Atom-Field Interaction in Optical Resonators

by

James Joseph Childs Jr.

B.A., Boston University (1980)

Submitted to the Department of Physics
in partial fulfillment of the requirements for the degree of

Doctor of Philosophy

at the

MASSACHUSETTS INSTITUTE OF TECHNOLOGY

February 1996

Author .. ..
:tment of Physics
October 30, 1995

Certified b .....
Michael S. Feld
Professor
Thesis Supervisor

Accepted by ....
George F. Koster
Chairman, Departmental Committee on Graduate Students

Atom-Field Interaction in Optical Resonators

by

James Joseph Childs Jr.

Submitted to the Department of Physics
on October 30, 1995, in partial fulfillment of the
requirements for the degree of
Doctor of Philosophy

Abstract

Normal-mode lineshapes are obtained in the strong and intermediate coupling regimes of atom-cavity interaction. The system consists of a beam of two-level ^{138}Ba atoms intersecting at right angles a standing-wave TEM_{00} mode of a low-loss cavity. The coupling regimes are realized with two cavities which differ only in finesse. Two experimental configurations are employed: The atoms or the cavity mode are weakly driven by tunable coherent laser light. In either case, both the light scattered out the resonator sides (from the atoms) as well as out the cavity end are simultaneously recorded as functions of laser frequency.

Lineshapes obtained are critically dependent upon excitation and observation schemes. Furthermore, dramatic manifestations of the standing-wave mode structure and intra-cavity atomic number fluctuations are observed with mean intra-cavity atomic number, $\langle \overline{N} \rangle \approx 1$. For strong coupling, one, two and three-peaked lineshapes are observed. In addition, two-peaked spectra observed in intermediate coupling demonstrate that lineshape splitting is not necessarily indicative of oscillatory atom-cavity energy exchange (normal-mode splitting).

The relationship between lineshapes and temporal evolution of the system is elucidated with a semiclassical model which accounts for intra-cavity atomic number fluctuations. The predicted lineshapes agree well with the experimental lineshapes in all configurations. Single-peaked lineshapes with widths twice the free-space natural linewidth reveal greatly enhanced *irreversible* spontaneous emission in the intermediate coupling regime, and two-peaked lineshapes indicate greatly enhanced *reversible* spontaneous emission (vacuum Rabi oscillations). In such experiments, a single intra-cavity atom does not constitute a true single atom experiment but, instead, requires on average several atoms interacting with the cavity mode simultaneously.

Thesis Supervisor: Michael S. Feld
Title: Professor

Acknowledgments

To my wife, Larisa Filipenco, whose love, support, and encouragement made this all possible. Her warmth, her selflessness, her sacrifices knew no bounds.

I wish to thank Professor Michael Feld for his faith, help, and patience throughout. He is a thoughtful advisor, coach, and friend. I have gained a great appreciation for his deep, intuitive approach to physics and remain indebted to him for his positive influence and inspiration. I also thank Dr. Ramanchandra Dasari who made the journey more enjoyable with dinner parties and friendly conversations. His expressed concerns for my well-being as well as others are only a few testaments to his warm spirit.

This thesis has benefited from the constructive comments of several people, namely Professors Dan Kleppner, Roy Glauber, and John King. I thank them for their help. I would also like to acknowledge and warmly thank Dr. Kyungwon An and Dr. Michael Otteson. Kyungwon not only provided much of the contents of section 2.3.3 and Appendix C, but also many hours of enjoyable companionship in the laboratory and constructive criticisms in our meetings. Michael joined the experiment for two months and contributed greatly to the laser stabilization setup.

There are many other friends and colleagues whose contributions took many forms. Among them I would like to thank Simone and Gee Rittenhouse for their love and support. Gee and I shared many enjoyable hours together. His wit, humour, and friendship during the rough times were truly a saving grace. (Our pick-and-roll had to be one of the most respected plays wherever we went.) I also thank Christian Schön for his friendship. Our lunch-time conversations and frequent gatherings are fondly remembered. Farideh Partovi, who brightened the office environment with her smile, was always willing to help with any problem, no matter how busy she was. Johnny Annese was also particularly helpful whenever I needed metal or machining advise. I also thank Professor Wolfgang Ketterle, who frequently loaned me whatever optics, electronics, or laser equipment I needed, especially during the final crunch time, and

Jon Bloch for his double-balanced mixer and RF generator.

From my earlier days, special thanks and acknowledgements go to Professor Dan Heinzen, now at the University of Texas at Austin, who took me under his wing and introduced me to experimental physics. He showed me how to align a dye laser, how to operate a lathe, and numerous other skills necessary to an experimental physicist. I also thank Professor John Thomas, now at Duke University, for his support and help, particularly with AO's. I enjoyed and benefited from our numerous discussions.

I thank Peggy Berkovitz for her administrative assistance; George Zonios for extra memory; Mike Kash, George Welch, and John Iu for their entertaining and enjoyable lab companionship; Tim Hutton and Professor Bill Dalby for their help and support; and Mike Donovan who not only demonstrated that a velocity selector was not the way to go, but also filled some of my lunch breaks with interesting points of view. I also would like to give a special thanks to my former supervisors, Carl Larsen and Dr. Robert DeWitt, for all their help. They made it possible for this work to be continued without interruption.

I would like to express my appreciation to Victor Filipenco for the many hours of informative and amusing conversations we shared. I thank my brother, Steve, for his timely assistance and my father, who taught me the value of hard work. Finally, I thank my mother for her unconditional support and love.

Contents

List of Figures

List of Tables

Chapter 1

Introduction

In 1917, the phenomenon of spontaneous emission was introduced in Einstein's celebrated treatment of a gas of atoms in thermal equilibrium with the surrounding radiation field [1]. Not only is spontaneous emission as well as stimulated emission and absorption necessary, but these processes also had to be directional in order to correctly obtain the Planck radiation distribution law. This provided further evidence for the existence of photons: The radiation field is composed of discrete packets of energy which also possess momentum that may be imparted (directionally) to interacting molecules or atoms. One of the earliest successes of the formally developed quantum theory of radiation is the natural occurrence of spontaneous emission, placed on an equal footing with simulated emission, in the description of a radiating atom. The Einstein A and B coeffficients could now be rigorously calculated in a theory capable of going far beyond the conditions and assumptions required in prior phenomenological derivations based on thermodynamics and rate equations.

To calculate the total spontaneous emission rate, Weisskopf and Wigner [2] applied perturbation theory to the interaction between the atom and the quantized field modes of free space. The vacuum surrounding the excited atom no longer plays a passive role, as it did in the preceding classical theories of radiation but, instead, couples to and perturbs the atom. Another celebrated result, also a consequence of the interaction between an atom and the vacuum, is the Lamb shift [3]. In free space, the vacuum is viewed as an ensemble of unexcited harmonic oscillators, the

electromagnetic field modes of free space, and these oscillators all couple to the atom. As a consequence of this ensemble, the spontaneous emission process is irreversible, i.e., the emitted energy does not return to the atom.

In the quantum theory of radiation, alteration of the surrounding vacuum by placing bounding surfaces naturally leads to changes in the atomic properties and, consequently, the spontaneous emission process. The first experimental demonstration of this involved a monomolecular layer of dye molecules deposited on a thin dielectric layer which lay on top of a metal mirror [4]. The fluorescence lifetime of the dye molecules exhibited a dependence on the thickness of the dielectric layer: For thicknesses less than the fluorescence wavelength, the lifetime increased.

For more dramatic effects, a natural system to consider is a cavity which is formed by contoured surfaces, with large electrical conductivity (or, equivalently, reflectivity), that either completely or partially enclose a radiating atom. The first experimental demonstration of inhibited spontaneous emission for this type of setup observed large changes in the damping rate of cyclotron motion of an electron in an electromagnetic trap [5]. With proper construction, a cavity can not only inhibit the atom from radiating its energy (increase of the excited atomic state lifetime), but also enhance the spontaneous radiation rate (decrease of the excited atomic state lifetime). Furthermore, if the interaction between the atom and the cavity field is strong enough and if the bounding cavity can store the emitted photon for a sufficient period of time, then the spontaneously emitted photon can be reabsorbed by the atom. This leads to an oscillatory exchange of energy between the atom and cavity field and the atomic emission may be viewed as *reversible* spontaneous emission. The resulting process has been popularly referred to in the literature as *vacuum Rabi oscillation* [6] by virtue of its similarity with the evolution of an atom subject to an intense, *external* laser field.

In this thesis, open optical resonators are used to investigate the lowest energy eigenstate structure of a composite atom-cavity system. In this type of cavity, the atom couples to an ensemble of free space modes as well as to a cavity mode. Note, however, that the cavity mode itself is coupled to free space modes via the finite reflectivity of the mirrors which make up the cavity. Not only the atom but also the

cavity mode can irreversibly lose energy. The resulting competition between the irreversible damping processes and the reversible atom-cavity energy exchange provides for a rich source of phenomena which may be characterized in three regimes: (1) Strong coupling, in which oscillatory energy exchange dominates, (2) weak coupling, in which radiative decay to free space (damping) dominates, and (3) intermediate coupling, where all processes are of similar strength.

1.1 Background

The study of an atom coupled to a single mode of a resonator, known as cavity quantum electrodynamics (QED), has undergone significant advances since Purcell first pointed out that a resonator could alter the atomic spontaneous emission rate [7]. Many of the initial experiments demonstrating suppression and/or enhancement of spontaneous emission were conducted in the microwave regime with Rydberg atoms [8, 9]. The advantages of this system are twofold: (1) Large dipole moments provide for large transition rates and (2) large wavelengths make feasible the construction of cavities whose dimensions are on the order of that wavelength [10]. Interestingly, investigations which utilized these low order mode cavities were also performed in the optical regime by placing two plane parallel mirrors, separated by 2.2 μm, in an atomic beam of properly prepared cesium atoms [11]. In the microwave experiments, direct measurement of the emitted photons is impossible. Instead, the atomic population levels are recorded after interaction with the cavity. In the optical regime, however, the emitted light can be measured directly.

Results in our laboratory demonstrated that substantial modifications of the spontaneous emission process is also possible in cavities with much larger dimensions, i.e., *high order* mode resonators. Large enhancement and suppression of spontaneous emission as well as cavity-enhanced radiative level shifts in the visible regime were observed in confocal and concentric geometry cavities [12, 13, 14]. These resonators have a degeneracy of modes which significantly alters the vacuum field density of states and gives rise to a large atom-cavity coupling (see also [15]). Note, however,

that these experiments were performed in the weak coupling regime because cavity damping dominated the atom-cavity interaction. We will discuss these special resonators further in Sec. 3.4.

Note that in the regime of weak atom-cavity coupling, perturbation theory is adequate to describe the system's behavior. Of great interest, however, is the strong coupling regime where a host of phenomena is possible. Evolution of the atomic radiator, as well as the cavity field, must be taken into account. Microwave researchers were the first to observe several interesting consequences of strong coupling which included quantum collapse and revival [16], Rabi oscillations [17, 18], and single-atom maser oscillation [19]. Improvements in resonator design have recently made this regime accessible at optical wavelengths. For example, experiments have demonstrated Rabi oscillations with many atoms coupled to a single field mode [20] and normal mode splitting for a single intra-cavity atom [21] as well as squeezed-state generation [22] and optical bistability with few atoms [23]. Normal mode splitting refers to the two-peaked frequency spectrum expected when oscillatory energy exchange occurs. The peaks correspond to each of the two nondegenerate frequencies (normal modes) of oscillation and their separation measures the oscillatory exchange rate of energy. Furthermore, single atom laser oscillation has recently been observed in our laboratory [24, 25].

The above experiments employed atomic beams, but enhanced spontaneous emission [26] as well as normal mode splitting [27] have also been observed in semiconductor devices, where practical as well as fundamental issues of cavity QED are studied [28, 29]. Recently, semiconductor technology has made possible the observation of normal mode splitting lineshapes in devices with only a few quantum wells (QW) [30], and even a single exciton within a single QW located at the anti-node of a low-order cavity mode [31]. In this experiment, the Rabi oscillations in the emitted intensity as well as the emission spectra were recorded. These studies are only a few in the recent activity toward realizing low-threshold and, therefore, more efficient microcavities (also recently demonstrated [32]). A commonly used parameter, called the spontaneous emission coefficient, β, is defined as the ratio of the (enhanced) spon-

taneous emission rate into the cavity mode to the total spontaneous emission rate (cavity mode plus all other free space modes). The larger the β parameter, the lower the threshold for laser oscillation. In the limit $\beta \rightarrow 1$ thresholdless lasing occurs [28]. Several areas of technology which may benefit from this research include optical communications, displays, and optical computing.

All of the above studies utilize standing-wave (SW) mode resonators, in which the coupling of the radiator to the cavity mode is position dependent. The effect of such mode structure on atom-cavity dynamics can be significant. For example, threshold in microcavities is dependent on the spontaneous emission coefficient, which is mode structure and, therefore, position dependent. Similarly, operation of the single-atom laser, which employs an atomic beam as the gain medium, is critically dependent on the location of the atom(s) within the cavity mode volume [33]. Unlike the microcavity case, in which it is possible to localize the radiators at specific positions within the cavity mode, atoms in an atomic beam can occupy any position within the cavity mode. This thesis will elucidate interesting consequences of this in the study of the normal mode structure of an SW cavity mode interacting with atoms in an atomic beam. Other interesting phenomena which rely on this SW mode structure include the effects of atomic motion in the cavity mode [34, 35], trapping, and squeezing [36, 22].

The first fully quantized treatment of an atom-cavity system was introduced by Jaynes and Cummings [37]. In this paper, a comparison of the fully quantized theory with a *semiclassical* theory, a theory in which the atoms are treated quantum mechanically but the radiation field is treated classically, is made. In particular, it is pointed out that previous semiclassical treatments (eg., [38]) involve approximations: In addition to the classical treatment of the radiation field, the molecules are given independent wave functions and are not treated as a single quantum mechanical system as was done in a formalism similar to that of Dicke's superradiant gas [39]. For the complete quantum mechanical treatment suggested, however, solution of the so-called Jaynes Cummings Hamiltonian for one or many atom(s) becomes tractable only under the assumption of a uniform mode function. To illustrate, consider the

Hamiltonian for atoms interacting with a cavity mode in which damping is neglected:

$$\hat{H} = \sum_{j=1}^{N} \left[\frac{1}{2}\hbar\omega_p \hat{\sigma}_z^j + \hbar\omega_p \hat{a}\hat{a}^\dagger + ig_j(\hat{a}^\dagger \hat{\sigma}_-^j - \hat{a}\hat{\sigma}_+^j) \right], \tag{1.1}$$

where $\hat{\sigma}_z^j$ is the atomic inversion operator, g_j is the coupling of the atom to the quantized cavity field mode with raising (lowering) operators $\hat{a}^\dagger$ ($\hat{a}$), and $\hat{\sigma}_+$ ($\hat{\sigma}_-$) is the atomic raising (lowering) operators for the j^{th} atom. If the cavity mode is described by a uniform mode function, $g_j = g_0$ for all j regardless of the j^{th} atom's position, and all the atoms are equally coupled to the mode. In analogy with the angular momentum formalism, one may introduce the operators

$$\hat{S}_z = \sum_{j=1}^{N} \hat{\sigma}_z^j, \qquad \hat{S}_\pm = \sum_{j=1}^{N} \hat{\sigma}_\pm^j, \tag{1.2}$$

so that the Hamiltonian, Eq. 1.1, may be rewritten as

$$H = \frac{1}{2}\hbar\omega_p \hat{S}_z + \hbar\omega_p \hat{a}\hat{a}^\dagger + ig_0(\hat{a}^\dagger \hat{S}_- - \hat{a}\hat{S}_+) \equiv H_0 + ig_0(\hat{a}^\dagger \hat{S}_- - \hat{a}\hat{S}_+). \tag{1.3}$$

The operators satisfy the commutation relations

$$[\hat{S}_z, \hat{S}_\pm] = \pm\hat{S}_\pm, \tag{1.4}$$

$$[\hat{S}_+, \hat{S}_-] = 2\hat{S}_z, \tag{1.5}$$

and a basis which forms simultaneous eigenstates of H_0 and the operator $\hat{S}^2 = \hat{S}_z^2 + (\hat{S}_+\hat{S}_- + \hat{S}_-\hat{S}_+)/2$ may be constructed [39]. This situation was treated in a frequently quoted paper by Tavis and Cummings [40]. If, however, an SW mode function, depicted in Fig. 1-1, is assumed so that all the g_j's are different, the treatment becomes more complicated. This point will be discussed later in connection with many-atom versus single-atom effects.

Atom-cavity systems have been studied theoretically in many different approaches, with predictions of a host of interesting features in both the classical and quantum

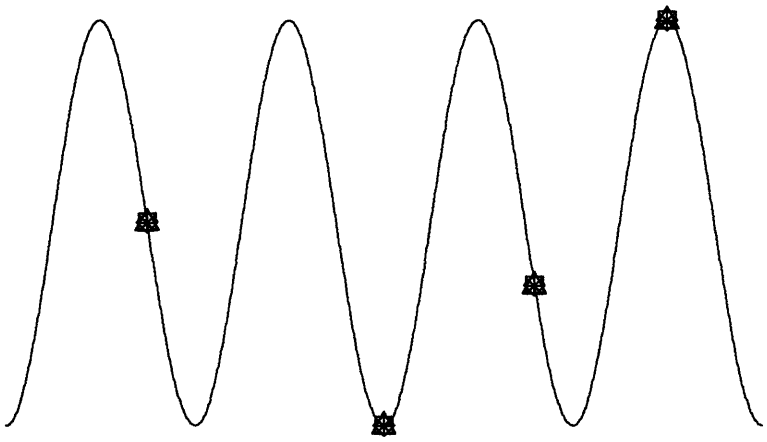

Figure 1-1: Atoms coupled to a standing-wave cavity mode

domains. Quantized field models have analyzed the statistical properties [41, 42] and/or structure [43] of the single-atom system over a range of system parameter values. Sanchez-Mondragon et al. [6] have presented the first fully quantum mechanical predictions of the spontaneous emission spectrum of a strongly coupled atom-cavity system with no cavity damping (see also Agarwal, who has calculated the atomic absorption [44] and spontaneous emission [45] spectra of such a system). Rice and Carmichael [46] have discussed nonclassical effects such as squeezing-induced line narrowing and spectral holes in the incoherent part of the fluorescence and transmission spectra, and Carmichael et al. [47] have discussed the role of squeezing in the spontaneous emission spectrum and weakly driven fluorescence spectrum of a damped, strongly coupled system. Models in which the emission field is quantized have been developed to study the strongly excited system [48, 49].

Quantized field models become increasingly more complicated to apply when the cavity field or the number of interacting atoms becomes large. Recent theoretical activity, however, holds promise of providing numerical simulations in fully quantized treatments of these more realistic systems: Quantum trajectory simulations are fully quantized treatments currently being applied to experimentally realizable systems

that include open, high-order cavities similar to those studied here (with one or many atoms) (see [50] and references therein).

1.2 Present Work

Many of the above mentioned phenomena are manifested in spectral lineshapes. For example, two-peaked lineshapes occur in normal-mode splitting, multi-resonance lineshapes are predicted to arise from atomic motion through the cavity mode, and broadened and narrowed Lorentzians demonstrate enhanced and suppressed spontaneous emission, respectively. These lineshapes are sensitive not only to the kind of resonator (standing/traveling wave, open/closed and degenerate/nondegenerate) and radiator (moving atoms in a beam or fixed excitons in a quantum well), but also to the excitation and observation geometry. In particular, normal-mode lineshapes in an atom-cavity system with an open optical resonator may be obtained either by exciting the atom from the side of the resonator, or the cavity mode through the end mirrors. In either case one may observe light scattered by the atom out the resonator side (sidelight) or transmitted out the resonator ends, Fig. 1-2. The various schemes can exhibit dramatically different lineshapes.

The core of this thesis consists of a detailed study of spectral lineshapes obtained in experiments with an atomic beam interacting with a single mode of an open optical resonator. All schemes mentioned above are performed with weak excitation to obtain the normal mode structure for this system. We utilize nondegenerate resonators ("super-cavity") but, in order to connect with other works, degenerate (concentric or confocal) and nondegenerate resonators are briefly compared. We obtain lineshapes in all three coupling regimes (strong, intermediate and weak coupling) and extract information about the spontaneous emission processes in such cavities.

One objective in studying these systems is the realization of the single atom limit in which only a single atom interacts with the cavity mode. This objective has not been realized in these experiments for very interesting reasons attributable to manifestations of the SW mode structure. Fluctuations in the number of intra-cavity

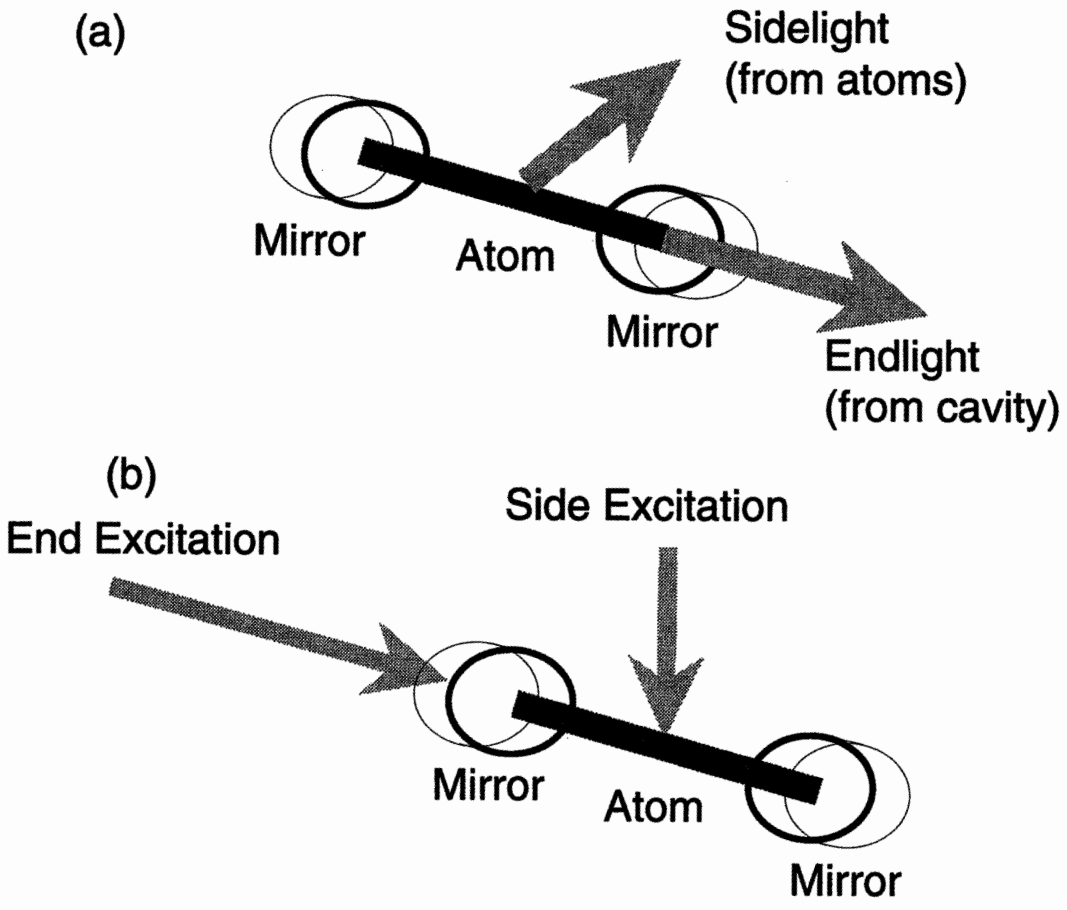

Figure 1-2: Diagram of the possible excitation and observation schemes.

atoms, defined in Chapter 3, are very important in this limit and have dramatic effects on the lineshapes for appropriately chosen schemes.

The analyses of our results utilize a semiclassical model in which all fields, cavity and probe, are treated classically via Maxwell's equations. This approach, of course, cannot provide information about effects that arise from the quantum coherence between the atoms and field: The semiclassical theory of this type arises from assuming, in the fully quantized theory, that the expectation of products of the atomic and field operators is equivalent to the product of their expectations. (Note that some semiclassical theories, such as those treating a strongly driven atom in free space (see, for example, the derivation of the Mollow spectrum, [51]), assume that the probe field is classical but the emission field (free space) is quantized.) Nonetheless, such a theory is applicable to our studies of normal mode structure and provides a tractable means for analyzing the various results.

1.2.1 Contributions

In summary, we provide a list of what this thesis demonstrates:

- Demonstration of the importance and effects of fluctuations in intra-cavity atomic number on experimental lineshapes.
- Clarification of the conditions for single atom effects in SW and degenerate resonators.
- First observation of normal mode splitting for a single intra-cavity atom in an "artifact-free" scheme.
- Large enhancement of spontaneous emission in intermediate coupling regime.
- Elucidation of the relationship between lineshapes and temporal evolution. In particular, we distinguish lineshape splitting (two-peaked lineshapes) from normal mode splitting (two nondegenerate normal mode frequencies) and demonstrate the conditions under which lineshape splitting implies oscillatory energy exchange.

- Utility of a semiclassical model in describing the various spectral lineshapes experimentally obtained.
- Investigation of saturation effects in an SW cavity mode in the strong coupling regime.
- Comparison of nondegenerate and degenerate resonators.

1.3 Organization of Thesis

In Chapter 2, we present the "fixed-atom" semiclassical model. This model assumes that either one stationary atom interacts with the cavity mode or, if there are many atoms, they all are equally coupled to the cavity. This provides the framework from which a more realistic model applicable to the experiments can be constructed (in Chapter 3).

Chapter 3 extends the model of chapter 2 to study an atomic beam interacting with a standing-wave cavity mode. The number of atoms and their positions (which determines each atom's coupling strength) within the mode fluctuate, giving rise to fluctuations in the number of intra-cavity atoms. Manifestations of these fluctuations are discussed and the lineshapes are compared with the fixed-atom lineshapes. The single atom limit is discussed and a study of saturation is briefly described.

Chapter 4 describes the experiments and their results are compared with theory.

Chapter 5 presents a summary of the present work. Possible future studies for this particular experimental arrangement are also presented.

Appendix A calculates a cavity transmission factor for transmission experiments.

Appendix B briefly describes broadband excitation of the atom-cavity system.

Appendix C discusses stimulated emission line narrowing.

Appendix D contains a reprint of the Physical Review Letter.

Chapter 2

Theory I

This chapter describes a semiclassical model which assumes a fixed number of atoms interacting with a single resonator mode described by a uniform mode function. The positions of the atom(s) is irrelevant, they are all coupled equally to the cavity mode. For a related work see [52]. The theory described below has also been applied to the study of optical bistability in atom-cavity systems, see [53].

2.1 Introduction

Consider a two-level atom with free-space atomic center frequency, ω_p, and transition dipole moment matrix element, μ, coupled to a mode of a resonator with frequency, ω_c, and volume, V. In a quantized field picture this system can be described using dressed states [54]. If we consider only the lowest lying states (those with zero or one quantum of excitation), neglect damping of the atom and cavity, and treat the coupling in the rotating wave approximation, the dressed state frequencies are

$$\Omega_{\pm}^{0} = \omega_p + \omega_- \pm \sqrt{\omega_-^2 + g_0^2}. \tag{2.1}$$

In this equation the atom-cavity mode coupling constant is defined as $g_0 = \mu E_{vac}/\hbar = \mu\sqrt{2\pi\hbar\omega_c/V}$, with $\omega_- = (\omega_c - \omega_p)/2$ the atom-cavity frequency detuning. The quantity E_{vac} corresponds to the RMS electric field associated with vacuum fluctuations

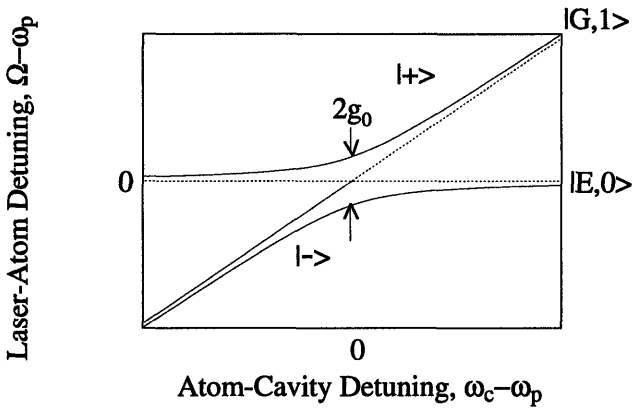

Figure 2-1: Dressed state diagram of the two lowest excited states of the atom-cavity system. $|G,1\rangle$ is the superposition state with one photon in the cavity and the atom in the ground state, and $|E,0\rangle$ is the superposition state with no photons in the cavity and the atom in the excited state. The dashed lines show the uncoupled states.

[55].

The forgoing treatment provides a simple, qualitative picture of the mode frequencies of the atom-cavity system, depicted in the dressed state diagram of Fig. 2-1. Essentially the same result is obtained classically if one considers the atom and cavity as coupled harmonic oscillators. Because of the coupling, the normal mode frequencies deviate from the uncoupled oscillator frequencies. For zero detuning (cavity tuned to the atomic center frequency, $\omega_- = 0$) the normal mode frequencies differ by $2g_0$. Physically, this normal mode frequency difference corresponds to the exchange rate of the energy of one quantum between the atom and the cavity field (*normal mode ringing*). Even for large detuning, $|\omega_-| \gg g_0$, the normal mode frequencies deviate slightly from the atom and cavity field uncoupled frequencies. For $\omega_- \ll -g_0$, the $|+\rangle$ dressed state is *atom-dominated* (i.e., the probability that the atom is excited is much greater than the probability that a photon is in the cavity) and the $|-\rangle$ state is *cavity-dominated.* For $\omega_- \gg g_0$, the reverse occurs. For $\omega_- = 0$, these states are a linear superposition of an excited atom, empty-cavity-mode product state and an unexcited atom, one-photon-cavity-mode product state.

Since decay is an essential feature of any physically realizable atom-cavity system, damping must be incorporated. The atom decays out the side of the resonator

via coupling to the free-space modes there and also emits into the resonator mode, which itself decays via coupling to free-space modes bounding the mirror surfaces. The inclusion of damping gives rise to three regimes for study: the strongly coupled regime, of which the preceding dressed states example is an extreme case; the intermediate coupling regime, in which the coupling strength is of the same order as the damping; and the weakly coupled regime, in which damping dominates the atom-cavity interaction. (These three regimes are defined more precisely in Sec. 2.3.1.) In the time domain, a strongly coupled, resonant ($\omega_- = 0$) system exhibits an oscillatory exchange of energy between the two oscillators (ringing), despite the presence of damping, whereas a weakly coupled, resonant system exhibits decay with no ringing, despite the presence of coupling. In the frequency domain, the spectral lineshape of the oscillators (studied, e.g., by monitoring the atomic fluorescence and the cavity transmission) is effected by the presence of coupling in various ways depending on the coupling regime and the experimental arrangement. For a resonant system in the strong coupling regime, the spectral lineshapes are two-peaked (lineshape *splitting*) but in the weak coupling regime they are single-peaked. The observation of lineshape splitting in the frequency domain, however, does not necessarily indicate ringing in the time domain. As will be discussed in Sec. 2.3.2, in the intermediate coupling regime there can be significant lineshape distortions, and a two-peaked structure can occur, *even in a resonant system with no ringing.* Most atom-cavity experiments are performed in the frequency domain by studying the emission or scattering in a succession of single-atom events. On average, this is equivalent to performing the experiment in the steady state. In fact, for the experiments described in Chapter 4, each atom reaches steady state very quickly so that the initial transient regime may be neglected.

As seen in Sec. 2.3.3, for arbitrary atom and cavity decay rates the spontaneous emission rate into the cavity mode for the resonant atom-cavity system may be written as

$$A_{cav} = \frac{2g_0^2}{\gamma_p + \gamma_c}, \tag{2.2}$$

with γ_p the atomic dipole moment decay rate and γ_c the cavity field decay rate into free-space modes. We will mainly specialize to open optical resonators, for which $\gamma_c = c(1-R)/2L$, with R the mirror reflectivity and L the cavity length. A_{cav} may be expressed in various ways. From an experimental point of view, it is useful to relate it to the resonator finesse $F = \pi c/2L\gamma_c = \pi/(1-R)$, and to the factor f, the ratio of power spontaneously emitted by a free-space dipole into a solid angle subtended by the cavity mirrors to the total free-space power spontaneously emitted [13]:

$$A_{cav} = \frac{2fF}{\pi}\frac{2\gamma_p\gamma_c}{\gamma_p+\gamma_c}. \tag{2.3}$$

Note that the parameter f is *not* the same as the spontaneous emission coefficient, β, which includes the effects of atom-cavity coupling. In fact,

$$\beta = \frac{A_{cav}}{2\gamma_p + A_{cav}}. \tag{2.4}$$

The total free-space spontaneous emission rate is

$$A_{free} = \frac{4\mu^2\omega_p^3}{3\hbar c^3}. \tag{2.5}$$

Equation 2.3 can also be expressed in terms of the atomic absorption cross section,

$$\sigma_0 = \frac{2Vg_0^2}{c\gamma_p} = \frac{4\pi\omega_p\mu^2}{c\hbar\gamma_p}, \tag{2.6}$$

to obtain,

$$A_{cav} = \frac{\sigma_0 c}{V}\frac{\gamma_p}{\gamma_p+\gamma_c}. \tag{2.7}$$

In general, the coupled atom-cavity system is best described in terms of the two normal modes. As mentioned above, three regimes of interest may be defined, according to the relative sizes of g_0, γ_c and γ_p. In strong coupling, the coupling constant g_0 dominates, and in weak coupling γ_c and/or γ_p dominate. (In a system of N atoms interacting with the cavity mode, the coupling constant is given by $\sqrt{N}g_0$.) The normal modes contain contributions from the properties of both oscillators. The

identification of separate, distinct atomic and cavity-mode oscillators is not possible in the strong and intermediate coupling regimes when the atom and cavity mode are resonant. With weak coupling, however, one normal mode resembles the atomic oscillator, and the other resembles the cavity oscillator. Changes in the decay rate and emission frequency resulting from the coupling will occur for the cavity oscillator, as well as for the atomic oscillator. The atomic emission rate, emission frequency, and lineshape can be significantly altered by the atom-cavity interaction.

In a weakly coupled system the spontaneous emission rate of the atom can be enhanced or suppressed and the atomic emission frequency can shift due to the presence of the resonator. Such changes in the atomic spontaneous emission rate have been observed at microwave [8, 9] as well as optical [11] wavelengths in systems with a low-order mode resonator/waveguide whose dimensions are on the order of the wavelength ($L \approx \lambda$). For visible wavelengths, spontaneous emission rate changes as well as vacuum radiative level shifts have been studied using specially designed open optical resonators ($L \gg \lambda$) with degenerate high-order modes [12, 13, 14]. In these experiments, the spontaneous emission rates and frequencies were extracted from lineshapes obtained in a scattering arrangement (Sec. 2.2.3). The lineshapes observed were single Lorentzians. In this limit, the total spontaneous emission rate is identical to the linewidth of the scattering lineshape, but this is not generally true. In Sec. 2.3 we will discuss the relationship between emission rates and linewidths obtained from scattering lineshapes, as well as from emission spectra. All of the preceding experiments have been performed in the broad cavity limit, where $\gamma_c \gg \gamma_p$. Enhancements as large as 42% have been observed [14]. We may write equation 2.2 in this limit to obtain the enhanced spontaneous emission rate, A_{enh}:

$$A_{cav} \rightarrow A_{enh} = \frac{2g_0^2}{\gamma_c}, \qquad \gamma_c \gg \gamma_p. \tag{2.8}$$

The spontaneous emission rates and vacuum radiative level shifts can also be analyzed using perturbation theory [2], since the atom interacts with a resonator mode that decays more rapidly than the atom. The changes in spontaneous emission

can be understood as arising from the alteration in the density of modes caused by the presence of the resonator [7, 56]. The resulting perturbation also gives rise to vacuum radiative level shifts analogous to the Lamb shift [13]. Note that perturbation theory, however, is no longer appropriate in the strong or intermediate coupling regimes or when the field mode damping rate is comparable with or slower than the atomic decay rate (i.e., narrow cavity limit, $\gamma_p \gg \gamma_c$). In these cases, the atom evolves on a time scale comparable with or faster than the field to which the atom is coupled.

As mentioned, the fluorescence and emission spectra of the atom-cavity system can exhibit a two-peaked lineshape for zero atom-cavity detuning in the strong or intermediate coupling regimes. One source of this two-peaked lineshape is the *normal mode ringing* that occurs in the time evolution of the two oscillators as energy is exchanged back and forth between the atom and cavity field, despite the presence of damping. This process has been described as *vacuum field Rabi oscillation* [6], although it should be clear from the foregoing discussion that it is purely classical in origin (see also [45, 20]). The terms *normal mode splitting* and *vacuum Rabi splitting* have frequently been used as well to describe the resulting lineshapes. In general, as will be discussed in Secs. 2.3.1 and 2.3.2, lineshape splitting in the frequency domain does not directly correspond to normal mode ringing in the time domain. The conditions that determine whether or not ringing will occur are not the same as those which determine whether or not lineshape splitting will occur.

In the visible wavelength regime, resonant atom-cavity systems have been studied with a small number of atoms coupled to a high-finesse "supercavity" optical resonator, and lineshape splitting has been observed [57, 21]. In these experiments the cavity mode was excited by a weak laser field and the transmission out the end of the cavity monitored as the laser frequency was swept through resonance. Lineshape splitting has also been observed in a similar experiment with a large number of atoms, each weakly coupled to a weakly excited nondegenerate resonator mode ($g_0 \ll \gamma_c, \gamma_p$, and $\sqrt{N}g_0$) [20]. This latter experiment also studied the time domain, where normal mode ringing was observed in the decaying output emission of the cavity mode. A model based on linear absorption and dispersion in a multi-atom medium was used

to provide a classical interpretation of this effect.

As previously discussed, an atom can undergo spontaneous emission into the resonator mode at a greatly enhanced rate. Under appropriate conditions, i.e., in the presence of cavity photons, single-atom stimulated emission into the resonator mode can also occur. The features of these two processes are very different. In enhanced spontaneous emission the linewidth increases with increasing emission rate [12, 13, 14]. In stimulated emission, however, the linewidth should *decrease* with increasing emission rate in a manner analogous to laser emission [58]. As will be discussed in Sec. 2.2.2, for incoherent excitation of the atom-cavity system we may write a rate equation for the average number of photons, ν, in the cavity mode:

$$\dot{\nu} = A_{cav}N_u + K(N_u - N_l)\nu - 2\gamma_c\nu, \tag{2.9}$$

where N_u and N_l are the average occupation probabilities (populations) of the upper and lower states of the atom, A_{cav} is the Einstein A coefficient for spontaneous emission into the cavity mode, defined above, and $K = A_{cav}$ is proportional to the Einstein B coefficient. We may solve for ν in the steady state to obtain the power emitted out the end mirrors (assuming cavity loss is negligible compared with transmission):

$$P = 2\gamma_c\hbar\omega\nu = \frac{N_u\hbar\omega A_{cav}}{1 - G_0}, \tag{2.10}$$

with

$$G_0 = \frac{(N_u - N_l)\sigma_0 L}{V(1-R)}\frac{\gamma_p}{\gamma_p + \gamma_c}. \tag{2.11}$$

Note that G_0 can be interpreted as the multi-pass gain of the atom-cavity system. When G_0 is negligible and $\gamma_c \gg \gamma_p$, we recover the usual enhanced spontaneous emission result. For positive gain, however, a further increase in emitted power occurs. This extra enhancement is due to stimulated emission. One is thus led to assess the possibility of studying stimulated emission in an atom-cavity system and its interplay with enhanced spontaneous emission. In Sec. 2.3.3, we will discuss the conditions for which stimulated emission can occur. Note that the above rate equation approach,

while useful in the description of conventional lasers, does not properly account for the underlying process which occurs in the recently realized single atom laser [25]. In this system, atom-cavity energy exchange occurs by means of quantized Rabi oscillations with no disruption of phase by incoherent pumping mechanisms. Excited atoms enter the cavity, undergo coherent evolution with the field, and exit the cavity.

The objective of our study is to develop a theoretical framework that describes various regimes of cavity QED emission. The present chapter describes a semiclassical model in which only the atom is quantized. This is particularly useful for exploring the inter-relationships among different cavity QED experimental schemes and for describing stimulated emission in an atom-cavity system and its relation to spontaneous emission. The model predicts both spectral features (linewidths and emission frequencies) and emission and decay rates. We restrict ourselves mostly to the case of weak excitation, in which the background atomic level populations are unperturbed. We study all regimes of the system parameters (specified by relative sizes of atom and cavity damping rates and coupling constant), showing agreement with quantized field calculations where they exist, and we explore the unique properties of the system when the inversion is allowed to become positive and there is net positive gain.

An atom-cavity system is a composite entity that exhibits characteristic lineshapes, decay rates, and emission rates. Its features can be studied in either emission or scattering experiments. In emission, the upper state of the atom, averaged over a series of successive events, is incoherently populated and the resulting spectrum of emitted radiation (emission spectrum) is studied or the total emitted power is studied (by either measuring the atomic population or the integral over the emission spectrum). The system response can also be observed in the transient regime, by initially exciting the atom or cavity mode and studying the emitted radiation. This can be considered as the *free-induction decay* of the atom-cavity system. In a scattering experiment, on the other hand, resonance fluorescence of the atom-cavity system in its ground state is studied by exciting the system with a monochromatic field and observing the scattered photons. In this case, one can study either the spectrum of scattered photons (resonance fluorescence spectrum) or the total power

scattered as a function of the excitation frequency (*excitation* spectrum). As will be discussed in Sec. 2.3, measurement of the excitation spectrum is equivalent to probing the absorption of the atom-cavity system. If the exciting field is weak, the resonance fluorescence spectrum will be monochromatic at the excitation frequency (elastic scattering) [59]. For strong excitation, however, nonmonochromatic spectral components (inelastic scattering) will also be present (e.g., the Mollow spectrum; see [51]). These are manifested as power broadening of the Lorentzian lineshape in the excitation spectrum [48]. As will be explained, equivalent information can be obtained in an emission experiment and a scattering experiment, and both types of experiments have been performed. Goy et al. [8], Hulet et al. [9], and Jhe et al. [11] have studied emission by monitoring the atomic state populations, whereas Heinzen et al. [12, 13, 14], Raizen et al. [57] and Thompson et al. [21] have employed scattering arrangements. Zhu et al. [20] have performed both types of experiments, but in the emission set-up they observed the time evolution of the emitted field directly. In the present chapter we connect the parameters measured in various experiments and clarify the relationships among linewidths, decay rates, and emission rates.

From a theoretical point of view, too, one can study either emission or scattering. A normal mode analysis of an atom-cavity system is presented (Sec. 2.2.1), from which the free-induction decay is obtained and decay rates extracted. Emission spectra can then be obtained from the Fourier transform of the transient solutions (Sec. 2.2.2). We then analyze the case of scattering (Sec. 2.2.3). In scattering, the excitation spectrum gives the absorption profile of the atom-cavity system, which is identical to the emission profile (see Sec. 2.3). Therefore, the lineshape of the excitation spectrum contains information about spontaneous emission enhanced or suppressed by the atom-cavity interaction. The connection between scattering and emission is discussed. In the time domain analysis, the system is given a prescribed set of initial conditions, and the evolution in time of the atom (via emission out the side of the cavity) or cavity field (via emission out the end of the cavity) is monitored as shown in Fig. 1-2(a). In a scattering experiment, either the atom or the cavity field can be probed (Fig. 1-2(b)), and the power scattered out the end mirrors (proportional

to the square of the cavity field) or the side of the resonator (proportional to the square of the atomic dipole moment) can be monitored. The various possibilities are analyzed below. In addition, we discuss the possibility of stimulated emission and absorption, and their relation to spontaneous emission, in Sec. 2.3.3.

2.2 Semiclassical Model

The analyses of this section are based on the coupled Maxwell-Schrödinger equations. Consider an atom-cavity system composed of N two-level atoms coupled to a single mode of a resonator. We are particularly interested in systems employing open optical resonators, but our results will be written in a form applicable to various other types. The atom is assumed to decay radiatively. Other homogeneous and inhomogeneous broadening mechanisms are assumed negligible. In Sec. 2.2.1, a normal mode analysis is performed from which transient solutions for the atomic dipole and the cavity field, as well as their Fourier transforms, are obtained. These results are then extended in Sec. 2.2.2 to the case of steady state emission, assuming an incoherent pumping mechanism. In Sec. 2.2.3, the scattering formalism is presented. In this case a driving field is included in the coupled Maxwell-Schrödinger equations as a source for exciting either the atom or the cavity mode. In each analysis two ensemble averaged observables are computed: the power scattered/emitted out the sides and out the ends of the resonator as a function of the excitation/emission frequency, respectively. From these quantities the spectral structure of the atom-cavity system is obtained. The linewidths obtained in the scattering analysis will later be compared to the decay rates obtained in the time domain analysis, and to the steady state emission rates. This model therefore elucidates the relationships between linewidths, decay rates and emission rates.

2.2.1 Normal Mode Analysis

We first study the time-dependent behavior of the atom-cavity system, prepared with a given set of initial conditions. The transient solutions provide decay rates and

emission frequencies, and their Fourier transforms provide the frequency content of the emitted radiation, none of which are obtainable in a scattering analysis. Furthermore, if we consider a steady state experiment in which an ensemble of these radiators is supplied at some rate, we may also obtain emission rates and emission spectra, as well as a rate equation for the cavity photon number. It is then possible to discuss stimulated emission/absorption in the atom-cavity system.

To obtain the transient solutions, we start with the Maxwell-Schrödinger equations:

$$\ddot{\mathbf{p}} + 2\gamma_p \dot{\mathbf{p}} + \omega_p^2 \mathbf{p} = -\frac{2\mu^2 \omega_p}{\hbar} \mathcal{N} \mathsf{E_c}, \tag{2.12}$$

$$\ddot{\mathsf{E}}_\mathsf{c} + 2\gamma_c \dot{\mathsf{E}}_\mathsf{c} + \omega_c^2 \mathsf{E_c} = \frac{4\pi\omega_p^2}{V} \mathbf{p}, \tag{2.13}$$

$$\dot{\mathcal{N}} + 2\gamma_p(\mathcal{N} - \mathcal{N}_0) = \frac{2(\dot{\mathbf{p}} + \gamma_p \mathbf{p})\mathsf{E_c}}{\hbar\omega_p}, \tag{2.14}$$

$$\mathcal{N} = N_u - N_l \quad ; \quad N = N_u + N_l, \tag{2.15}$$

with $\mathbf{p}$ the atomic dipole and $\mathsf{E_c}$ the resonator field evaluated at the position of the atom. The vector notation is suppressed because we assume they are all parallel. This is a valid assumption so long as the cavity mirrors exhibit no birefringence. The atom is assumed to have a dipole moment decay rate, γ_p (the decay rate into all modes except the cavity mode, i.e., out the sides). If we interpret these equations as describing the average atom-cavity behavior due to a succession of single-atom events, the atom can be considered to have an inversion, $\mathcal{N}$, with decay rate γ_p and $\mathcal{N}_0$ the inversion in the absence of $\mathsf{E_c}$ (*background* inversion). Note that

$$2\gamma_p = A_{free}(1 - f). \tag{2.16}$$

In most cases, $f \ll 1$ (see, however, Heinzen et al., [12, 13, 14]). The population equation 2.14 is essentially a statement of energy balance. It can be rewritten as the rate of energy flow into the upper state of the atom:

$$\hbar\omega_p \dot{N}_u = [\hbar\omega_p N_u^0 \cdot 2\gamma_p] - [\hbar\omega_p N_u \cdot 2\gamma_p - (\dot{\mathbf{p}} + \gamma_p \mathbf{p})\mathsf{E_c}]. \tag{2.17}$$

The two bracketed quantities represent the energy supply and energy loss contributions to N_u, respectively. The N_u^0 term represents the rate of supply of background population, if any, to the upper state. The N_u term describes the power emitted out the side of the resonator. Finally, the last term describes the interaction of the atomic dipole with the cavity field, which results in the power scattered out the ends of the resonator.

In this chapter we assume a weak cavity field so that the level populations are unperturbed (i.e., $\mathcal{N} \approx \mathcal{N}_0$) and Eq. 2.14 may be neglected. We will leave $\mathcal{N}$ arbitrary in most of the following equations for future use, however. In particular, in Sec. 2.3.2, we will assume that $\mathcal{N}_0 = -1$, and in Sec. 2.3.3 we will allow the inversion to be positive as well as negative.

We assume normal mode solutions of the form:

$$\mathbf{p}(t) = \mathrm{Re}[p(t)] = \mathrm{Re}[p_0 e^{i\lambda t}], \tag{2.18}$$

and

$$\mathsf{E_c}(t) = \mathrm{Re}[E_c(t)] = \mathrm{Re}[E_0 e^{i\lambda t}], \tag{2.19}$$

with λ the normal mode frequencies. Note that λ is a complex quantity whose real part represents the actual normal mode frequency and imaginary part the decay constant of the excited normal mode. The following secular equations for λ are obtained from Eqs. 2.12 and 2.13:

$$[\omega_p^2 - \lambda^2 + 2i\lambda\gamma_p]p_0 = -\frac{2\mu^2\omega\mathcal{N}}{\hbar}E_0, \tag{2.20}$$

$$[\omega_c^2 - \lambda^2 + 2i\lambda\gamma_c]E_0 = \frac{4\pi\omega^2}{V}p_0. \tag{2.21}$$

In general, only numerical solutions for λ are possible. In the present case, however, damping, atom-cavity detuning, and coupling are all much smaller than the optical frequency, and we may find approximate analytic solutions to Eqs. 2.20 and 2.21 by assuming $\omega^2 - \lambda^2 \approx 2\lambda(\omega - \lambda)$, a condition equivalent to the near-resonance condition

employed in the frequency domain. Equations 2.20 and 2.21 then become:

$$\mathcal{L}_p(\lambda)p_0 = -\frac{i\mu^2\mathcal{N}}{\hbar}E_0, \tag{2.22}$$

$$\mathcal{L}_c(\lambda)E_0 = \frac{2\pi\omega_p}{V}p_0, \tag{2.23}$$

with the complex Lorentzian factors

$$\mathcal{L}_{c,p}(x) = -i(x - \omega_{c,p}) - \gamma_{c,p}, \tag{2.24}$$

where x is an arbitrary variable. We shall refer to $\mathcal{L}_q$ as a *Lorentzian factor*; the actual Lorentzian is $1/|\mathcal{L}_q(x)|^2$. The resulting secular equation for λ is

$$[\mathcal{L}_c(\lambda)\mathcal{L}_p(\lambda) - \mathcal{N}g_0^2]E_0 \equiv \mathcal{L}_+(\lambda)\mathcal{L}_-(\lambda)E_0 = 0, \tag{2.25}$$

with complex Lorentzian factors

$$\mathcal{L}_\pm(x) = -i(x - \lambda_\pm), \tag{2.26}$$

with

$$\lambda_\pm = \Omega_\pm + i\Gamma_\pm, \tag{2.27}$$

and

$$\Gamma_\pm = \gamma_+ \pm I, \tag{2.28}$$

$$\Omega_\pm = \omega_+ \pm R, \tag{2.29}$$

with $\Omega_\pm$, $\Gamma_\pm$, I, and R all real, and

$$2R^2 = (\omega_-^2 - \mathcal{N}g_0^2 - \gamma_-^2) + \sqrt{(\omega_-^2 - \mathcal{N}g_0^2 - \gamma_-^2)^2 + 4\omega_-^2\gamma_-^2}, \tag{2.30}$$

$$2I^2 = -(\omega_-^2 - \mathcal{N}g_0^2 - \gamma_-^2) + \sqrt{(\omega_-^2 - \mathcal{N}g_0^2 - \gamma_-^2)^2 + 4\omega_-^2\gamma_-^2} \tag{2.31}$$

where

$$\omega_{\pm} = \frac{\omega_c \pm \omega_p}{2}; \qquad \gamma_{\pm} = \frac{\gamma_c \pm \gamma_p}{2}. \tag{2.32}$$

For the special case of zero atom-cavity detuning ($\omega_- = 0$), Eqs. 2.30 and 2.31 become

$$2R_0^2 = -(\mathcal{N}g_0^2 + \gamma_-^2) + |\mathcal{N}g_0^2 + \gamma_-^2|, \tag{2.33}$$

$$2I_0^2 = (\mathcal{N}g_0^2 + \gamma_-^2) + |\mathcal{N}g_0^2 + \gamma_-^2|. \tag{2.34}$$

As seen from Eqs. 2.33 and 2.34 for the resonant atom-cavity system, R_0 is zero when $\mathcal{N}g_0^2 > -\gamma_-^2$ and I_0 is zero when $\mathcal{N}g_0^2 < -\gamma_-^2$. We shall term an atom-cavity system operating in these two regimes as *over-damped* and *under-damped*, respectively. For the special case $\mathcal{N} = -1$, discussed in what follows, these conditions become

$$g_0^2 < \gamma_-^2, \qquad \text{over-damped;} \tag{2.35}$$

$$g_0^2 > \gamma_-^2, \qquad \text{under-damped.} \tag{2.36}$$

For an over-damped system, the decay rates will differ but the normal mode frequencies are degenerate. For an under-damped system, however, the reverse is true.

Both R and I of Eqs. 2.28 and 2.29 are real quantities and, in taking the square root in Eqs. 2.30 and 2.31, the proper sign must be chosen. Our convention is as follows: for $\mathcal{N}g_0^2 > -\gamma_-^2$, the sign of I is $\gamma_-/|\gamma_-|$ and the sign of R is $\omega_-/|\omega_-|$; for $\mathcal{N}g_0^2 < -\gamma_-^2$, the sign of R is positive and the sign of I is $-\omega_-\gamma_-/|\omega_-\gamma_-|$. In both cases, if ω_- or γ_- are zero, the plus sign should be chosen. With this convention the $\mathcal{L}_+$ factor is associated with the cavity and the $\mathcal{L}_-$ factor is associated with the atom in the weak coupling limit. Note that $\Omega_\pm$ are the frequencies of the normal modes whose decay rates are $\Gamma_\pm$. In the strong coupling limit Ω_+ is the higher frequency and Ω_- the lower frequency normal mode. If we let $\gamma_c, \gamma_p \to 0$, then $\Omega_\pm \to \Omega_\pm^0$, the eigenfrequencies given in Eq. 2.1, as is easily verified.

The general solutions for the dipole and the field may be written in complex form:

$$p(t) = p_0^+ e^{i\lambda_+ t} + p_0^- e^{i\lambda_- t}, \tag{2.37}$$

$$E_c(t) = E_0^+ e^{i\lambda_+ t} + E_0^- e^{i\lambda_- t}, \tag{2.38}$$

where $p_0^\pm$ and $E_0^\pm$ are complex constants to be determined by the initial conditions. Invoking Eqs. 2.22 and 2.23 for each normal mode, the following additional relations must hold between the complex constants:

$$\mathcal{L}_p(\lambda_+)p_0^+ = -\frac{i\mu^2\mathcal{N}}{\hbar}E_0^+, \qquad \mathcal{L}_c(\lambda_+)E_0^+ = \frac{2\pi i\omega}{V}p_0^+, \tag{2.39}$$

$$\mathcal{L}_p(\lambda_-)p_0^- = -\frac{i\mu^2\mathcal{N}}{\hbar}E_0^-, \qquad \mathcal{L}_c(\lambda_-)E_0^- = \frac{2\pi i\omega}{V}p_0^-, \tag{2.40}$$

We consider two types of initial conditions: the system begins with all the energy either in the dipole (which we denote with the superscript $\epsilon = p$) or in the cavity field (which we denote with the superscript $\epsilon = c$). In Sec. 2.2.3, it will be seen that these conditions correspond to the driven-atom case ($\epsilon = p$) and the driven-cavity case ($\epsilon = c$), respectively, of the scattering arrangement. In general, the evolution of the decaying atom-cavity system depends in detail on the specific initial values of the dipole and its time derivative as well as the field and its time derivative. To order g_0/ω_p and $\gamma_c, \gamma_p/\omega_p$, however, the emission properties depend only on the initial distribution of energy between the two oscillators, and not on the particular distribution of energy within a given oscillator (i.e., the distribution of energy between kinetic and potential energy of the atomic dipole or the distribution of energy between the electric and magnetic fields of the cavity). This can be understood by observing that energy is rapidly exchanged from kinetic to potential in the atom and from electric to magnetic in the cavity field (at a rate of order $\omega \gg \gamma_c, \gamma_p, g_0$), whereas it is transferred between oscillators much more slowly (at a rate of order g_0) and to the surroundings (at a rate of order γ_c, γ_p). Therefore, to simplify the algebra, we choose the following convenient initial values, expressed in complex form:

1. *Dipole initially excited* ($\epsilon = p$):

$$p^{\epsilon=p}(t=0) = P_0, \qquad E_c^{\epsilon=p}(t=0) = 0, \tag{2.41}$$

where P_0 is a real quantity. The solutions corresponding to these initial conditions may be written

$$p^{\epsilon=p}(t) = \frac{P_0}{i(\lambda_- - \lambda_+)}\{\mathcal{L}_c(\lambda_+)e^{i\lambda_+ t} - \mathcal{L}_c(\lambda_-)e^{i\lambda_- t}\}, \tag{2.42}$$

and

$$E_c^{\epsilon=p}(t) = \frac{(2\pi i\omega/V)P_0}{i(\lambda_- - \lambda_+)}\{e^{i\lambda_- t} - e^{i\lambda_+ t}\}. \tag{2.43}$$

The corresponding conditions for the cavity field are:

2. *Cavity field initially excited* ($\epsilon = c$):

$$p^{\epsilon=c}(t=0) = 0, \qquad E_c^{\epsilon=c}(t=0) = E_0, \tag{2.44}$$

where E_0 is now a real quantity, with solutions:

$$p^{\epsilon=c}(t) = \frac{(i\mu^2\mathcal{N}/\hbar)E_0}{i(\lambda_- - \lambda_+)}\{e^{i\lambda_- t} - e^{i\lambda_+ t}\}, \tag{2.45}$$

and

$$E_c^{\epsilon=c}(t) = \frac{E_0}{i(\lambda_- - \lambda_+)}\{\mathcal{L}_p(\lambda_+)e^{i\lambda_+ t} - \mathcal{L}_p(\lambda_-)e^{i\lambda_- t}\} \tag{2.46}$$

With the forgoing solutions, note that for the case $\epsilon = p$ the initial conditions of Eq. 2.41 imply that $\dot{E}_c(t=0) = Re[\dot{E}_c(t=0)] = 0$. Similarly, for the case $\epsilon = c$, the initial conditions of Eq. 2.44 imply $\dot{p}(t=0) = 0$. Thus we initially have all of the energy in the appropriate oscillator, as required.

The power emitted out the sides of the resonator is proportional to the square of the atomic dipole moment and the power emitted out the cavity ends is proportional to the square of the cavity electric field. In particular, the instantaneous power emitted out the sides of the resonator is obtained by applying Larmor's formula to

the dipole emitter:

$$P_{side}(t) = \frac{2\ddot{\mathbf{p}}(t)^2}{3c^3}(1-f) \approx \frac{2\omega^4 \mathbf{p}(t)^2}{3c^3}(1-f), \tag{2.47}$$

with f defined in the introduction of this chapter. The instantaneous power out the cavity ends is given by:

$$P_{ends}(t) = \eta_{cav} 2\gamma_c \frac{\mathsf{E_c}(t)^2 V}{4\pi}, \tag{2.48}$$

with $\eta_{cav} = \frac{T}{1-R}$ the output coupling factor (throughput) for a cavity with mirror transmission T and reflectivity R ($1 - R = T + A_L$, with A_L the mirror loss), and $\mathbf{p}(t)$ and $\mathsf{E}_c(t)$ the real parts of the preceding solutions for the case of interest. Note that the field mode is normalized such that $\int E^2 dV = E_c^2 V$.

The power spectra, which provide information about the frequency content of the decaying oscillators, are proportional to the complex conjugate squares of the Fourier transforms of Eqs. 2.42, 2.43 and Eqs. 2.45, 2.46. We define the Fourier transform of the complex function, $F(t)$, as

$$\mathcal{F}(\Omega) = \int_{-\infty}^{\infty} \frac{dt}{\sqrt{2\pi}} F(t) e^{-i\Omega t}, \tag{2.49}$$

and neglect the anti-resonant terms to obtain for the $\epsilon = p$ case,

$$\mathrm{p}^{\epsilon=p}(\Omega) = \frac{P_0}{2\sqrt{2\pi}} \left(\frac{\mathcal{L}_c(\Omega)}{\mathcal{L}_+(\Omega)\mathcal{L}_-(\Omega)} \right), \tag{2.50}$$

$$\mathcal{E}_c^{\epsilon=p}(\Omega) = -\frac{i2\pi\omega}{2\sqrt{2\pi V}} P_0 \left(\frac{1}{\mathcal{L}_+(\Omega)\mathcal{L}_-(\Omega)} \right), \tag{2.51}$$

where now the Lorentzian factors are functions of the Fourier transform variable Ω. In Eq. 2.50 we have used the identity

$$\mathcal{L}_c(\Omega) = \frac{\mathcal{L}_c(\lambda_+)\mathcal{L}_-(\Omega) - \mathcal{L}_c(\lambda_-)\mathcal{L}_+(\Omega)}{i(\lambda_- - \lambda_+)}. \tag{2.52}$$

Similarly, the Fourier transforms of Eqs. 2.45 and 2.46, neglecting the anti-resonant

terms, are:

$$p^{\epsilon=c}(\Omega) = \frac{i\mu^2\mathcal{N}}{2\sqrt{2\pi}\hbar}E_0\left(\frac{1}{\mathcal{L}_+(\Omega)\mathcal{L}_-(\Omega)}\right), \tag{2.53}$$

$$\mathcal{E}_c^{\epsilon=c}(\Omega) = \frac{E_0}{2\sqrt{2\pi}}\left(\frac{\mathcal{L}_p(\Omega)}{\mathcal{L}_+(\Omega)\mathcal{L}_-(\Omega)}\right). \tag{2.54}$$

In Eq. 2.54 we have used the identity

$$\mathcal{L}_p(\Omega) = \frac{\mathcal{L}_p(\lambda_+)\mathcal{L}_-(\Omega) - \mathcal{L}_p(\lambda_-)\mathcal{L}_+(\Omega)}{i(\lambda_- - \lambda_+)}. \tag{2.55}$$

2.2.2 Emission Analysis and the Photon Rate Equation

The transient solutions of the preceding section can be used to obtain expressions for the power emitted under steady state incoherent excitation of the atom-cavity system. Consider such a system in which initially excited atomic dipoles, P_0, are supplied at some constant rate, Λ (atoms/sec). An individual, excited atomic dipole interacts with the cavity and evolves according to Eq. 2.42. Averaged over a succession of incoming dipoles with random phases, the net effect is steady state atom-cavity emission, which may be studied in the frequency domain. Note that in this section, the average background inversion, $\mathcal{N}_0$, may take on values between ± 1. To calculate this *emission spectrum*, we first note that the total power emitted out the side of the resonator is determined with Larmor's formula and the supply rate:

$$P_{side} = (1-f)\Lambda\frac{2\omega^4}{3c^3}\int dt \left\langle [\mathbf{p}^{\epsilon=p}(t)]^2 \right\rangle_{ave}, \tag{2.56}$$

where the time average, denoted by $<>_{ave}$ in Eq. 2.56 is over an optical cycle. Using Parseval's theorem and the fact that $< \mathbf{p}(t)^2 >_{ave} = |p(t)|^2/2$, we get

$$P_{side} = (1-f)\Lambda\frac{\omega^4}{3c^3}\int d\Omega |p^{\epsilon=p}(\Omega)|^2. \tag{2.57}$$

Thus, we obtain for the *spontaneous emission power spectrum* out the resonator side,

$$\mathcal{P}_{side}(\Omega) = \Lambda\frac{P_0^2\omega^4}{24\pi c^3}\left|\frac{\mathcal{L}_c(\Omega)}{\mathcal{L}_+(\Omega)\mathcal{L}_-(\Omega)}\right|^2 (1-f). \tag{2.58}$$

Similarly, the total power emitted out both ends of the cavity is simply the total steady state energy maintained inside the cavity, multiplied by the cavity decay rate, $2\gamma_c$:

$$P_{ends} = \eta_{cav}\Lambda 2\gamma_c \frac{V}{4\pi}\int dt \left\langle [\mathsf{E_c}^{\epsilon=p}(t)]^2 \right\rangle_{ave}. \tag{2.59}$$

Therefore we obtain:

$$P_{ends} = \eta_{cav}\Lambda \frac{\gamma_c V}{4\pi}\int d\Omega |\mathcal{E}^{\epsilon=p}(\Omega)|^2, \tag{2.60}$$

from which the *cavity emission spectrum* is:

$$\mathcal{P}_{ends}(\Omega) = \eta_{cav}\Lambda \frac{P_0^2}{4\mu^2}\hbar\omega \frac{\sigma_0 c}{V}\frac{\gamma_p\gamma_c}{4\pi}\left|\frac{1}{\mathcal{L}_+(\Omega)\mathcal{L}_-(\Omega)}\right|^2. \tag{2.61}$$

The above arguments have been applied to the $\epsilon = p$ case of initially excited dipoles. However, one could exploit the symmetry of this system and consider incoherently exciting the cavity mode (e.g. with thermal photons) at some rate Λ. The above arguments would then apply to the $\epsilon = c$ case.

The resulting emission spectra all contain the product of two Lorentzians with factors $|\mathcal{L}_\pm(\Omega)|^2$, which characterize the two normal modes of the system. For the initially-excited-atom case ($\epsilon = p$) these two Lorentzians in the power spectrum out the side are multiplied by the empty cavity lineshape factor, $|\mathcal{L}_c(\Omega)|^2$. Similarly, for the initially-excited-cavity case ($\epsilon = c$) the two Lorentzians in the power out the end are multiplied by the free-space atomic lineshape factor, $|\mathcal{L}_p(\Omega)|^2$. These additional lineshape factors are discussed below in Sec. 2.3.2.

We may now obtain a rate equation governing the average number of photons in the resonator mode due to emission. Consider the atom-cavity system discussed above, in which atoms are excited into the upper state via incoherent pumping at a rate Λ. First, if no resonator is present (free-space) we can relate the initial supply rate, Λ, and P_0 to N_u^0 using the correspondence principle for the excited state population,

$$P_{side} = N_u \hbar\omega 2\gamma_p, \tag{2.62}$$

to obtain the steady state power emitted with no cavity field:

$$P^0_{side} = \Lambda \frac{\omega^4}{3c^3} \int d\Omega |p^{\epsilon=p}_{hom}(\Omega)|^2 (1-f) = N^0_u \hbar\omega 2\gamma_p, \tag{2.63}$$

where $p^{\epsilon=p}_{hom}(\Omega)$ is the Fourier transform of the homogeneous solution to the dipole equation, Eq. 2.12, given by:

$$p^{\epsilon=p}_{hom}(\Omega) = \frac{1}{2\sqrt{2\pi}} \frac{P_0}{\mathcal{L}_p(\Omega)}, \tag{2.64}$$

which gives

$$N^0_u = \frac{\Lambda}{8\gamma_p} \left(\frac{P_0}{2\mu}\right)^2. \tag{2.65}$$

We evaluate the integral in Eq. 2.57 by the method of residues, use Eq. 2.62 and substitute Eq. 2.65 to obtain the excited state population in the cavity:

$$N_u = N^0_u \left[1 + \left(\frac{\gamma_c}{\gamma_p + \gamma_p}\right) \frac{G'}{1-G'}\right], \tag{2.66}$$

where

$$G' \equiv \mathcal{N} \frac{\sigma c}{2\gamma_c V}, \tag{2.67}$$

and

$$\sigma \equiv \frac{\sigma_0}{1 + \left(\frac{\omega_c - \omega_p}{\gamma_p + \gamma_c}\right)^2}, \tag{2.68}$$

with the peak atomic absorption cross section, σ_0, defined in Eq. 2.6.

Using Eq. 2.65 and evaluating the integral in Eq. 2.60, the total power emitted out the resonator ends may then be written as

$$P_{ends} = \eta_{cav} N^0_u \hbar\omega 2\gamma_p \left(\frac{\sigma c}{2\gamma_c V}\right) \left(\frac{\gamma_c}{\gamma_c + \gamma_p}\right) \frac{1}{1-G'}, \tag{2.69}$$

or, substituting Eq. 2.66 and writing Eq. 2.69 in the form of a steady state rate equation for the number of photons in the resonator mode via a correspondence

principle for ν analogous to Eq. 2.62,

$$P_{ends} = \eta_{cav} N_u \hbar\omega 2\gamma_p \left(\frac{\sigma c}{2\gamma_c V}\right)\left(\frac{\gamma_c}{\gamma_c+\gamma_p}\right)\frac{1}{1-G'} = \eta_{cav}\nu\hbar\omega 2\gamma_c, \tag{2.70}$$

with G the single-atom gain, given by

$$G = G'\left(\frac{\gamma_p}{\gamma_p+\gamma_c}\right) = \mathcal{N}\frac{\sigma c}{2\gamma_c V}\frac{\gamma_p}{\gamma_p+\gamma_c}. \tag{2.71}$$

Rearranging, we obtain the photon rate equation (cf. Eq. 2.9):

$$\dot{\nu} = 0 = \underbrace{N_u\left(\frac{\sigma' c}{V}\right)}_{\substack{\text{spontaneous}\\ \text{emission}}} + \underbrace{(N_u - N_l)\left(\frac{\sigma' c}{V}\right)\nu}_{\substack{\text{stimulated emission}\\ \text{and absorption}}} - \underbrace{2\gamma_c\nu}_{\substack{\text{resonator}\\ \text{loss}}}, \tag{2.72}$$

where

$$\sigma' \equiv \sigma\frac{\gamma_p}{\gamma_p+\gamma_c}. \tag{2.73}$$

The physical features of these equations are discussed in Sec. 2.3.3, below.

Note that as a check for our model, it is straightforward to verify conservation of energy, i.e., that the rate of energy loss out the ends and side equals the total energy supply rate. Assuming $\eta_{cav} = 1$ and using Eqs. 2.66 and 2.69, we obtain after some algebra

$$P^0_{side} = N^0_u \hbar\omega 2\gamma_p = P_{ends} + P_{side}. \tag{2.74}$$

The results of this section can also be derived in the elastic scattering analysis of the next section, with the assumption of broadband excitation. We consider this situation in Appendix B, and discuss an atom-cavity experiment in which atomic excitation with a broadband light source is used to study emission.

2.2.3 Elastic Scattering Analysis

We now turn to a description of scattering. The atom is considered to be in the ground state ($\mathcal{N}_0 = -1$), and we provide for an external laser field to excite the atom

or cavity mode. Driving terms are then added to the right hand side of the coupled Maxwell-Schrödinger equations:

$$\ddot{\mathbf{p}} + 2\gamma_p\dot{\mathbf{p}} + \omega_p^2\mathbf{p} = -\frac{2\mu^2\omega_p}{\hbar}\mathcal{N}(\mathsf{E_c} + \delta_{\epsilon p}\mathsf{E}_L^p), \tag{2.75}$$

$$\ddot{\mathsf{E}}_\mathsf{c} + 2\gamma_c\dot{\mathsf{E}}_\mathsf{c} + \omega_c^2\mathsf{E}_\mathsf{c} = \frac{4\pi\omega_p^2}{V}\mathbf{p} + \delta_{\epsilon c}\beta\mathsf{E}_L^c, \tag{2.76}$$

$$\dot{\mathcal{N}} + 2\gamma_p(\mathcal{N} - \mathcal{N}_0) = \frac{2(\dot{\mathbf{p}} + \gamma_p\mathbf{p})(\mathsf{E_c} + \delta_{\epsilon p}\mathsf{E}_L^p)}{\hbar\omega_p}, \tag{2.77}$$

with $\mathsf{E}_L^{c,p}$ the applied monochromatic excitation field at frequency Ω for the driven cavity, atom cases, respectively. As we restrict ourselves to weak excitation (elastic scattering), $\mathsf{E_c}$ and $\mathbf{p}$ will also be monochromatic at the same frequency. In a manner analogous to the normal mode analysis, the Kroenicker delta functions, $\delta_{\epsilon p}$ and $\delta_{\epsilon c}$ are introduced for convenience in choosing either the atom ($\epsilon = p$) or the cavity mode ($\epsilon = c$) to be driven by the excitation field, (Fig. 1-2(b)). The quantity α describes the coupling of E_L^c into the resonator field mode and is calculated in Appendix A to be

$$\alpha^2 = 8\Omega^2\eta_{cav}\left(\frac{c}{2L}\right)\gamma_c. \tag{2.78}$$

As was done in the previous section, the population equation may be rewritten as the rate of energy flow into the upper state of the atom:

$$\hbar\omega_p\dot{N}_u = [\delta_{\epsilon p}(\dot{\mathbf{p}} + \gamma_p\mathbf{p})\mathsf{E}_L^p] - [\hbar\omega_p N_u \cdot 2\gamma_p - (\dot{\mathbf{p}} + \gamma_p\mathbf{p})\mathsf{E_c}]. \tag{2.79}$$

This equation is similar to Eq. 2.17, with $N_u^0 = 0$ and an additional term appearing in the first brackets which describes the excitation of the atomic dipole when E_L^p is coupled to the atom $\epsilon = p$. All other terms have the same interpretations given in the normal mode analysis section. However, note that in the case of E_L^c coupled to the cavity $\epsilon = c$, the second term in the second brackets includes the component of the excitation field coupled into the cavity, as well as the field radiated by the atomic dipole (Eq. 2.84, below).

We consider a monochromatic excitation field in the form $\mathsf{E}_L^{c,p} = Re[E_L^{c,p}e^{i\Omega t}]$,

and write Eqs. 2.75, 2.76, and 2.77 in the slowly-varying envelope approximation, in which $\mathbf{p} = Re[pe^{i\Omega t}]$, $\mathsf{E_c} = Re[E_c e^{i\Omega t}]$, with E_c and p slowly varying amplitudes, and neglect non-resonant contributions. This gives

$$\dot{p} - \mathcal{L}_p(\Omega)p = \frac{i\mu^2}{\hbar}\mathcal{N}(E_c + \delta_{\epsilon p}E_L^p), \tag{2.80}$$

$$\dot{E}_c - \mathcal{L}_c(\Omega)E_c = -\frac{2\pi i\omega_p}{V}p + \delta_{\epsilon c}\left(\frac{\alpha}{2i\Omega}\right)E_L^c, \tag{2.81}$$

$$\dot{\mathcal{N}} + 2\gamma_p(\mathcal{N} - \mathcal{N}_0) = -\frac{Im[p(E_c + \delta_{\epsilon p}E_L^p)^*]}{\hbar}, \tag{2.82}$$

where $\mathcal{L}_{c,p}(\Omega)$ is defined in Eq. 2.24. Note that the right hand side of Eq. 2.82 is the time average of the right hand side of Eq. 2.77 after the slowly varying envelope approximation has been made. For the scattering configurations described in this chapter, $E_L^{c,p}$ is a weak coherent source. So long as the cavity and excitation fields are small, the atomic level populations will not change appreciably from their background values, $\mathcal{N} \approx \mathcal{N}_0 = -1$.

Setting the time varying terms in Eqs. 2.80, 2.81, and 2.82 equal to zero, we can solve for the steady state value of E_c as a function of the exciting laser frequency, Ω. Solving Eq. 2.80 for p and substituting into Eq. 2.81, we get

$$E_c^{\epsilon=p,c}(\Omega) = \delta_{\epsilon p}\frac{\mathcal{N}g_0^2E_L^p}{\mathcal{L}_c(\Omega)\mathcal{L}_p(\Omega) - \mathcal{N}g_0^2} - \delta_{\epsilon c}\frac{(\alpha/2i\Omega)\mathcal{L}_p(\Omega)E_L^c}{\mathcal{L}_c(\Omega)\mathcal{L}_p(\Omega) - \mathcal{N}g_0^2}, \tag{2.83}$$

and

$$p^{\epsilon=p,c}(\Omega) = -\frac{\mathcal{N}(i\mu^2/\hbar)E_L^{c,p}}{\mathcal{L}_c(\Omega)\mathcal{L}_p(\Omega) - \mathcal{N}g_0^2}[\delta_{\epsilon p}\mathcal{L}_c(\Omega) - \delta_{\epsilon c}(\alpha/2i\Omega)]. \tag{2.84}$$

We may relate the scattered power out the resonator ends to the cavity field at the atom as follows:

$$P_{ends}^{\epsilon=p,c}(\Omega) = \eta_{cav}(2\gamma_c)\frac{|E_c^{\epsilon=p,c}(\Omega)|^2V}{8\pi}. \tag{2.85}$$

Substituting the expressions from Eq. 2.83, $E_c^{\epsilon=p,c}(\Omega)$ into Eq. 2.85, after some rear-

rangement we obtain the power scattered out the ends for the driven-atom case:

$$P_{ends}^{\epsilon=p}(\Omega) = \eta_{cav}\frac{I_L}{I_s}\hbar\omega\gamma_p^2\gamma_c\frac{g_0^2}{|\mathcal{L}_+(\Omega)\mathcal{L}_-(\Omega)|^2}, \tag{2.86}$$

with $I_L = cE_L^2/8\pi$ the intensity of the excitation field and I_s the saturation intensity, defined by $\sigma_0 I_s/\hbar\omega = \gamma_p$. Again, $\mathcal{L}_\pm(\Omega)$ are defined in Eq. 2.26. For the driven-cavity case, the power transmitted through the output mirror at frequency Ω is

$$P_{end}^{\epsilon=c}(\Omega) = \eta_{cav}^2 I_L a\frac{\gamma_c^2|\mathcal{L}_p(\Omega)|^2}{|\mathcal{L}_+(\Omega)\mathcal{L}_-(\Omega)|^2}, \tag{2.87}$$

with $a = V/L$. Note that Eqs. 2.86 and 2.87 exhibit a dependence on exciting laser frequency equivalent to the dependence of the corresponding emission spectra (Eq. 2.61 and the complex conjugate square of Eq. 2.54, respectively) on emission frequency.

According to the discussion following Eq. 2.79, the total power scattered out the sides of the resonator for both cases ($\epsilon = p, c$) should be given by $\hbar\omega_p N_u \cdot 2\gamma_p$. We may solve Eq. 2.82 in the steady state for $\mathcal{N}$ using Eq. 2.84 to lowest order in I_L/I_s to obtain

$$\mathcal{N}(\Omega) = \frac{\mathcal{N}_0}{1+\frac{1}{2}\left|\frac{p(\Omega)}{\mu\mathcal{N}}\right|^2} \approx \left(1-\frac{1}{2}\left|\frac{p(\Omega)}{\mu}\right|^2\right), \tag{2.88}$$

which may be written in terms of N_u as ($\mathcal{N}_0 \approx -1$)

$$N_u(\Omega) \approx \left|\frac{p(\Omega)}{2\mu}\right|^2, \tag{2.89}$$

with the dipole, $p(\Omega)$, given by the appropriate choice in Eq. 2.84 (we have suppressed the superscript $\epsilon = p, c$ for convenience). Multiplying Eq. 2.89 by $\hbar\omega 2\gamma_p$ and noting that

$$\hbar\omega 2\gamma_p\left|\frac{p(\Omega)}{2\mu}\right|^2 = \frac{\omega^4}{3c^3}|p(\Omega)|^2(1-f), \tag{2.90}$$

we may write the total power scattered out the side of the resonator in the form:

$$N_u^{\epsilon=p,c}(\Omega)\hbar\omega_p 2\gamma_p = P_{side}^{\epsilon=p,c}(\Omega), \tag{2.91}$$

where

$$P_{side}^{\epsilon=p,c}(\Omega) = \frac{\omega_p^4}{3c^3}|p^{\epsilon=p,c}(\Omega)|^2(1-f). \tag{2.92}$$

Note, however, that N_u cannot be measured directly in a scattering experiment without destroying the phase coherence of the excitation-scattering process.

Equation 2.92 has an interesting interpretation if we calculate the scattering out the side using Larmor's formula for a single dipole radiator. Since p in Eq. 2.80 is the total dipole moment of a single atom, we write

$$P_{side}^{\epsilon=p,c} = \frac{2\omega_p^4 < \mathbf{p}^2 >_{ave}}{3c^3}(1-f), \tag{2.93}$$

where the brackets again indicate time averaging. Using

$$< \mathbf{p}^2 >_{ave} = \frac{1}{2}|p^{\epsilon=p,c}(\Omega)|^2, \tag{2.94}$$

Eq. 2.93 is easily seen to be identical to Eq. 2.92.

For the driven-atom case, Eq. 2.92 becomes

$$P_{side}^{\epsilon=p}(\Omega) = \frac{I_L}{I_s}(\hbar\omega_p\gamma_p^2)\frac{\gamma_p|\mathcal{L}_c(\Omega)|^2}{|\mathcal{L}_+(\Omega)\mathcal{L}_-(\Omega)|^2}, \tag{2.95}$$

and for the driven-cavity case,

$$P_{side}^{\epsilon=c}(\Omega) = \eta_{cav}\frac{I_L}{I_s}(\hbar\omega_p\gamma_p^2)\frac{\gamma_p(\alpha/2\Omega)^2}{|\mathcal{L}_+(\Omega)\mathcal{L}_-(\Omega)|^2}. \tag{2.96}$$

Again, note the similarity in frequency dependence to the corresponding emission spectra of the previous section. Similarly for N_u we use

$$\left|\frac{\mu E_L}{\hbar}\right|^2 = \frac{\sigma_0 I_L}{\hbar\omega_p}2\gamma_p = 2\frac{I_L}{I_s}\gamma_p^2, \tag{2.97}$$

together with Eq. 2.89, 2.83, and 2.84 to obtain for the driven atom case,

$$N_u^{\epsilon=p}(\Omega) \approx \frac{I_L}{4I_s}\frac{\gamma_p^2|\mathcal{L}_c(\Omega)|^2}{|\mathcal{L}_+(\Omega)\mathcal{L}_-(\Omega)|^2}, \tag{2.98}$$

and for the driven-cavity case,

$$N_u^{\epsilon=c}(\Omega) \approx \frac{I_L}{4I_s} \frac{\gamma_p^2(\alpha/2\Omega)^2}{|\mathcal{L}_+(\Omega)\mathcal{L}_-(\Omega)|^2}. \tag{2.99}$$

The quantities $\Omega_\pm$ and $\Gamma_\pm$ contained in $\mathcal{L}_+(\Omega)$ take on different forms depending on the strength of the coupling (as discussed in Sec. 2.2.1). In the absence of an atom coupled to the cavity, Eq. 2.87 reduces to the empty cavity transmission function (proportional to $|\mathcal{L}_c(\Omega)|^{-2}$ because $\mathcal{L}_+(\Omega) = \mathcal{L}_c(\Omega)$ and $\mathcal{L}_-(\Omega) = \mathcal{L}_p(\Omega)$, see Sec. 2.3.2) and, of course, no scattered radiation is seen out the side (Eq. 2.92). The presence of the atom modifies the spectral lineshape. For the driven-atom case, the power out the end, Eq. 2.86, also depends on the presence of an atom in the cavity because the light is indirectly coupled into the cavity via the atom illuminated by the side excitation field.

As mentioned above, by comparing these scattering results with the results for emission with $\mathcal{N}_0 = -1$, we find that the complex conjugate squares of Eqs. 2.50 and 2.51 have the same dependence on frequency as the corresponding expressions derived here for the driven-atom case (Eqs. 2.95 and 2.86, respectively), and that the complex conjugate squares of Eqs. 2.53 and 2.54 are identical in frequency dependence to Eqs. 2.96 and 2.87 for the driven-cavity case. Recall, however, the different interpretations of Ω. In Sec. 2.2.2, Ω is a frequency component of the emission spectrum, whereas in this section it is the frequency of scattering (equal to the excitation laser frequency). We have thus shown that the lineshapes of the emission spectra and corresponding excitation spectra are identical. As seen in the next section, when the gain is small and the atom is uninverted, the emission is purely spontaneous, and the emission rate is identical to the linewidth of the emission spectrum in the broad cavity, weak coupling limit. Therefore, in this case the linewidth of the excitation spectrum is also equal to the emission rate. This provides the basis for interpreting the excitation spectral linewidths as spontaneous emission rates, as has been done in some experiments.

2.3 Results and Discussion

In Sec. 2.3.1 the results of the normal mode analysis are studied to obtain the transient response (decay rates, normal mode ringing, etc.) of the atom-cavity system with one atom coupled to the cavity mode. In Sec. 2.3.2 the results of the scattering and emission sections are used to study the lineshapes of the excitation spectra (or, equivalently, the spontaneous emission spectra) for the different coupling regimes in both narrow and broad cavity limits. Finally, in Sec. 2.3.3 the photon rate equation and emission results derived in Sec. 2.2.2 are studied in various regimes of interest. One such regime includes the situation in which the lower level of the two-level atom can also decay and $\mathcal{N}$ can take on positive, as well as negative, values.

Before discussing the results of Sec. 2.2, it is perhaps worthwhile to review how scattering relates to emission in an atom-cavity system. The scattering analysis developed above provides the excitation spectrum, i.e., the total power coherently scattered as a function of the excitation frequency. The monochromatic excitation field induces an atomic dipole moment whose radiated field coherently interferes with the excitation field. So long as the excitation intensity is small compared to the saturation intensity, the scattered photons are monochromatic at the excitation frequency. In this case Eqs. 2.86 and 2.96 reflect the normal mode structure of the atom-cavity system in its ground state ($\mathcal{N}_0 = -1$). The correspondence between scattering and absorption should be noted. Every photon of the excitation field that is absorbed by the atom-cavity system is radiated as scattered light. Thus, energy conservation (optical theorem, [60]) requires that the total scattered power equals the power absorbed from the excitation field. The resulting excitation spectrum is thus equivalent to the absorption spectrum.

Equivalently, we can study the emission spectrum of an atom-cavity system in which the atom, averaged over many events, has a background excited state population. By the principle of detailed balance [61] both the scattering arrangement, which gives absorption, and the emission arrangement must provide the same spectral information about the normal mode structure. The emission rate in each frequency

interval must be the same as the absorption rate in that same frequency interval. Furthermore, we can identify the two terms in the absorption cross section, proportional to $P_{side}(\Omega)$ and $P_{ends}(\Omega)$, as corresponding to the *spontaneous emission* to the side (free space) and the total emission out the ends of the resonator mode, respectively. This explains how one can extract spontaneous emission information from the scattering analysis, as is done below. In particular, with $\mathcal{N} \approx \mathcal{N}_0 = -1$ and negligible gain, only spontaneous emission occurs, and the emission rate is just the spontaneous emission rate. In the broad cavity limit with weak coupling we can interpret the linewidth of the excitation spectrum out the end as a measure of the enhanced spontaneous emission rate, even though we do not monitor emission rates at all. We note that in a scattering experiment one cannot measure the excited state population without disrupting the coherent interaction, because to do so would violate the energy-time uncertainty relation. Hence, it is not possible to directly explore per-atom emission rates in coherent scattering. Nevertheless, we do obtain equivalent information about emission rates from the linewidth measurements. However, when incoherent excitation is used the coherence is destroyed and it is possible to measure the average occupation probability of the excited state without significantly perturbing the light-atom interaction process. This explains the relationship of the steady state emission experiment for the special case with $\mathcal{N} = -1$ to the scattering experiment, and the reason why the same spectral lineshape is obtained in each. Note that it is also possible to destroy the coherence via broadband excitation.

As discussed in the introduction, a resonant ($\omega_- = 0$) atom-cavity system without damping always exhibits two distinct normal mode frequencies unless the inversion is positive. We assume a system with negative steady state inversion. (The case of positive steady state inversion shall be considered in Sec. 2.3.3.) In the time domain, energy would forever oscillate between the atom and the cavity field at the normal mode frequency difference and, in the frequency domain, all spectra would exhibit two distinct delta functions at the normal mode frequencies. A resonant, system without damping is thus always strongly coupled. With damping, however, three possible regimes arise within which the resonant, atom-cavity system acquires

distinct characteristics:

$$g_0^2 \ll \gamma_-^2 \qquad \text{weak coupling,} \tag{2.100}$$

$$\left.\begin{array}{ll} (1) & g_0^2 \leq \gamma_-^2 \\ (2) & \gamma_-^2 < g_0^2 < \frac{\gamma_c^2+\gamma_p^2}{2} \end{array}\right\} \qquad \text{intermediate coupling,} \tag{2.101}$$

$$g_0^2 \gg \frac{\gamma_c^2+\gamma_p^2}{2} \qquad \text{strong coupling.} \tag{2.102}$$

Note that the over-damped system (with $\Omega_+ = \Omega_-$ and $\Gamma_+ \neq \Gamma_-$), Eq. 2.35, is divided into two regimes; the weak coupling regime and case (1) of the intermediate coupling regime. Similarly, the under-damped system (with $\Omega_+ \neq \Omega_-$ and $\Gamma_+ = \Gamma_-$), Eq. 2.36, is divided into two regimes; case (2) of the intermediate coupling regime and the strong coupling regime. In the weak coupling regime the system undergoes decay with no ringing and the emission (or scattering) lineshapes of both oscillators are single-peaked. In the strong coupling regime, on the other hand, the system exhibits two distinct normal mode frequencies and ringing is observable in the oscillators despite the presence of damping. In this case the emission (or scattering) lineshapes of both oscillators exhibit two peaks. In the intermediate coupling regime, however, the interplay between coupling and damping gives rise to subtle atom-cavity behavior. When the coupling is slightly less than $|\gamma_-|$, case (1), the normal mode frequencies are degenerate and the oscillators decay with no ringing, but the frequency domain emission or excitation lineshape may nonetheless exhibit two peaks. When the coupling is slightly greater than $|\gamma_-|$, case (2), the degeneracy of the normal mode frequencies is lifted; nevertheless, lineshapes may exhibit only one peak. In fact, in the intermediate coupling regime, lineshape features will depend on which oscillator is excited and which oscillator is observed. Therefore, there is no simple correlation between ringing in the time domain and a two peak structure in the frequency domain. The choice of the boundary between the intermediate and strong coupling regimes will be made clear in the discussions of the strong coupling regime in Secs. 2.3.1 and 2.3.2.

2.3.1 Transient Response: Free Induction Decay

Turning to the results of the time domain study of Sec. 2.2.1, we consider the atom to be in the absorbing state ($\mathcal{N} \approx \mathcal{N}_0 = -1$) and analyze the effects of coupling in the time dependent behavior of each oscillator in the weak, intermediate and strong coupling regimes in parts (1), (2), and (3) of this section, respectively. The weak coupling regime gives rise to pure decay and the strong coupling regime exhibits ringing in the emitted power.

1. Weak Coupling

First consider the weak coupling regime, $g_0^2 \ll \gamma_-^2$. Neglecting terms of order $(g_0/\gamma_-)^2$ and higher in Eqs. 2.28 and 2.29, we get:

$$\begin{aligned} \mathcal{L}_c(\lambda_+) &\approx 0, \\ \mathcal{L}_c(\lambda_-) &\approx -(\gamma_c - \gamma_p), \end{aligned} \tag{2.103}$$

where, in the second equation we have neglected ω_- by assuming that $|\omega_-| < |\gamma_-|$.

a. Broad Cavity Limit. In the broad cavity limit ($\gamma_c \gg \gamma_p$), $\epsilon = p$ case, we may substitute Eqs. 2.103 into the solutions for the atom and cavity field, Eqs. 2.42 and 2.43, to get

$$\begin{aligned} \mathbf{p}^{\epsilon=p}(t) &\approx P_0 e^{-\Gamma_- t} cos\Omega_- t, \\ \mathsf{E_c}^{\epsilon=p}(t) &\approx \tfrac{2\pi\omega P_0}{V\gamma_c}(e^{-\Gamma_+ t} - e^{-\Gamma_- t})\sin\Omega_- t, \end{aligned} \tag{2.104}$$

where

$$\Gamma_- \approx \gamma_p - \frac{\mathcal{N} g_0^2/\gamma_c}{\left(\frac{\omega_c - \omega_p}{\gamma_c}\right)^2 + 1}, \tag{2.105}$$

$$\Omega_- \approx \omega_p + \frac{\mathcal{N} g_0^2(\omega_c - \omega_p)}{(\omega_c - \omega_p)^2 + \gamma_c^2}, \tag{2.106}$$

$$\Gamma_+ \approx \gamma_c + \frac{\mathcal{N} g_0^2/\gamma_c}{\left(\frac{\omega_c - \omega_p}{\gamma_c}\right)^2 + 1}, \tag{2.107}$$

and terms only to first order in $(g_0/\gamma_c)^2$ have been kept. Initially (up to times of order $\Gamma_+^{-1} \approx \gamma_c^{-1}$), the field decays faster than the atom ($\Gamma_+ \gg \Gamma_-$). After this short

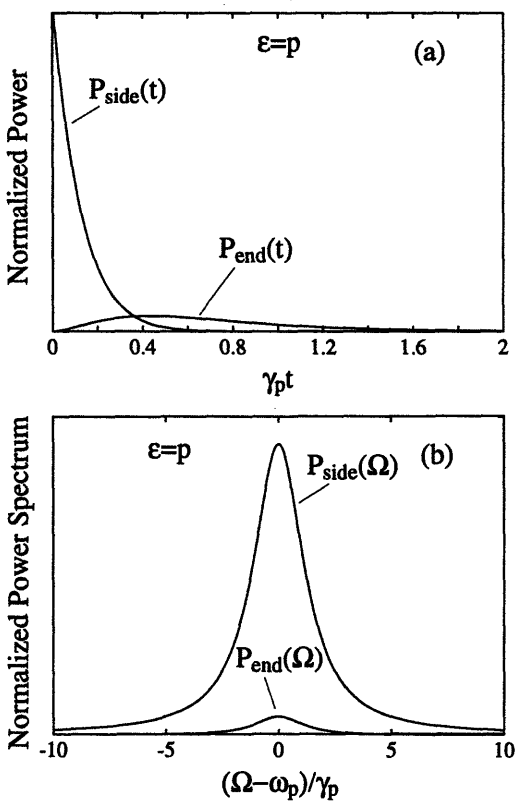

Figure 2-2: Weak coupling regime. (a) Power emitted out the side, $P_{side}^{\epsilon=p}(t)$ (atom), and out the ends, $P_{ends}^{\epsilon=p}(t)$, of the cavity as a function of time for the case $\epsilon = p$ and (b) the corresponding emission spectra. For this plot $g_0/\gamma_p = 1$ and $\gamma_c/\gamma_p = 4$.

period, however, both the atom and field decay at Γ_-, the enhanced decay rate, and the decay rates out the side and ends of the cavity are the same (see Fig. 2-2(a)). Using Eqs. 2.47 and 2.48 for the emitted power time-averaged over an optical cycle, we obtain:

$$P_{side}^{\epsilon=p}(t) \approx \left(\frac{P_0}{2\mu}\right)^2 \hbar\omega 2\gamma_p e^{-\Gamma t}, \tag{2.108}$$

and

$$P_{ends}^{\epsilon=p}(t) = \eta_{cav}\left(\frac{P_0}{2\mu}\right)^2 \hbar\omega A_{cav}(e^{-\Gamma_+ t} - e^{-\Gamma_- t})^2, \tag{2.109}$$

which, after a short time of order γ_c^{-1}, becomes:

$$P_{ends}^{\epsilon=p}(t) = \eta_{cav}\left(\frac{P_0}{2\mu}\right)^2 \hbar\omega A_{cav} e^{-\Gamma t}, \tag{2.110}$$

with A_{cav} given by Eq. 2.8 in the broad cavity limit and with:

$$\Gamma = 2\Gamma_- \approx 2\gamma_p + \frac{g_0^2/\gamma_c}{[(\omega_c - \omega_p)/\gamma_c]^2 + 1}, \tag{2.111}$$

since $\mathcal{N} \approx -1$ (see Figs. 2-3(b) and 2-4(b)). A frequency shift also arises (Figs. 2-3(a) and 2-4(a)), with the atom-cavity system now oscillating at $\Omega_- = \omega_0 + \delta\omega_0$, where

$$\delta\omega_0 \approx -\frac{g_0^2}{\gamma_c}\frac{(\omega_c - \omega_p)/\gamma_c}{[(\omega_c - \omega_p)/\gamma_c]^2 + 1}. \tag{2.112}$$

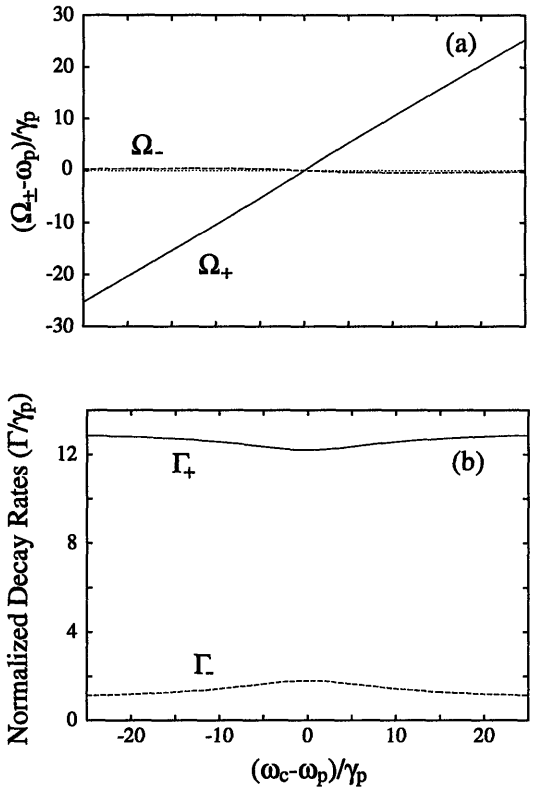

Figure 2-3: The normal modes for a weakly coupled atom-cavity system as functions of atom-cavity detuning: (a) The frequencies and (b) their associated decay rates. In these plots, $g_0/\gamma_p = 3$ and $\gamma_c/\gamma_p = 13$ (broad cavity, weak coupling limit).

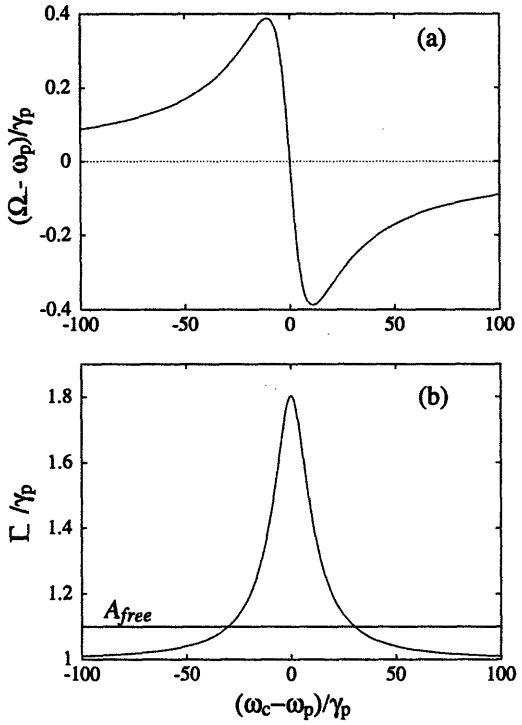

Figure 2-4: Expanded view of the atomic oscillator normal mode frequency (a) and the associated decay rate (b). The straight lines represent the uncoupled (free-space) values for the corresponding parameters. Note the frequency pulling (a) from the free-space value (vacuum radiative level shift) and the enhancement ($\Delta \approx 0$) and suppression ($|\Delta| \gg 0$) in the emission linewidth.

This is the regime of enhanced and suppressed spontaneous decay. The decay rate and oscillation frequency of the atom-cavity system are dominated by the atom, and we may interpret this regime as one in which the atom's decay rate and transition frequency are perturbed by the presence of the cavity. Because of the damping, the normal mode frequencies (a) now cross at $\omega_- = 0$ despite the coupling. In this limit, curves labeled Ω_- and Γ_- correspond to the normal mode that is atom dominated, and curves labeled Ω_+ and Γ_+ correspond to the normal mode that is cavity dominated. Note that the frequency pulling and decay rate changes occur for both oscillators. The numerator of the second term in Eqs. 2.105 and 2.111 shows the enhancement, (compare Eq. 2.8), and the detuning factor in the denominator gives rise to suppression. The frequency shift can be interpreted as a frequency pulling effect due to the interaction of the cavity oscillator with the atomic oscillator. In a QED calculation (Wigner-Weisskopf perturbation theory), the frequency shift

(vacuum radiative level shift) and the enhanced decay rate can be interpreted as arising from a perturbation in the free-space mode density induced by the cavity [13]. This point of view is only appropriate in the broad cavity, weak coupling limit. Note also that the above treatment assumes single mode interaction and neglects the effect of all other cavity modes. Within these limits, these results agree with the perturbation calculations and experimental results for decay rates and level shifts. Note also that, using $2\gamma_p = A_{free}(1-f)$, Eq. 2.111 can be expressed in terms of A_{free} to obtain the decay rate for large solid angle (degenerate) resonators:

$$\Gamma \approx A_{free}\left(1 - f + \frac{2g_0^2/\gamma_c A_{free}}{[(\omega_c - \omega_p)/\gamma_c]^2 + 1}\right), \tag{2.113}$$

which corresponds to our previous results [14, 12, 13]. The first term on the right hand side is the contribution to the decay rate due to spontaneous emission out the sides and the second term is the contribution due to emission out the ends of the resonator.

b. Narrow Cavity Limit. In a similar manner we obtain, for the narrow cavity limit ($\gamma_c \ll \gamma_p$), ($\epsilon = p$) case

$$\begin{aligned} \mathbf{p}^{\epsilon=p}(t) &\approx P_0 e^{-\Gamma_- t}\cos\Omega_- t, \\ \mathsf{E_c}^{\epsilon=p}(t) &\approx \tfrac{2\pi\omega P_0}{V\gamma_p}(e^{-\Gamma_- t} - e^{-\Gamma_+ t})\sin\Omega_+ t, \end{aligned} \tag{2.114}$$

where

$$\Gamma_+ \approx \gamma_c - \frac{\mathcal{N}g_0^2\gamma_p}{(\omega_c - \omega_p)^2 + \gamma_p^2}, \tag{2.115}$$

$$\Omega_+ \approx \omega_c + \frac{\mathcal{N}g_0^2(\omega_c - \omega_p)}{(\omega_c - \omega_p)^2 + \gamma_p^2}, \tag{2.116}$$

$$\Gamma_- \approx \gamma_p + \frac{\mathcal{N}g_0^2\gamma_p}{(\omega_c - \omega_p)^2 + \gamma_p^2}, \tag{2.117}$$

and we have again kept terms only to first order in $(g_0/\gamma_p)^2$. The cavity field is now determined by the resonator properties after a short time of order $\Gamma_-^{-1} \approx \gamma_p^{-1}$ and its

power decay rate, Γ, is

$$\Gamma = 2\Gamma_+ \approx 2\gamma_c + \frac{2g_0^2/\gamma_p}{[(\omega_c - \omega_p)/\gamma_p]^2 + 1}. \tag{2.118}$$

A frequency shift also arises, the oscillation occurring at $\Omega_- = \omega_c + \delta\omega_c$, where

$$\delta\omega_c \approx -2\gamma_c \left(\frac{g_0^2}{2\gamma_c\gamma_p}\right) \frac{(\omega_c - \omega_p)/\gamma_p}{[(\omega_c - \omega_p)/\gamma_p]^2 + 1}, \tag{2.119}$$

This regime can be termed "enhanced/suppressed cavity decay". The cavity oscillator's decay rate and oscillation frequency are perturbed by the atomic oscillator. In the narrow cavity limit ($\epsilon = p$), the atom is dominated by the Γ_- decay rate ($\approx \gamma_p$) but the cavity decays at Γ_+ ($\approx \gamma_c$) after a short time of order Γ_-^{-1}. In this case the decay rate out the side is different from the decay rate out the end of the cavity, whereas in the broad cavity limit, atom excitation case the decay rate out the side equals the decay rate out the end. Therefore, in the broad cavity limit, ($\epsilon = p$) case, one decay rate can be associated with the atom-cavity system as a whole. This is not so for the ($\epsilon = p$) case in the narrow cavity limit.

Because of the symmetry between the two oscillators, the results for the cavity excitation case ($\epsilon = c$) in the weak coupling regime may be obtained by simply exchanging the atom with the field in the above arguments. Note that, in any case, the weak coupling condition always leads to pure exponential decay in the time domain of both oscillators.

2. Intermediate Coupling

In this section, as well as the following section for strong coupling, we specialize to the case of zero atom-cavity detuning for simplicity ($\omega_c = \omega_p = \omega$). If the coupling strength is less than $|\gamma_-|$, case (1), (over-damped regime, Eq. 2.36) the oscillation frequencies are degenerate and there are two normal mode decay rates:

$$\begin{aligned} \Gamma_\pm &= \gamma_+ \pm \gamma_s, \\ \Omega_\pm &= \omega, \end{aligned} \tag{2.120}$$

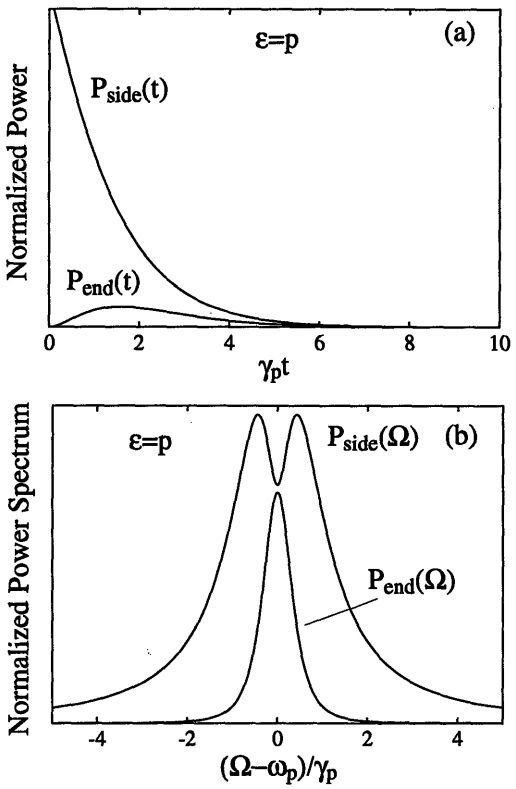

Figure 2-5: Intermediate coupling regime with lineshape splitting but no ringing. (a) The time behavior of the atom and cavity field for case (1) of the intermediate coupling regime, $\epsilon = p$. (b) The spectra of the atom and cavity field. In this plot, $g_0/\gamma_p = 0.3$, $\gamma_c/\gamma_p = 0.3$, and $\omega_- = 0$.

where

$$\gamma_s = \sqrt{\gamma_-^2 - |\mathcal{N} g_0^2|}. \tag{2.121}$$

Using the above, we obtain the following solutions for the $\epsilon = p$ case from Eqs. 2.42 and 2.43:

$$\begin{aligned} \mathbf{p}^{\epsilon=p}(t) &\approx \tfrac{P_0}{2\gamma_s}[(\gamma_s - \gamma_-)e^{-\Gamma_- t} - (\gamma_s + \gamma_-)e^{-\Gamma_+ t}]\cos\omega t, \\ \mathsf{E_c}^{\epsilon=p}(t) &\approx \tfrac{\pi\omega P_0}{V\gamma_s}(e^{-\Gamma_- t} - e^{-\Gamma_+ t})\sin\omega t. \end{aligned} \tag{2.122}$$

The power emitted out the sides and ends of the cavity are again given by Eqs. 2.56 and 2.59, respectively. Equations 2.122 hold in both the weak and intermediate coupling regimes, case (1), which we discuss here. The atom-cavity system again exhibits exponential decay at two slightly different rates (since g_0 is comparable to $|\gamma_-|$, γ_s is small compared to γ_+), Fig. 2-5(a). There is, of course, no ringing. Note that the sign of γ_s must be chosen in accordance with the convention discussed in Sec. 2.2.1. De-

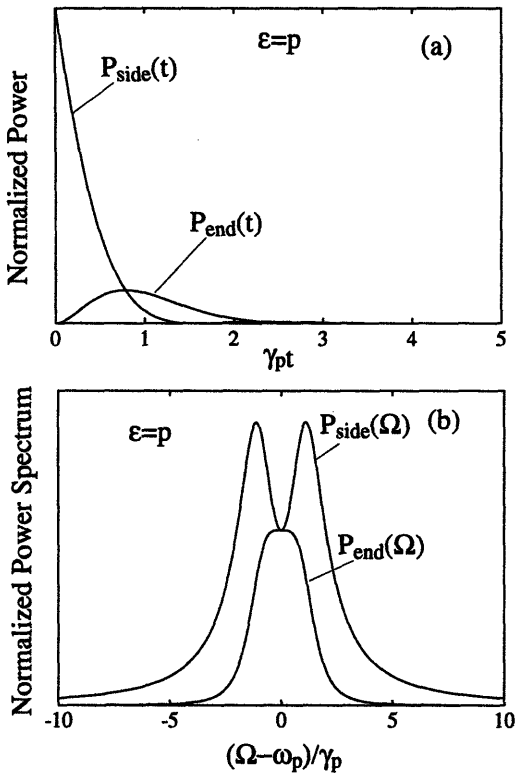

Figure 2-6: Intermediate coupling regime of atom-cavity emission. (a) The time behavior of the atomic population ($\propto P_{side}^{\epsilon=p}(t)$) and cavity field energy ($\propto P_{ends}^{\epsilon=p}(t)$) for the intermediate coupling regime, $\epsilon = p$, with $g_0/\gamma_p = 0.9$ and $\gamma_c/\gamma_p = 1$ (case 2). (b) The corresponding emission spectra.

spite the lack of ringing, the atomic emission spectrum (or excitation spectrum) shows splitting. Hence, the presence of splitting in the emission or excitation spectrum is not a sufficient condition for ringing.

If the coupling strength is greater than $|\gamma_-|$ (under-damped regime), then $I_0 = 0$ in Eq. 2.34 and power decay rates for the two normal modes (from Eqs. 2.28 and 2.34) are equal, whereas the oscillation frequencies (from Eqs. 2.29 and 2.33) are nondegenerate:

$$\begin{aligned} \Gamma &= 2\Gamma_\pm = 2\gamma_+, \\ \Omega_\pm &= \omega \pm g_s, \end{aligned} \tag{2.123}$$

where

$$g_s = \sqrt{|\mathcal{N} g_0^2| - \gamma_-^2}. \tag{2.124}$$

In this under-damped regime the solutions given by Eqs. 2.42 and 2.43 ($\epsilon = p$) for

the (real) atomic dipole moment is:

$$\mathbf{p}^{\epsilon=p}(t) = Re[p^{\epsilon=p}(t)] = P_0(\cos g_s t + \frac{\gamma_-}{g_s}\sin g_s t)\cos\omega t e^{-\gamma_+ t}, \tag{2.125}$$

and for the (real) cavity field is:

$$\mathsf{E_c}^{\epsilon=p}(t) = Re[E_c^{\epsilon=p}(t)] = \frac{2\pi\omega P_0}{V g_s}\sin\omega t \sin g_s t e^{-\gamma_+ t}. \tag{2.126}$$

The power emitted out the sides and ends of the cavity are again given by Eqs. 2.56 and 2.59, respectively. These equations hold for both the intermediate coupling regime, case (2), and the strong coupling regime, discussed below. Case (2) of the intermediate coupling regime requires that $\gamma_-^2 < g_0^2 < \frac{\gamma_c^2+\gamma_p^2}{2}$. This condition implies that $g_s^2 < \gamma_+^2$ and normal mode ringing is negligible and obscured by damping. As an example, we consider the case where the coupling, atomic and cavity decay rates are comparable, $\gamma_c = \gamma_p$, $g_0 = 0.9\gamma_p$. Figure 2-6 shows the side and end power emitted as functions of time. Note the presence of splitting in the atomic emission spectrum but not the cavity field. In this case ringing is negligible and is not clearly observable in the time domain. These cases are discussed further in the frequency domain analysis (Sec. 2.3.2).

When the atom-cavity detuning is large compared to $|\gamma_-|$, Eqs. 2.120 and 2.123 are no longer appropriate. In this case, the system becomes simply an empty cavity and free atomic dipole, i.e., the $+/-$ modes resemble the empty cavity/atomic dipole, respectively, and the atom and cavity field behave as though the other were not present.

3. Strong Coupling: Normal Mode Ringing

We now consider the regime of strong coupling ($g_0 \gg \gamma_-$). As in Eqs. 2.108 and 2.109, the time-averaged power emitted from each oscillator is proportional to the squares

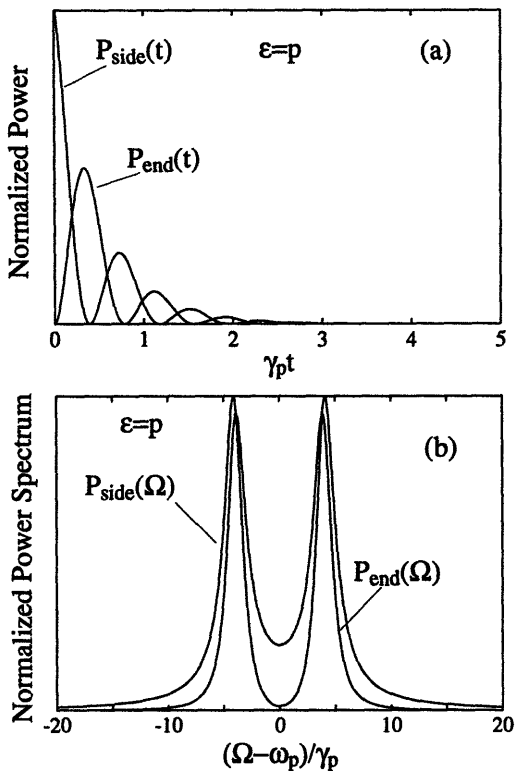

Figure 2-7: Ringing regime of atom-cavity emission. (a) The transient atomic population and cavity field energy and (b) the corresponding emission spectra in the underdamped regime, $\epsilon = p$, with $g_0/\gamma_p = 4$ and $\gamma_c/\gamma_p = 1$. Note the larger splitting in the atomic lineshape, $P_{side}^{\epsilon=p}(\Omega)$, due to the Lorentzian factor in the numerator.

of Eqs. 2.125 and 2.126 and the relative phases differ by π:

$$P_{side}^{\epsilon=p}(t) \approx \left(\frac{P_0}{2\mu}\right)^2 \hbar\omega 2\gamma_p e^{-2\gamma_+ t}\cos^2 g_s t, \tag{2.127}$$

and

$$P_{ends}^{\epsilon=p}(t) \approx \left(\frac{P_0}{2\mu}\right)^2 \hbar\omega A_{cav} e^{-2\gamma_+ t}\sin^2 g_s t, \tag{2.128}$$

where we have neglected terms of order γ_-/g_s or higher. As can be seen in the solutions for the dipole and cavity field, Eqs. 2.125–2.128, normal mode ringing physically represents the energy exchange between the cavity oscillator and the atomic oscillator. This process continues until the energy is dissipated. The loss of energy occurs via radiative coupling of the oscillators to the surrounding free-space modes. The decay rates of the normal modes are the average of the decay rates of the two uncoupled

oscillators. This may be physically explained by the fact that each normal mode consists of an equal contribution of a cavity oscillator and an atomic oscillator. As the energy is exchanged, the damping rate of each oscillator shares equally in leaking energy to the surroundings. Note that the condition, $g_0^2 > \gamma_-^2$, is not a sufficient condition for observing normal mode ringing in any practical sense. For example, as seen in Fig. 2-6(a), the oscillations in the transient behavior of both the atom, $P_{side}(t)$, and the cavity field, $P_{end}(t)$, in case (2) of the intermediate coupling regime are negligible. Significant ringing requires that $g_0^2 \gg (\gamma_c^2 + \gamma_p^2)/2$. This condition can be derived by requiring $g_s > \gamma_+$ in Eqs. 2.127 and 2.128; it insures that more than one oscillation occurs before the emitted power decays to $e^{-2\pi}$ of its initial value (Fig. 2-7(a) illustrates this case). When defined in this way, the condition for strong coupling is identical to that given in the frequency domain (Sec. 2.3.2).

2.3.2 Excitation and Emission Spectra

We now turn to the study of steady state lineshapes obtained in the frequency domain analyses. As discussed in the introduction (Sec. 2.1), steady state emission experiments and scattering experiments provide equivalent information; they exhibit the same spectral profiles and, thus, can be analyzed together. Therefore, the results of the following lineshape analyses of the excitation spectra obtained in a scattering arrangement are equally applicable to the spontaneous emission spectra obtained in an emission arrangement. Note, however, that in the case of scattering $\mathcal{N} = \mathcal{N}_0 = -1$. The spontaneous emission spectrum for an atom coupled to a cavity mode has been calculated in the QED framework (see Eq. (6) of [47]), and the result is equivalent to Eq. 2.58.

1. Weak Coupling

In the weak coupling limit, where $g_0^2 \ll (\gamma_c - \gamma_p)^2/4$, the spectral features of the power spectra, $P^{\epsilon=p,c}_{end,side}(\Omega)$ (compare Eqs. 2.58 and 2.61) are determined by the narrower of the two Lorentzian factors, $\mathcal{L}_{\pm}(\Omega)$.

a. Broad Cavity Limit. If we assume the broad cavity limit ($\gamma_c \gg \gamma_p$), we get from Eqs. 2.86, 2.87, 2.95, and 2.96:

$$P^{\epsilon=p}_{ends}(\Omega) \approx \eta_{cav}\hbar\omega_p \left(\frac{I_L}{2I_s}\right) \frac{g_0^2}{\gamma_c} \left[\frac{\gamma_c^2}{(\Omega-\omega_c)^2+\gamma_c^2}\right] \left[\frac{\gamma_p^2}{(\Omega-\Omega_-)^2+\Gamma_-^2}\right], \tag{2.129}$$

$$P^{\epsilon=p}_{side}(\Omega) \approx \hbar\omega_p 2\gamma_p \left(\frac{I_L}{2I_s}\right) \left[\frac{\gamma_p^2}{(\Omega-\Omega_-)^2+\Gamma_-^2}\right], \tag{2.130}$$

$$P^{\epsilon=c}_{end}(\Omega) \approx \eta_{cav}^2 I_L a \left[\frac{\gamma_c^2}{(\Omega-\omega_c)^2+\gamma_c^2}\right], \tag{2.131}$$

$$P^{\epsilon=c}_{side}(\Omega) \approx \eta_{cav} \frac{\hbar\omega_p 2\gamma_p}{1-R} \left(\frac{I_L}{2I_s}\right) \left[\frac{\gamma_c^2}{(\Omega-\omega_c)^2+\gamma_c^2}\right] \left[\frac{\gamma_p^2}{(\Omega-\Omega_-)^2+\Gamma_-^2}\right], \tag{2.132}$$

where Γ_- and Ω_- are given in Eqs. 2.105 and 2.106 and terms only to first order in $(g_0/\gamma_c)^2$ and I_L/I_s have been kept. In Eqs. 2.129 and 2.132 the broad cavity

lineshape is slowly varying over the atomic lineshape, hence the lineshapes are essentially determined by the atomic properties (i.e., by $\mathcal{L}_-(\Omega)$, see Fig. 2-2(b)); the spectral linewidth and frequency shifts are given by Eqs. 2.111 and 2.112 respectively (see Figs. 2-3 and 2-4). Changes in the emission rate and frequency manifest themselves in the spectral linewidth and center frequency of the excitation spectrum. The suppression (enhancement) arises from the destructive (constructive) interference, respectively, of the multiply reflected fields within the cavity. Note that the empty cavity lineshape in Eq. 2.130 has been approximated by unity because $\gamma_c \gg \Gamma_-$. For the driven-cavity case, the scattering lineshape observed from the sides of the cavity, Eq. 2.132, is the same as that observed out the cavity end in the driven-atom case, Eq. 2.129. In contrast, the forward scattered lineshape out the end of the cavity, Eq. 2.131, is approximately constant near the atomic frequency, because the factor $|\mathcal{L}_p(\Omega)/\mathcal{L}_-(\Omega)|^2$ in that equation is approximately unity (since $\Gamma_- \approx \gamma_p$ and $\Omega_- \approx \omega_p$). In this regime the cavity simply acts as a broadband transmission filter, with a slight modification induced by the atom. However, when we consider the strong or intermediate coupling regimes below it will be seen that the transmission lineshape can be altered dramatically by the coupling.

Rewriting Eqs. 2.98 and 2.99 in this limit, we obtain:

$$N_u^{\epsilon=p}(\Omega) \approx \left(\frac{I_L}{2I_s}\right) \frac{\gamma_p^2}{(\Omega-\Omega_-)^2+\Gamma_-^2}, \tag{2.133}$$

$$N_u^{\epsilon=c}(\Omega) \approx \frac{\eta_{cav}}{1-R}\left(\frac{I_L}{2I_s}\right) \frac{\gamma_p^2}{(\Omega-\Omega_-)^2+\Gamma_-^2}. \tag{2.134}$$

As expected, the atomic state population follows the slightly perturbed atomic lineshape. If Eqs. 2.133 and 2.134 are used in Eqs. 2.130 and 2.132, respectively, then the power scattered out the side is simply proportional to the average excited state population induced by the excitation field (as in the emission case). Also note that given the intensity at the atom for $\epsilon = c$, $I_c^{\epsilon=c} = c|E_c^{\epsilon=c}|^2/8\pi$, we can write

$$N_u^{\epsilon=c}(\Omega) \approx \left(\frac{I_c^{\epsilon=c}(\Omega)}{2I_s}\right) \frac{\gamma_p^2}{(\Omega-\omega_p)^2+\gamma_p^2}, \tag{2.135}$$

which exhibits the expected relation between the atomic population and the (weak) cavity field intensity.

b. Narrow Cavity Limit. In the narrow cavity limit ($\gamma_c \ll \gamma_p$), we obtain from Eqs. 2.86, 2.87, 2.95, and 2.96:

$$P_{ends}^{\epsilon=p}(\Omega) \approx \eta_{cav}\hbar\omega_p \left(\frac{I_L}{2I_s}\right) \frac{g_0^2}{\gamma_c} \left[\frac{\gamma_p^2}{(\Omega-\omega_p)^2+\gamma_p^2}\right] \left[\frac{\gamma_c^2}{(\Omega-\Omega_+)^2+\Gamma_+^2}\right], \tag{2.136}$$

$$P_{side}^{\epsilon=p}(\Omega) \approx \hbar\omega_p 2\gamma_p \left(\frac{I_L}{2I_s}\right) \left[\frac{\gamma_p^2}{(\Omega-\omega_p)^2+\gamma_p^2}\right], \tag{2.137}$$

$$P_{end}^{\epsilon=c}(\Omega) \approx \eta_{cav}^2 I_L a \left[\frac{\gamma_c^2}{(\Omega-\Omega_+)^2+\Gamma_+^2}\right], \tag{2.138}$$

$$P_{side}^{\epsilon=c}(\Omega) \approx \eta_{cav}\frac{\hbar\omega_p 2\gamma_p}{1-R} \left(\frac{I_L}{2I_s}\right) \left[\frac{\gamma_p^2}{(\Omega-\omega_p)^2+\gamma_p^2}\right] \left[\frac{\gamma_c^2}{(\Omega-\Omega_+)^2+\Gamma_+^2}\right], \tag{2.139}$$

where Γ_+ and Ω_+ are given in Eqs. 2.115 and 2.116, respectively, and we have again kept terms only to first order in $(g_0/\gamma_p)^2$ and I_L/I_s. The lineshapes out the ends of the resonator are now determined by the resonator properties, $\mathcal{L}_+(\Omega)$. The cavity oscillator's decay rate and emission frequency are perturbed by the atomic oscillator, and in the excitation spectrum this manifests itself as changes in the resonator linewidth and center frequency. This can be seen, for example, in the case $\epsilon = c$ of Eq. 2.138, where the lineshape of the transmitted power is perturbed from that of the empty cavity (again $|\mathcal{L}_p(\Omega)/\mathcal{L}_-(\Omega)|^2 \approx 1$). The emission out the side shows a lineshape, Eq. 2.139, with a narrow cavity-like structure, since the atom can scatter light only when the cavity field builds up in the resonator. For the driven-atom case, however, the scattered lineshape out the side of the cavity, Eq. 2.137, is approximately that of the atomic lineshape ($|\mathcal{L}_c(\Omega)/\mathcal{L}_+(\Omega)|^2 \approx 1$), and the lineshape out the end is approximated by the modified narrow-cavity lineshape on top of the much broader atomic lineshape.

We summarize briefly the results of this section for the special case of the resonant atom-cavity system ($\omega_c = \omega_p = \omega$). In the regime of weak coupling and broad or narrow cavity limits, the $\mathcal{L}_{p,c}(\Omega)$ Lorentzian factors in the numerators of Eqs. 2.95

and 2.87 are approximately canceled by the appropriate Lorentzian factors, $\mathcal{L}_+(\Omega)$ or $\mathcal{L}_-(\Omega)$, in the denominator. In general, the linewidths (half-widths) $\Gamma_\pm$ are

$$\Gamma_\pm = \gamma_+ \pm \gamma_- \sqrt{1 + \mathcal{N}\left(\frac{g_0}{\gamma_-}\right)^2}, \tag{2.140}$$

so that in the broad or narrow cavity limit with weak coupling we get

$$\begin{aligned} \Gamma_+ &\approx \gamma_c + O\left(\mathcal{N}\tfrac{g_0^2}{\gamma_-}\right), \\ \Gamma_- &\approx \gamma_p - O\left(\mathcal{N}\tfrac{g_0^2}{\gamma_-}\right). \end{aligned} \tag{2.141}$$

In the broad cavity limit the $\mathcal{L}_c(\Omega)$ Lorentzian factor is canceled by $\mathcal{L}_+(\Omega)$ and in the narrow cavity limit the $\mathcal{L}_p(\Omega)$ Lorentzian factor is canceled by $\mathcal{L}_-(\Omega)$, as described above.

2. Intermediate Coupling

In the intermediate coupling regime (Eq. 2.101) lineshape distortions can arise, and two-peaked spectra can occur, even in the absence of ringing. For case (1) of the intermediate coupling regime in either the broad or narrow cavity limit, if $g_0^2 < \gamma_-^2$, i.e., the coupling strength is slightly less than γ_-, then the normal mode oscillation frequencies are degenerate and the decay rates are approximately equal (Eq. 2.120). Therefore, in the narrow cavity limit $P_{side}^{\epsilon=p}(\Omega)$, given in Eq. 2.95, will exhibit lineshape splitting, since the *square* of a broad Lorentzian (with full width $2\gamma_+ \approx \gamma_p$ centered at frequency, ω) is divided by a narrow Lorentzian (with full width $2\gamma_c < 2\gamma_p$, also centered at frequency, ω) (see Fig. 2-5(b)). Note that for this case, the dip in the lineshape at resonance provides another example of the suppression of fluorescence for an atom in a cavity similar to that studied in the weak coupling, broad cavity limit. In the ideal limit that $\gamma_c \to 0$, no scattering of light out the side occurs for $\Omega = \omega_c = \omega_p$. Furthermore, from Eq. 2.83 we obtain

$$E_c^{\epsilon=p}(\Omega = \omega_c) = -E_L^p, \tag{2.142}$$

so that a non-zero field persists in the resonator. From Eq. 2.142, we can see that the cavity field has the same amplitude as the driving field, but is shifted 180^o out of phase. Thus, the total field at the position of the atom is zero and the atom stops radiating (see Eq. 2.80). With the laser probe frequency far off resonance ($\Omega \gg \omega_c = \omega_p$, for example), the atom radiates out the side and no scattering into the cavity mode occurs. As the probe laser frequency approaches the cavity frequency within the cavity resonance bandwidth, (enhanced) scattering into the cavity mode increases with a resulting suppression in scattered light out the resonator side. Also note that this argument holds *regardless* of the coupling strength. This effect has also been interpreted in the dressed-state picture [62].

Similarly, in the broad cavity limit $P_{end}^{\epsilon=c}(\Omega)$, given in Eq. 2.87, will exhibit lineshape splitting. As discussed in Sec. 2.3.1, this case gives rise to pure exponential decay with no ringing. Thus, a two-peaked lineshape is possible even in the over-damped regime ($g_0 < \gamma_-$) in which normal mode ringing cannot occur. Again, lineshape splitting may occur without ringing. For this case, the suppression of transmission near resonance that gives rise to the dip in the lineshape has a simple interpretation. It is simply due to the loss of light via scattering by the atom out the side of the resonator. (Note that a similar effect has been discussed in a paper by Rice and Carmichael in connection with squeezing appearing in the spectrum of transmitted light of a weakly driven cavity containing a single atom [46].) We can conclude this study of the over-damped regime in intermediate coupling by noting that in order to observe splitting in a regime where no oscillatory energy exchange is possible, one must *drive/excite and observe* the oscillator with the greatest damping.

Case (2) of the intermediate coupling regime always gives rise to two nondegenerate frequencies and equal decay rates for the normal modes of the resonant atom-cavity system. Because decay dominates, normal mode ringing is negligible. In either the broad or narrow cavity limit, the emission or scattering lineshape of one oscillator may exhibit splitting while the other oscillator's lineshape does not. Since the linewidths are broader than the frequency separation in the $\mathcal{L}_\pm(\Omega)$ Lorentzian factors, $P_{side}^{\epsilon=c}(\Omega)$, Eq. 2.96, and $P_{end}^{\epsilon=p}(\Omega)$, Eq. 2.86, will not exhibit two peaks but, rather, a

distorted squared-Lorentzian lineshape. On the other hand, $P_{side}^{\epsilon=p}(\Omega)$, Eq. 2.95, in the narrow cavity limit and $P_{ends}^{\epsilon=c}(\Omega)$, Eq. 2.87, in the broad cavity limit will exhibit lineshape splitting. For the special case $\gamma_c = \gamma_p = \gamma$, Eqs. 2.95 and 2.87 will exhibit splitting if $g_0^2 > 0.3\gamma^2$. Equations 2.127 and 2.128 are valid in this limit, and we plot the emitted power of the atom and cavity field and the corresponding emission (or excitation) spectra in Fig. 2-6 with $g_0^2 = 0.8\gamma^2$. As can be seen, even though the atom exhibits a prominent splitting in its emission/excitation spectrum, the cavity spectrum does not, and ringing in the transient evolution of the oscillators is negligible.

We now summarize the results of this section. The presence of a two-peaked structure in the excitation or emission spectrum is not simply correlated with the existence of normal mode ringing in the time domain. As pointed out in Sec. 2.2, and as is seen in the excitation spectra above, when one observes the power scattered/emitted by the oscillator which is initially excited or which is being driven (Eqs. 2.50 and 2.54, or Eqs. 2.87 and 2.95, respectively), the spectrum of power scattered or emitted contains an extra factor, $|\mathcal{L}_{c,p}(\Omega)|^2$, in the numerator which is not present in the spectrum of the oscillator which is not being driven or excited, respectively. This factor depends upon the initial conditions, i.e., on which oscillator is initially excited or on which oscillator is being driven. The presence of $|\mathcal{L}_{c,p}(\Omega)|^2$ in the numerator can create a two-peaked spectrum, *even when normal mode ringing cannot occur.* These numerator factors may be viewed as *artifacts* of this type of coupled oscillator system that are manifested in particular choices of the excitation and observation scheme. They arise from *interference* effects between the dipole, cavity, and excitation fields independent of the atom-cavity coupling strength. They have obvious effects on lineshape splitting, but do not effect the actual normal mode frequency separation (see also the next section). To illustrate, Fig. 2-5 is a plot of spectra in the intermediate coupling regime for the case $\epsilon = p$, in which $g_0/\gamma_p = 0.3$ and $\gamma_c/\gamma_p = 0.3$ and no ringing can occur. However, it should be noted that in the broad or narrow cavity limits, the results of this section show that no two-peaked spectra can occur in either oscillator for intermediate coupling, case (1), if one drives (excites) the narrowest (or

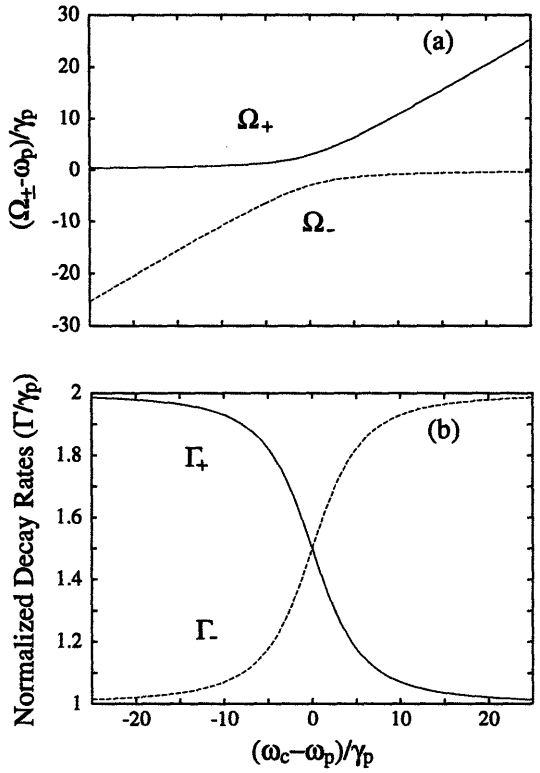

Figure 2-8: Strongly coupled atom-cavity system. The normal mode frequencies (a) and the corresponding decay rates (b) as functions of atom-cavity detuning. In this case $g_0/\gamma_p = 3$ and $\gamma_c/\gamma_p = 2$. Note that the normal mode frequencies are nondegenerate and the associated decay rates are equal at zero atom-cavity detuning.

least damped) oscillator.

3. Strong Coupling

We now turn to the strongly coupled system, where the normal mode frequencies differ substantially and their linewidths (equal to the decay rates) are equal, as discussed in Sec. 2.3.1. Equations 2.123 apply to this case as well, but now $g_s \gg \gamma_+$. In this case the normal modes are split by $2g_s$. For large atom-cavity detuning the excitation spectrum exhibits two peaks in all cases. The condition for observing a two-peaked structure in the excitation and emission spectra of both oscillators is $g_0^2 > (\gamma_c^2+\gamma_p^2)/2$. This condition is determined by requiring that there be three distinct frequencies at which the slopes of $P_{ends}^{\epsilon=p}(\Omega)$ and $P_{side}^{\epsilon=c}(\Omega)$ (i.e., the function $\frac{1}{|\mathcal{L}_+(\Omega)\mathcal{L}_-(\Omega)|^2}$) become zero. (This is the same condition in the time domain for observing more than one oscillation

period before the emitted power decays to $e^{-2\pi}$ of the initial power emitted.) In this regime the lineshapes of the emission/excitation spectra for both the atomic and cavity field oscillators exhibit splitting regardless of which oscillator is being excited and ringing is observed. With increasing coupling strength the effect of the $\mathcal{L}_{c,p}(\Omega)$ factor on $P_{end}^{\epsilon=c}(\Omega)$, Eq. 2.87, and $P_{side}^{\epsilon=p}(\Omega)$, Eq. 2.95, decreases. Figure 2-7 shows the transient behavior and spectral lineshapes of the atom and cavity field oscillators for the case $\epsilon = p$, with $g_0/\gamma_p = 4$ and $\gamma_c/\gamma_p = 1$. Note that the $\mathcal{L}_c(\Omega)$ factor causes the atomic lineshape splitting, $P_{side}^{\epsilon=p}(\Omega)$, to be slightly larger than the lineshape splitting for the field, $P_{ends}^{\epsilon=p}(\Omega)$. Figure 2-8 shows the normal mode frequencies and linewidths (equal to the decay rates) of the emission spectra.

To summarize, the presence of splitting in $P_{ends}^{\epsilon=p}(\Omega)$, Eq. 2.86, and $P_{side}^{\epsilon=c}(\Omega)$, Eq. 2.96, is directly correlated with non-negligible normal mode ringing. Therefore, in order to study the direct manifestation of normal mode ringing via a lineshape splitting in the frequency domain in an unambiguous manner, one should either drive the atom and observe the power scattered out the cavity mirror ends, or drive the cavity and observe scattering from the atom out the cavity sides.

4. Single Normal Mode Excitation

In the scattering analysis of Sec. 2.2.3, we assumed that either the atom or the cavity was excited by a coherent laser field, and Eq. 2.83 for the cavity field was written to reflect these two choices. However, it is also possible to excite *both* the atom and field simultaneously. Under the appropriate conditions, it is then possible to excite only one of the two normal modes of the atom-cavity system. We briefly consider this possibility. Notice that both terms of Eq. 2.83 are then present, and that one probe field may differ from the other in both amplitude and phase. The single mode excitation condition occurs when the two probe fields, $E_L^{\epsilon=p}$ and $E_L^{\epsilon=c}$, satisfy the following relation:

$$g_0^2 E_L^{\epsilon=p} + \left(\frac{\alpha}{2i\Omega}\right) \mathcal{L}_p(\Omega) E_L^{\epsilon=c} = \xi \mathcal{L}_{\pm}(\Omega), \tag{2.143}$$

with ξ a constant of proportionality. For a resonant system, this gives:

$$\frac{E_L^{\epsilon=p}}{E_L^{\epsilon=c}} = \pm \frac{\sqrt{2\eta_{cav}\gamma_c c/2L}}{g_0} e^{\pm i\phi}, \tag{2.144}$$

with the relative phase of the two fields given by:

$$\phi = \tan^{-1}\left(\frac{\gamma_-}{g_s}\right). \tag{2.145}$$

The choice of sign ($\pm$) selects the normal mode with lineshape proportional to $|\mathcal{L}_\pm(\Omega)|^{-2}$, respectively. The cavity field lineshape then follows a Lorentzian lineshape, even in the strong coupling limit, with Lorentzian factor $\mathcal{L}_+(\Omega)$ or $\mathcal{L}_-(\Omega)$. In other words, we can selectively excite *either one* of the normal modes of a strongly coupled atom-cavity system and study its lineshape. Instead of two peaks, a single Lorentzian would be seen either up-shifted or down-shifted relative to the uncoupled (degenerate) oscillator frequencies. In the time domain, this corresponds to choosing the initial conditions so that only the symmetric or anti-symmetric mode of a coupled oscillator system is excited. Note that for $\gamma_- \approx 0$ we obtain $\phi = \pi/2$.

2.3.3 Stimulated Emission and Absorption

Insight into the effects of stimulated emission/absorption and its relation to enhanced spontaneous emission in the atom-cavity system can be obtained from the emission results. We now investigate the consequences of positive, as well as negative, inversion on the emission power and spectral linewidth. Note that to attain positive steady state inversion, we must select an atomic system with an unstable lower state which decays more rapidly than the upper state. In the following discussion we will continue to restrict our analysis to the small signal regime, so that $\mathcal{N} \approx \mathcal{N}_0$, in order to avoid the effects of population saturation.

From the photon rate equation, Eq. 2.72, together with Eqs. 2.71 and 2.73, it can be seen that G accounts for stimulated emission and absorption. Note that the numerator of Eq. 2.70, the spontaneous emission term, is just $N_u\hbar\omega A_{cav}$. We can

thus identify spontaneous emission, as well as stimulated emission and absorption, and their effects on the average number of photons in the cavity, i.e., the steady state emitted power. We also have expressions for the expected spectral linewidths of the emitted power in various regimes of interest (Sec. 2.3.2). Therefore, we can study the relationship between the total emitted power and the emission linewidth, as well as elucidate the roles played by stimulated and spontaneous emission processes.

According to Eq. 2.61 the emission spectrum in a resonant atom-cavity system exhibits a lineshape described by the product of two Lorentzian functions with widths Γ_- and Γ_+, respectively (see Eq. 2.140). Note from the discussion below Eqs. 2.33 and 2.34 that a resonant atom-cavity system with positive inversion exhibits only one emission frequency, regardless of coupling strength. As seen in Eq. 2.140, the emission linewidth of the atom-cavity system exhibits narrowing if the inversion is positive and exhibits broadening if the inversion is negative. (See Appendix C for discussion and proof.)

We may write the total emission rate per atom of the atom-cavity system using Eqs. 2.62 and 2.70 as follows:

$$A = \frac{P_{end} + P_{side}}{N_u \hbar\omega} = 2\gamma_p + \frac{A_{cav}}{1-G}, \tag{2.146}$$

with the emission rate out the ends (using Eq. 2.70) given by

$$A_{ends} = \frac{A_{cav}}{1-G}. \tag{2.147}$$

Note that for small multi-pass gain and to first order in $(g_0^2/\gamma_c\gamma_p)$, $A_{ends} \approx A_{cav}$. It is interesting to compare the emission rate, A, to the atom-cavity linewidth. As shown below, the two are equal only under special circumstances.

In the broad cavity limit of a weakly coupled, resonant atom-cavity system ($\gamma_c \gg \gamma_p$, $g_0^2 \ll \gamma_c^2$), stimulated processes are negligible compared to spontaneous emission: From Eq. 2.72,

$$\frac{\text{stimulated emission rate}}{\text{spontaneous emission rate}} = \nu; \tag{2.148}$$

but ν from Eq. 2.70 in this limit is

$$\nu = N_u \left(\frac{1}{\gamma_c^2}\right) \frac{\sigma_0 c}{2V} \gamma_p = N_u \left(\frac{g_0}{\gamma_c}\right)^2 ; \tag{2.149}$$

and thus

$$\frac{\text{stimulated emission rate}}{\text{spontaneous emission rate}} = \nu = N_u \left(\frac{g_0}{\gamma_c}\right)^2 \ll 1. \tag{2.150}$$

Similarly, for the absorption processes we have

$$\frac{\text{absorption rate}}{\text{cavity loss rate}} = \frac{N_l \left(\frac{\sigma' c}{V}\right) \nu}{2\gamma_c \nu} = N_l \left(\frac{g_0}{\gamma_c}\right)^2 \ll 1. \tag{2.151}$$

The multi-pass gain, Eq. 2.71, is small, $|G| \ll 1$, and the total emission rate is simply the enhanced spontaneous emission rate. The linewidth is given by Eq. 2.105, which we may write in the following form, to first order in $(g_0^2/\gamma_c\gamma_p)$:

$$\Gamma = 2\Gamma_- \approx 2\gamma_p(1 - G'). \tag{2.152}$$

For $\mathcal{N} \approx -1$, the emission linewidth (see also Eq. 2.111) is equal to the total emission rate, Eq. 2.146. For any other value of the inversion, the total emission rate is not the same as the linewidth. Also note that if the inversion is *positive*, the emission linewidth *narrows*. This process can be identified as spontaneous emission line narrowing, since stimulated emission and absorption are negligible.

In contrast, in the narrow cavity limit ($\gamma_p \gg \gamma_c$) the stimulated emission rate can be comparable to, or even greater than, the spontaneous emission rate regardless of the coupling strength, and the gain can be non-negligible. The linewidth is now given by Γ_+ (Eq. 2.115) rather than Γ_-, and is similar in form to Eq. 2.152. In this case $G' \approx G$, and the $(1-G)$ term in the denominator of Eq. 2.146 can significantly depart from unity. For positive inversion, the emission rate increases with gain, becoming larger than that for pure spontaneous emission, and the resulting emission linewidth is further narrowed. This is a manifestation in the atom-cavity system of stimulated emission line-narrowing. For negative inversion, the total emission rate is reduced

compared to that for spontaneous emission; again, only for $\mathcal{N} = -1$ and $|G| \ll 1$ is the (broadened) linewidth the same as the total emission rate. Of course, when the gain becomes appreciable, $\mathcal{N}$ may deviate from $\mathcal{N}_0$, giving rise to further interesting behavior.

As mentioned above, in the narrow cavity limit stimulated emission can become appreciable, and can produce significant line narrowing. One might expect that stimulated emission and line narrowing are always correlated, just as they are in a laser. However, this notion breaks down in a strongly coupled atom-cavity system. For example, consider a two-level atom, the lower level of which is allowed to decay, but at a rate larger than that of the upper level. In the narrow-cavity limit ($g_0, \gamma_p \gg \gamma_c$), the mean photon number can be much larger than 1, as discussed above, so that photons are emitted mostly by stimulated emission. However, if the atom-cavity coupling is sufficiently strong ($g_0 \gg \gamma_p \gg \gamma_c$) and we assume that $f \ll 1$ so that $A_{free} \approx 2\gamma_p$, the spontaneous emission rate into the resonator mode can exceed even the free-space spontaneous emission rate of the upper level by a factor

$$\frac{A_{cav}}{A_{free}} = \frac{\left(\frac{\sigma_0' c}{V}\right)}{A_{free}} \xrightarrow{\gamma_c \ll \gamma_p} \left(\frac{g_0}{\gamma_p}\right) \gg 1. \tag{2.153}$$

In this case the upper-state total spontaneous emission rate ($A \approx A_{free} + A_{ends}$) can be made greater than that of the lower state, resulting in a negative steady-state inversion. (The inversion is slightly negative because the atom is strongly saturated by the large number of resonator-mode photons. In fact, a single photon in the mode is enough to saturate an atom which is coupled to it.) Therefore, we can have the remarkable situation in which an atom emits photons primarily by stimulated emission, even though its inversion remains negative.

2.4 Summary

We have developed a semiclassical model to study the emission and scattering properties of an atom-cavity system in which the atom(s) are fixed and the resonator

mode function is uniform. The semiclassical picture describes the properties of a single atom-cavity system, averaged over a series of successive events. The inclusion of damping gives rise to a host of interesting effects. In a normal mode analysis, the model describes decay rates and oscillation frequencies of the atom and cavity field in the time domain and their associated power spectra in the frequency domain. The model thus provides the normal mode structure for the system. Manifestations of coupling were seen in the spectral lineshapes in the weak, intermediate and strong coupling regimes. The results of enhanced and suppressed spontaneous emission and vacuum radiative level shifts were derived. The relationships between normal mode ringing and lineshape splitting were studied. The spectral lineshapes observed in the frequency domain are directly connected to the oscillator decay rates observed in the time domain. However, the relationships exhibit subtle behavior. For example, lineshapes exhibiting two symmetric peaks can be obtained in the absence of normal mode ringing. Therefore, the presence of a two-peaked structure in the excitation or emission spectra is not necessarily an indication of normal mode ringing. An emission analysis using the time domain results and their Fourier transforms provides emission rates as well as the lineshapes of the emission spectra.

The scattering formalism applied to the atom-cavity system in its ground state provides lineshapes which contain information about normal mode structure. We found that the same lineshapes are obtained in the emission analysis for the special case with inversion, $\mathcal{N} = -1$. The scattering lineshapes therefore provide atom-cavity spontaneous emission information as well. In particular, we studied the relationship between emission rates and linewidths. It was shown in the Wigner-Weisskopf limit (broad cavity, weak coupling) that emission rates and excitation linewidths are equal with enhanced spontaneous emission occurring in the $\mathcal{N} = -1$ case. In general, however, the emission rate and linewidth are not the same. When the steady state inversion does not equal -1, the linewidth associated with enhanced spontaneous emission is reduced, and for positive inversion a line narrowing occurs, despite the absence of stimulated emission and absorption.

The emission picture enables us to study the atom-cavity system for positive, as

well as negative, inversion, and thus to discuss the possibility of stimulated emission in an atom-cavity system and distinguish it from enhanced spontaneous emission. Only spontaneous emission (enhanced or suppressed) occurs in an atom-cavity system with negligible gain. In this case the linewidth is broadened for zero atom-cavity detuning and narrowed for large atom-cavity detuning. The resonant system exhibits a linewidth which is broadened (narrowed) if the inversion is negative (positive). With significant gain and positive inversion, however, the emission rate is further increased compared to the spontaneous emission rate and the linewidth is further narrowed by stimulated emission. Stimulated emission can play an important role in the atom-cavity radiation process and we have discussed the conditions under which stimulated emission line narrowing can occur. We also considered the system excited with broadband light and derived a photon rate equation identical to the equation obtained in the incoherently pumped system (see Appendix B).

Interestingly, in the strong coupling regime it may also be possible to experimentally observe (excite) each normal mode separately by properly chosen laser fields (amplitudes and relative phases) that drive both the atom and cavity simultaneously in a scattering arrangement. The resulting excitation spectrum would then exhibit a single Lorentzian in the strong coupling regime. This lineshape is just the particular normal mode which was chosen to be excited and is characterized by the Lorentzian factor $\mathcal{L}_+(\Omega)$ or $\mathcal{L}_-(\Omega)$. Later we will discuss the experimental difficulties associated with this proposal.

Chapter 3

Theory II

The model described in the previous chapter assumes that all atoms interacting with the cavity are equally coupled to the mode and that fluctuations in the number of atoms are negligible. In experiments which utilize semiconductor microcavities, for example, the radiators can be fixed in position at the node or anti-node to within small fractions of a wavelength. The results of the previous chapter may then be applied without any additional assumptions. In this case one needs only to replace $\mathcal{N}g_0^2 \longrightarrow -Ng_0^2$ ($\mathcal{N} \approx -N$) in the results of that chapter to generalize to the case of many atoms (or radiators). Additional examples to which the simple model of the previous chapter may be applied without further modification include those experiments with degenerate resonators (eg., concentric or confocal). Section 3.4 describes the two kinds of resonators that have been used in cavity QED studies (degenerate and nondegenerate) and discusses their fundamental and practical differences.

In the experiments to be described in the next chapter, however, an atomic beam interacts with a single SW mode of an open optical resonator. Either the atoms or the cavity mode is weakly driven by a coherent laser probe (both schemes are performed) and the power scattered out the side and out the end of the resonator are measured as functions of the probe frequency. Since the atomic beam extends over many optical wavelengths of the standing-wave mode structure, the coupling strength for each interacting atom is no longer the same. In this chapter, we extend the theory of the previous chapter to model these experiments.

During the course of the experiment, the number of atoms in the mode and their positions fluctuate. Since each atom's coupling strength to the cavity is dependent upon its position, these fluctuations may be manifested in the measured lineshapes. In Sec. 3.1 the semiclassical equations for many, fixed atoms interacting with a SW mode are introduced. For a fixed distribution of N atoms in the mode, a convenient parameter, the intracavity atomic number, $\overline{N}$, is defined. The lineshapes obtained in the various schemes all depend upon this parameter. With the above mentioned fluctuations, $\overline{N}$ becomes a continuous random variable with an associated distribution function. It is therefore necessary to perform an average over the fixed-atom lineshapes in order to realize the results of the experiment.

Fluctuations become important and can have a dramatic effect on the resulting lineshapes when the number of interacting atoms is small. In particular, we study the regime for which $\langle\overline{N}\rangle \approx 1$ where the brackets indicate the average of $\overline{N}$ over the distribution. As will be verified below, the total number of atoms interacting with the mode at any given time, N, must be greater than one to realize $\langle\overline{N}\rangle \approx 1$ so that such experiments do not constitute single atom experiments. We will discuss this point in Sec. 3.2.5.

Expressions for the excitation spectra, the power scattered as functions of coherent probe laser frequency, are derived in all schemes. In Sec. 3.2, simple examples are presented to elucidate certain aspects of the spectra in intermediate, as well as strong coupling regimes. A brief investigation of saturation and its effects is conducted in Sec. 3.3.

3.1 Atoms in a Standing Wave Cavity

The scalar form of the Maxwell–Schrödinger equations (see Eqs. 2.75–2.77) may be used since all dipole and field vectors will be parallel (we assume no birefringence in the cavity mirrors):

$$\ddot{\mathsf{p}}_j(t) + 2\gamma_p \dot{\mathsf{p}}_j(t) + \omega_p^2 \mathsf{p}_j(t) = -\frac{2\mu^2\omega_p}{\hbar}\mathcal{N}_j[\mathsf{E}_\mathsf{c}(\vec{r}_j,t) + \delta_{\epsilon p}\mathsf{E}_L^p(\vec{r}_j,t)], \tag{3.1}$$

$$\ddot{\mathsf{E}}_{\mathsf{c}}(\vec{r},t)+2\gamma_c\dot{\mathsf{E}}_{\mathsf{c}}(\vec{r},t)+\omega_c^2\mathsf{E}_{\mathsf{c}}(\vec{r},t)=-4\pi\ddot{\mathsf{P}}(\vec{r},t)+\delta_{ec}\alpha\mathsf{E}_L^c(\vec{r},t), \tag{3.2}$$

$$\dot{\mathcal{N}}_j+2\gamma_p(\mathcal{N}_j-\mathcal{N}_0^j)=\frac{2[\dot{\mathbf{p}}_j(t)+\gamma_p\mathbf{p}_j(t)][\mathsf{E}_{\mathsf{c}}(\vec{r}_j,t)+\delta_{ep}\mathsf{E}_L^p(\vec{r}_j,t)]}{\hbar\omega_p}, \tag{3.3}$$

with the polarization field, $\mathsf{P}(\vec{r},t)$, and the cavity field, $\mathsf{E}_{\mathsf{c}}(\vec{r},t)=Re[E_c(\vec{r},t)]$ where

$$\mathsf{P}(\vec{r},t)=Re\left[\sum_{j=1}^{N}p_j(t)\delta^3(\vec{r}-\vec{r}_j)\right], \qquad E_c(\vec{r},t)=E_0\psi(\vec{r})\mathcal{E}(t), \tag{3.4}$$

with $p_j(t)$ the (complex) dipole moment and $\vec{r}_j$ the position of the j^{th} atom ($j=1,\ldots,N$), and with N the total number of atoms. All assumptions and conditions made in Chapter 2 regarding the domain of validity of this model are in effect here as well. The end excitation field is $\mathsf{E}_L^c(\vec{r},t)=Re[E_L^c(\vec{r},t)]$, and the side excitation field is $\mathsf{E}_L^p(\vec{r},t)=Re[E_L^p(\vec{r},t)]$ where

$$E_L^c(\vec{r},t)=E_L^c(t)\psi(\vec{r}), \qquad E_L^p(\vec{r},t)=E_L^p(t)\phi(\vec{r}), \tag{3.5}$$

with mode functions

$$\psi(\vec{r})=e^{-\left(\frac{x^2+y^2}{\omega_0^2}\right)}\sin kz, \qquad \phi(\vec{r})=e^{-\left(\frac{r}{\omega_l}\right)^2}, \tag{3.6}$$

where $r^2=x^2+z^2$. We assume that the atoms interact with only the TEM_{00} cavity mode. The orientation of the coordinate axes, assumed throughout the text, is depicted in Fig. 3-1. Note that the end excitation field is mode–matched to the (SW) TEM_{00} cavity mode, with waist ω_0, whereas the side excitation field is a TEM_{00} traveling wave with arbitrary waist, ω_l. Furthermore, we neglect dipole–dipole interactions since atomic beam densities are low. Shown in Fig. 3-2 is a "snapshot" of the situation represented here. The height of each atom in the figure (dots) is a representation of its coupling strength to the mode. Normalization of the cavity mode field yields

$$\frac{1}{4\pi}\int E_0^2\psi^2(\vec{r})dV=\frac{\hbar\omega}{2}\Longrightarrow E_0=\sqrt{\frac{2\pi\hbar\omega}{V}}, \tag{3.7}$$

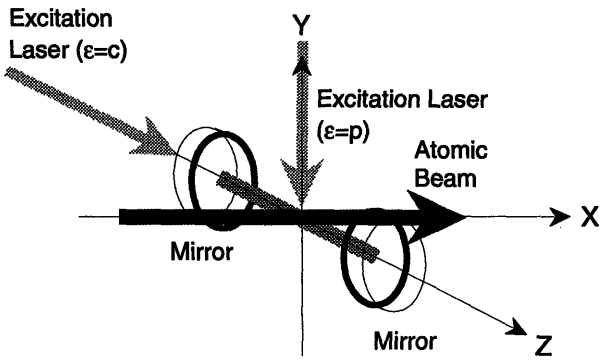

Figure 3-1: Orientation of the coordinate system used in the text. The optical axis defines the z axis.

with $V = \frac{1}{4}\pi\omega_0^2 L$ the mode volume.

Multiplying Eq. 3.2 by $\frac{E_0\psi(\vec{r})}{4\pi}$ and integrating over all space we obtain

$$\ddot{p}_j(t) + 2\gamma_p\dot{p}_j(t) + \omega_p^2 p_j(t) = -\frac{2\mu^2\omega_p}{\hbar}\mathcal{N}_j[E_0\psi(\vec{r}_j)\mathcal{E}(t) + \delta_{\epsilon p}E_L^p(t)\phi(\vec{r}_j)],, \tag{3.8}$$

$$\ddot{\mathcal{E}}(t) + 2\gamma_c\dot{\mathcal{E}}(t) + \omega_c^2\mathcal{E}(t) = -\frac{2E_0}{\hbar\omega}\sum_{j=1}^{N} p_j(t)\psi(\vec{r}_j) + \delta_{\epsilon c}\alpha\frac{E_L^c}{E_0}, \tag{3.9}$$

$$\dot{\mathcal{N}}_j + 2\gamma_p(\mathcal{N}_j - \mathcal{N}_0^j) = \frac{2[\dot{\mathbf{p}}_j(t) + \gamma_p\mathbf{p}_j(t)][\mathsf{E}_\mathsf{c}(\vec{r}_j,t) + \delta_{\epsilon p}\mathsf{E}_L^p(\vec{r}_j,t)]}{\hbar\omega_p}. \tag{3.10}$$

Note that Doppler and transit time broadening effects can be studied if atomic motion through the cavity mode is included by assuming the appropriate time dependence for the $\vec{r}_j$'s. For simplicity, however, we neglect such effects since these will be small in the experiments to be described.

We now assume coherent driving fields and the slowly varying envelope approximations, as in Eqs. 2.80–2.82 of Sec. 2.2.3, by replacing $\mathcal{E}(t) \to \mathcal{E}(t)e^{i\Omega t}$, $E_L^{c,p}(t) \to E_L^{c,p}(t)e^{i\Omega t}$, and $p_j(t) \to p_j(t)e^{i\Omega t}$ to obtain (keeping the same notation for the slowly varying amplitudes)

$$\dot{p}_j - \mathcal{L}_p(\Omega)p_j = \frac{i\mu^2}{\hbar}\mathcal{N}_j[E_0\psi(\vec{r}_j)\mathcal{E}(t) + \delta_{\epsilon p}E_L^p\phi(\vec{r}_j)], \tag{3.11}$$

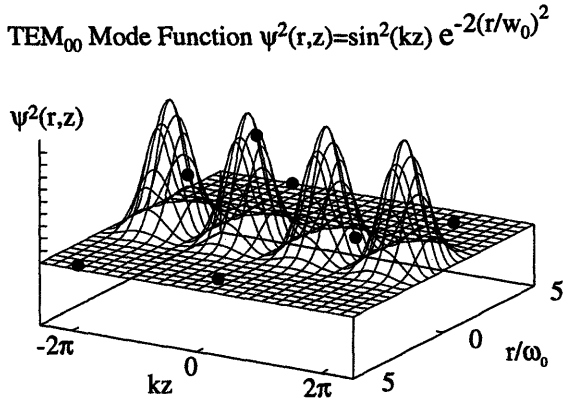

Figure 3-2: Atoms coupled to a TEM_{00} standing-wave cavity mode with mode function $\psi(r,z)$. z is along the optical axis and r is the radial distance from the mode center with waist ω_0

$$\dot{\mathcal{E}}(t) - \mathcal{L}_c(\Omega)\mathcal{E}(t) = -\frac{iE_0}{\hbar}\sum_{j=1}^{N} p_j(t)\psi(\vec{r}_j) + \delta_{\epsilon c}\left(\frac{\alpha}{2i\Omega}\right)\frac{E_L^c}{E_0}, \tag{3.12}$$

$$\dot{\mathcal{N}}_j(t) + 2\gamma_p(\mathcal{N}_j(t) - \mathcal{N}_j^0) = -\frac{Im[p_j(t)(E_0\psi(\vec{r}_j)\mathcal{E}(t) + \delta_{\epsilon p}E_L^p\phi(\vec{r}_j))^*]}{\hbar}, \tag{3.13}$$

where Ω represents the driving field's frequency.

3.1.1 Cavity Excitation.

Before obtaining the steady state solutions of Eqs. 3.11–3.13, note that a coherent, weighted sum of the dipoles (a "macroscopic" dipole) excites the cavity mode (Eqs. 3.9 and 3.12) for the driven cavity case. Multiplying Eq. 3.11 by $\psi(\vec{r}_j)$ and summing over j gives

$$\dot{P}(t) - \mathcal{L}_p(\Omega)P(t) = -\frac{i\mu^2}{\hbar}[E_0\overline{N}\mathcal{E}(t)], \tag{3.14}$$

for the "macroscopic" dipole oscillator,

$$P(t) = \sum_{j=1}^{N} p_j(t)\psi(\vec{r}_j), \tag{3.15}$$

and

$$\dot{\mathcal{E}}(t) - \mathcal{L}_c(\Omega)\mathcal{E}(t) = -\frac{iE_0}{\hbar}P(t) + \delta_{\epsilon c}\left(\frac{\alpha}{2i\Omega}\right)\frac{E_L^c}{E_0}, \tag{3.16}$$

for the cavity field oscillator. Therefore for the $\epsilon = c$ case, Eqs. 3.11 and 3.12 reduce to two simple, coupled oscillator equations.

The steady state solutions for the driven cavity case, which are generalizations of Eqs. 2.83 and 2.84 with $\epsilon = c$, are

$$p_j^{\epsilon=c}(\Omega) = -\frac{i\mu^2}{\hbar}\frac{\alpha}{2i\Omega}\left[\frac{\psi(\vec{r}_j)E_L^c}{\mathcal{L}_p(\Omega)\mathcal{L}_c(\Omega) + \overline{N}g_0^2}\right], \tag{3.17}$$

and

$$\mathcal{E}^{\epsilon=c}(\Omega) = -\frac{\alpha}{2i\Omega}\frac{E_L^c}{E_0}\left[\frac{\gamma_c\mathcal{L}_p(\Omega)}{\mathcal{L}_p(\Omega)\mathcal{L}_c(\Omega) + \overline{N}g_0^2}\right], \tag{3.18}$$

where

$$\overline{N} = \sum_{j=1}^{N}\psi^2(\vec{r}_j), \qquad g_0 = \frac{\mu E_0}{\hbar}. \tag{3.19}$$

In these expressions we assume weak excitation so that level populations do not change significantly and the inversion equation (3.13) may be neglected ($\mathcal{N}_j \approx -1$ for all j). Solutions which include the population equation will be discussed later when considering the role of saturation (Sec. 3.3).

Intra-cavity Atomic Number

As mentioned in the introduction to this chapter, we define $\overline{N}$ to be the number of *intra-cavity* atoms when N atoms, an integer number, are randomly dropped in the atomic beam volume which overlaps the cavity mode volume (for an illustration, see Fig. 3-2). Details of this will be provided below. It should only be noted here that, on average, $\overline{N}$ will not be the same as the total number of atoms in the experiment (i.e., the number of atoms in the atomic beam, N). To obtain $\overline{N} = N$ all atoms must fall at anti-nodes along the cavity axis so that $\psi(\vec{r}_j) = 1$ for all j. This is an extremely unlikely occurrence.

During the course of the atomic beam experiment, both N and the atomic positions will fluctuate. Thus $\overline{N}$ is a continuous random variable which will have an

associated probability distribution. We must therefore perform an ensemble average, described below in Sec. 3.2.2, to compare theory with experiment. The power emitted out the end therefore follows from

$$P_{end}^{\epsilon=c}(\Omega) = \eta_{cav}\hbar\omega 2\gamma_c \left\langle \frac{\int |E_0\psi(\vec{r})\mathcal{E}^{\epsilon=c}(\Omega)|^2 dV}{8\pi} \right\rangle_{ave}. \tag{3.20}$$

Evaluating the integral using Eq. 3.7 and substituting Eq. 3.18, we obtain

$$P_{end}^{\epsilon=c}(\Omega) = T_0\hbar\omega\gamma_c \left\langle \left| \frac{\mathcal{L}_p(\Omega)}{\mathcal{L}_p(\Omega)\mathcal{L}_c(\Omega) + \overline{N}g_0^2} \right|^2 \right\rangle_{ave}, \tag{3.21}$$

with

$$T_0 = 2\eta_{cav}^2 I_L \frac{V}{L}, \tag{3.22}$$

the empty cavity peak transmission and where $\langle\rangle_{ave}$ now denotes the required ensemble average (compare Eq. 2.87).

To obtain the total power scattered out the side of the cavity, however, we must incoherently add each dipole's contribution, using Larmor's formula (Eq. 2.92). The random positions of the dipoles imply random relative phases of their fields emitted out the side. Thus,

$$P_{side}^{\epsilon=c}(\Omega) = \frac{\omega^4}{3c^3} \left\langle \sum_{j=1}^{N} |p_j^{\epsilon=c}(\Omega)|^2 \right\rangle_{ave} (1-f), \tag{3.23}$$

with $p_j^{\epsilon=c}(\Omega)$ given in Eq. 3.17. Substitution gives

$$P_{side}^{\epsilon=c}(\Omega) = \left|\frac{\alpha}{2i\Omega}\right|^2 \frac{I_L}{I_s}\hbar\omega\gamma_p^2 \left\langle \frac{\overline{N}\gamma_p}{|\mathcal{L}_p(\Omega)\mathcal{L}_c(\Omega) + \overline{N}g_0^2|^2} \right\rangle_{ave} (1-f), \tag{3.24}$$

with I_L and I_s defined following Eq. 2.86 (compare Eq. 2.96). Since the experiments to be described are performed with cavities for which $f \approx 10^{-4}$, we will suppress the $(1-f)$ factor henceforth. Of course, any discussions involving the degenerate resonators, concentric or confocal, cannot neglect this term since typically $f \approx 10^{-1}$. However, as pointed out in the introduction, the results of this chapter do not apply

to degenerate cavities.

3.1.2 Atom Excitation.

The steady state solutions for the driven atom case, which are generalizations of Eqs. 2.83 and 2.84 with $\epsilon = p$, are

$$p_j^{\epsilon=p}(\Omega) = \frac{i\mu^2 E_L^p}{\hbar \mathcal{L}_p(\Omega)} \left[\phi(\vec{r}_j) - \psi(\vec{r}_j) \frac{g_0^2 \sum_{k=1}^N \psi(\vec{r}_k)\phi(\vec{r}_k)}{\mathcal{L}_p(\Omega)\mathcal{L}_c(\Omega) + \overline{N} g_0^2} \right], \tag{3.25}$$

and

$$\mathcal{E}^{\epsilon=p}(\Omega) = -\frac{\mu E_L^p}{\hbar} \frac{g_0 \sum_{j=1}^N \psi(\vec{r}_j)\phi(\vec{r}_j)}{\mathcal{L}_p(\Omega)\mathcal{L}_c(\Omega) + \overline{N} g_0^2}. \tag{3.26}$$

Using Eq. 3.20 with the appropriate $\epsilon = p$ terms, the total power emitted out the cavity ends is (compare Eq. 2.86)

$$P_{ends}^{\epsilon=p}(\Omega) = \eta_{cav} \frac{I_L}{I_s} \hbar\omega \gamma_p^2 \gamma_c \left\langle \frac{N' g_0^2}{|\mathcal{L}_p(\Omega)\mathcal{L}_c(\Omega) + \overline{N} g_0^2|^2} \right\rangle_{ave}. \tag{3.27}$$

Similarly, the total power scattered out the cavity side is (compare Eq. 2.95)

$$P_{side}^{\epsilon=p}(\Omega) = \frac{I_L}{2I_s} \gamma_p \hbar\omega \frac{\gamma_p^2}{|\mathcal{L}_p(\Omega)|^2} \left\langle N_{exc} - \frac{N' g_0^2 [2Re(\mathcal{L}_c(\Omega)\mathcal{L}_p(\Omega)) + \overline{N} g_0^2]}{|\mathcal{L}_p(\Omega)\mathcal{L}_c(\Omega) + \overline{N} g_0^2|^2} \right\rangle_{ave}, \tag{3.28}$$

where

$$N_{exc} = \sum_{j=1}^N \phi^2(r_j), \qquad N' = \left(\sum_{j=1}^N \phi(\vec{r}_j)\psi(\vec{r}_j) \right)^2. \tag{3.29}$$

In comparing these results with the fixed atom results of Sec. 2.2.3, the interference of the individual dipoles has a significant effect on the sidelight lineshapes for the dipole emission out the side. This point will be further dramatized in the experimental results.

To simplify the above expressions, we consider the special case in which all atoms are excited uniformly ($\phi(\vec{r}_j) = 1$). In this case $N_{exc} \equiv N$. Furthermore, we can write

$$N' = \left(\sum_{j=1}^N \psi(\vec{r}_j) \right)^2 = \overline{N} + \sum_{j \neq k} \psi(\vec{r}_j)\psi(\vec{r}_k). \tag{3.30}$$

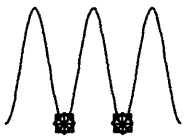

Figure 3-3: $N_{exc} = 2$, $N' = 0$, $\overline{N} = 0$.

In performing the ensemble average, the second term in Eq. 3.30 will occur with alternating signs so that any term which it multiplies will average to zero. Thus N' may be replaced by $\overline{N}$ to get:

$$P_{ends}^{\epsilon=p}(\Omega) = \eta_{cav}\frac{I_L}{I_s}\hbar\omega\gamma_p^2\gamma_c\left\langle\frac{\overline{N}g_0^2}{|\mathcal{L}_p(\Omega)\mathcal{L}_c(\Omega)+\overline{N}g_0^2|^2}\right\rangle_{ave}; \tag{3.31}$$

and

$$P_{side}^{\epsilon=p}(\Omega) = \frac{I_L}{2I_s}\gamma_p\hbar\omega\gamma_p^2\left[\frac{\langle N\rangle_{ave}-1}{|\mathcal{L}_p(\Omega)|^2}+\left\langle\frac{|\mathcal{L}_c(\Omega)|^2}{|\mathcal{L}_p(\Omega)\mathcal{L}_c(\Omega)+\overline{N}g_0^2|^2}\right\rangle_{ave}\right]. \tag{3.32}$$

The lineshape for the sidelight, when exciting the atoms, contains a contribution from two terms: A free-atom lineshape proportional to $\langle N\rangle - 1$ and a "single atom" lineshape with an effective coupling given by $\sqrt{\overline{N}}g_0$.

3.2 Discussion

To elucidate the results of the previous section, we consider simple cases of two atoms fixed at various positions along the SW cavity mode axis and neglect fluctuations. If both are located at the nodes and equally excited ($\phi(\vec{r}_j) = 1$ for $j = 1, 2$), then $\overline{N} = N' = 0$ in the above equations (Fig. 3-3). For the driven cavity case only the transmitted (empty cavity) signal survives (Eq. 3.33) and for the driven atom case

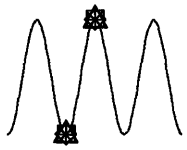

Figure 3-4: $N_{exc} = 2$, $N' = 1$, $\overline{N} = 1$.

only the side signal survives (Eq. 3.34):

$$P_{end}^{\epsilon=c}(\Omega) = T_0 \hbar\omega \frac{\gamma_c}{|\mathcal{L}_c(\Omega)|^2}, \qquad P_{side}^{\epsilon=c}(\Omega) = 0; \tag{3.33}$$

$$P_{ends}^{\epsilon=p}(\Omega) = 0, \qquad P_{side}^{\epsilon=p}(\Omega) = N_{exc} \frac{I_L}{2I_s} \gamma_p \hbar\omega \frac{\gamma_p^2}{|\mathcal{L}_p(\Omega)|^2}. \tag{3.34}$$

For $\epsilon = c$, atoms not coupled to the cavity mode give rise to an empty cavity transmission lineshape and for $\epsilon = p$, they give rise to a free atom lineshape signal out the side.

Now consider one atom at a node and the other at an anti-node (Fig. 3-4). The resulting expressions for the various observable signals are:

$$P_{ends}^{\epsilon=c}(\Omega) \propto \left| \frac{\mathcal{L}_p(\Omega)}{\mathcal{L}_p(\Omega)\mathcal{L}_c(\Omega) + g_0^2} \right|^2, \qquad P_{side}^{\epsilon=c}(\Omega) \propto \left| \frac{1}{\mathcal{L}_p(\Omega)\mathcal{L}_c(\Omega) + g_0^2} \right|^2; \tag{3.35}$$

$$P_{ends}^{\epsilon=p}(\Omega) \propto \left| \frac{1}{\mathcal{L}_p(\Omega)\mathcal{L}_c(\Omega) + g_0^2} \right|^2, \; P_{side}^{\epsilon=p}(\Omega) \propto \left| \frac{\mathcal{L}_c(\Omega)}{\mathcal{L}_p(\Omega)\mathcal{L}_c(\Omega) + g_0^2} \right|^2 + \frac{1}{|\mathcal{L}_p(\Omega)|^2}. \tag{3.36}$$

In this case both side and end signals for $\epsilon = c$ as well as the end signal for $\epsilon = p$, (Eqs. 3.35 and 3.36), give rise to the expected single-atom lineshapes, similar to those derived in the previous chapter. However, the side signal for the driven atom case ($\epsilon = p$) contains an additional term. It arises from the uncoupled atom which nonetheless is excited by the side probe and radiates as a free atom. Thus, excitation of the atom-cavity system from the side includes the contribution of uncoupled atoms

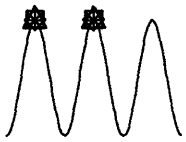

Figure 3-5: $N_{exc} = 2$, $N' = 0$, $\overline{N} = 2$.

to the sidelight signal.

Placing two atoms at consecutive anti-nodes of the resonator, Fig. 3-5, gives $\psi(\vec{r}_1) = -\psi(\vec{r}_2)$ because $r = 0$ and $\sin kz_1 = -\sin kz_2$. We therefore have

$$P_{ends}^{\epsilon=c}(\Omega) \propto \left| \frac{\mathcal{L}_p(\Omega)}{\mathcal{L}_p(\Omega)\mathcal{L}_c(\Omega) + 2g_0^2} \right|^2, \qquad P_{side}^{\epsilon=c}(\Omega) \propto \left| \frac{2}{\mathcal{L}_p(\Omega)\mathcal{L}_c(\Omega) + 2g_0^2} \right|^2; \quad (3.37)$$

$$P_{ends}^{\epsilon=p}(\Omega) = 0, \qquad P_{side}^{\epsilon=p}(\Omega) \propto \frac{1}{|\mathcal{L}_p(\Omega)|^2}. \quad (3.38)$$

The driven cavity results, Eqs. 3.37, exhibit an effective coupling parameter ($\sqrt{2}g_0$) which is larger than the single atom coupling, g_0, because of the cooperative nature of the interaction (coherent). The driven atom case, Eqs. 3.38, on the other hand, gives quite different results which are explained as follows: The side probe forces the dipoles to oscillate in phase. However, since they are located at two consecutive anti-nodes, they must oscillate *out of phase* with respect to each other for their respective scattered fields to constructively interfere with the cavity field. The net result is *no* scattering into the cavity because of destructive interference. Since the scattering out the side is *incoherently* added, free atom lineshapes occur as in the previous dipole configuration, but no contribution due to the presence of the cavity arises since there is no cavity field.

Finally, the solutions for two atoms located at alternate anti-nodes, see Fig. 3-6,

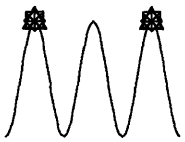

Figure 3-6: $N_{exc} = 2$, $N' = 4$, $\overline{N} = 2$.

are

$$P_{ends}^{\epsilon=c}(\Omega) \propto \left| \frac{\mathcal{L}_p(\Omega)}{\mathcal{L}_p(\Omega)\mathcal{L}_c(\Omega) + 2g_0^2} \right|^2, \qquad P_{side}^{\epsilon=c}(\Omega) \propto \left| \frac{2}{\mathcal{L}_p(\Omega)\mathcal{L}_c(\Omega) + 2g_0^2} \right|^2; \quad (3.39)$$

$$P_{ends}^{\epsilon=p}(\Omega) \propto \left| \frac{2}{\mathcal{L}_p(\Omega)\mathcal{L}_c(\Omega) + 2g_0^2} \right|^2, \qquad P_{side}^{\epsilon=p}(\Omega) \propto \frac{2|\mathcal{L}_c(\Omega)|^2}{|\mathcal{L}_p(\Omega)\mathcal{L}_c(\Omega) + 2g_0^2|^2}. \quad (3.40)$$

In this case all fields add constructively and a non-zero cavity field exists in the driven atom case, $P_{ends}^{\epsilon=p}(\Omega)$, in contrast with the previous example.

In describing the various lineshapes recorded, the notation "CC", "CP", "PC", or "PP" will be used to denote a particular "excitation-observation" scheme. For example, "CP" implies the arrangement in which the cavity (C) is excited by the probe and the light scattered out the cavity side by the atom (P) is measured. Similarly, "PC" refers to excitation of the atom directly by a side probe and observation of the light scattered out the resonator end. Note that the $P_{ends}^{\epsilon=c}(\Omega)$ and $P_{side}^{\epsilon=p}(\Omega)$ lineshapes (schemes labeled as CC and PP, respectively) can give rise to nonzero signals in the absence of atom-cavity coupling: In the PP scheme, an atom at a node radiates out the side as though no cavity is present. The same situation for the CC scheme gives rise to an empty cavity signal. The CP and PC signals ($P_{side}^{\epsilon=c}(\Omega)$ and $P_{ends}^{\epsilon=p}(\Omega)$, respectively), on the other hand, arise only when the atom is coupled to the cavity.

3.2.1 Coupling Regimes

In Sec. 2.3, three regimes were defined in order to characterize lineshapes for a fixed atom(s): (1) Weak coupling in which single-peaked lineshapes result from exponential decay, (2) Intermediate Coupling for both single and two-peaked lineshapes, and (3) Strong Coupling in which two-peaked lineshapes result from oscillatory energy exchange. In this chapter, we desire a single parameter to characterize the coupling regimes under study. Given the complexities introduced by fluctuations, we define this parameter for a single, optimally coupled atom. It therefore is dependent only upon the properties of the cavity and atom, and not the atomic location or number:

$$\xi = \left(\frac{2g_0}{\gamma_c - \gamma_p} \right)^2 . \tag{3.41}$$

Three regimes may then be characterized as follows: (1) strong coupling ($\xi \gg 1$); (2) intermediate coupling ($\xi \approx 1$) and (3) weak coupling ($\xi \ll 1$). Note that ξ also determines the mathematical condition for the existence of two nondegenerate normal modes of oscillation, i.e., $\xi \leq 1$ and $\xi > 1$ give rise to degenerate (overdamped) and nondegenerate (underdamped) normal mode frequencies, respectively (see Eqs. 2.35 and 2.36).

3.2.2 Ensemble Averages

The required ensemble averages for the lineshapes derived in Sec. 3.1 are performed in a computer simulation: Many trials, each consisting of random placement of a large, but fixed, number of atoms ($\propto \rho_0$, the atomic beam density) in a volume defined by the atomic beam, are performed. In each trial, only those atoms, N, falling within a small fraction of the atomic beam, centered on the cavity mode axis, are included in the sum to estimate $\overline{N}$ (Eq. 3.19). The volume of this fraction is chosen large enough so that all atoms outside, if included, would make a negligible contribution to $\overline{N}$. As an example, the situation depicted in Fig. 3-2 may be considered. However, the atomic beam in this case spans only two wavelengths whereas the atomic beam spans

$\approx$ 400 nodes in the actual experimental setup!

From trial to trial, both the number of atoms, N, and their positions will fluctuate (i.e., from "snapshot" to "snapshot"). The lineshapes derived in Sec. 3.1 depend upon intra-cavity atomic number, $\overline{N}$, and therefore may be sensitive to fluctuations in $\overline{N}$, particularly when $\overline{N}$ is small. To clearly see this, note that these fluctuations are characterized by two distribution functions, $P(N)$ and $\mathrm{P}(\overline{N})$. The distribution for the intra-cavity atomic number is shown in Fig. 3-7(a) for several values of ρ_0 ($\propto \langle\overline{N}\rangle$). The distribution for N follows the usual Poissonian distribution function as expected and is not shown. These computer generated curves are determined by the number of times a particular value of $\overline{N}$ occurs in the simulation, divided by the total number of trials. The curves in (b-e) are lineshapes for specific values of $\overline{N}$, i.e., with no fluctuations. They are obtained from the appropriate fixed-atom equations in Sec. 3.1, in which $\mathcal{N}g_0^2$ is replaced by $-\overline{N}g_0^2$. (Also see the discussion for the two-atom cases in this section, above.) For a given $\langle\overline{N}\rangle$, the resulting ensemble averaged lineshape is calculated as a weighted average of these lineshapes with the appropriate $\mathrm{P}(\overline{N})$ distribution in (a).

3.2.3 Intermediate Coupling Regime

To investigate lineshapes in the intermediate coupling regime, we asssume the following values for the system parameters: $F = 2.7 \times 10^4$, $L = 1$ mm, $R = 150$ cm, and $\lambda = 553.5$ nm. These values correspond to those used in Fig. 2-5 of Sec. 2.3.1 for the single, fixed atom case, where $g_0/\gamma_p = 0.3$, and $\gamma_c/\gamma_p = 0.3$ ($\xi = 0.86$, narrow cavity limit). In this regime, the two normal mode frequencies are degenerate and no oscillatory exchange of energy can occur with one atom. Nonetheless, a two-peaked lineshape arises, as seen in Fig. 2-5(b) for an optimally coupled atom. To see the effects of fluctuations, we now compare this result with the computed lineshapes for several values of beam density, shown in Fig. 3-8 for the driven atom case ($\epsilon = p$). Several points should be noted in Fig. 3-8. First, trace (a) exhibits a splitting (barely visible) in the sidelight lineshape of the atom (light scattered out the resonator side). This surprising feature has been discussed in Sec. 2.3.1 and again in Sec. 2.3.2 with

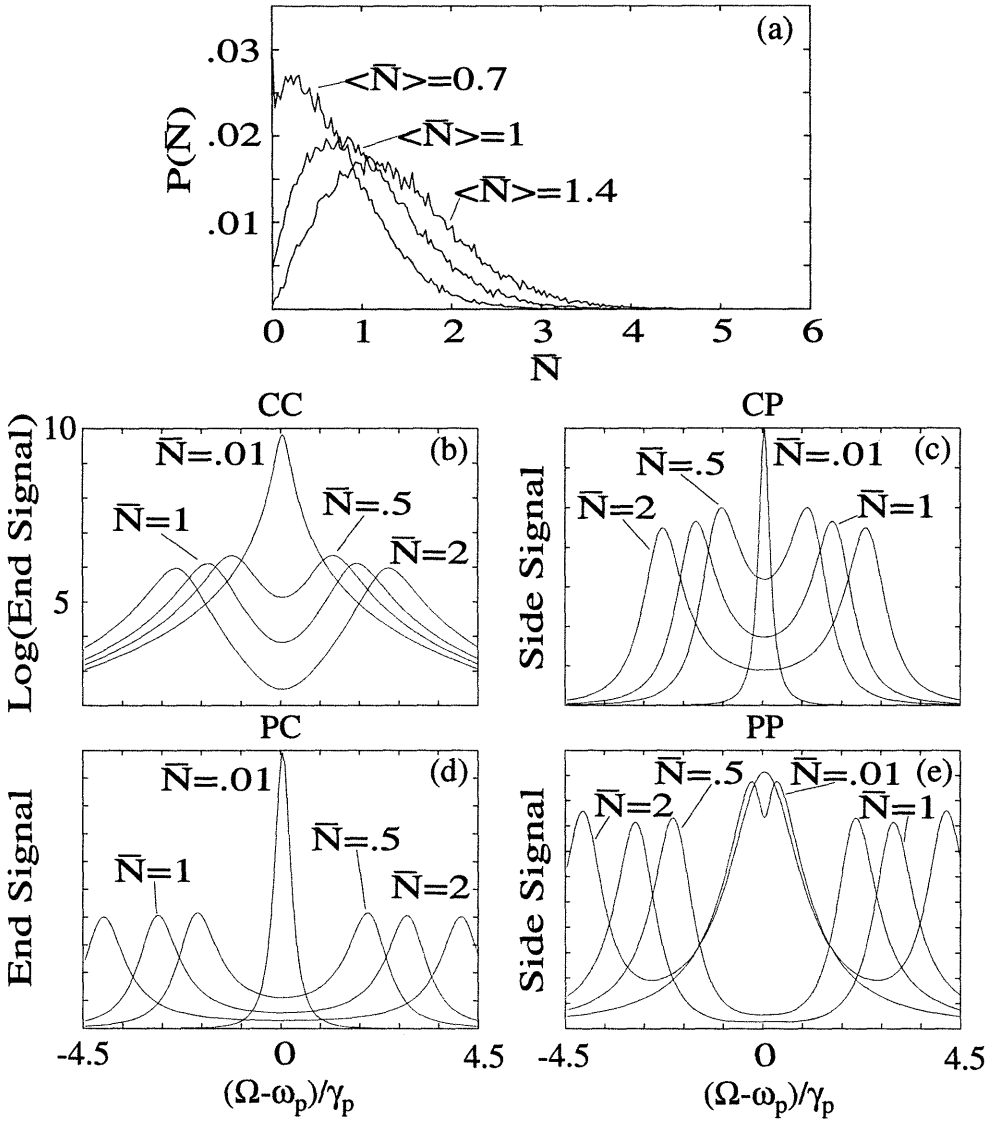

Figure 3-7: (a) Probability distribution, $P(\overline{N})$. (b-e) Fixed-atom lineshapes for five values of $\overline{N}$ in the strong coupling regime ($\xi = 16$). All possible schemes are shown: (b) CC, (c) CP, (d) PC, and (e) PP. Note the log scale in (b) only.

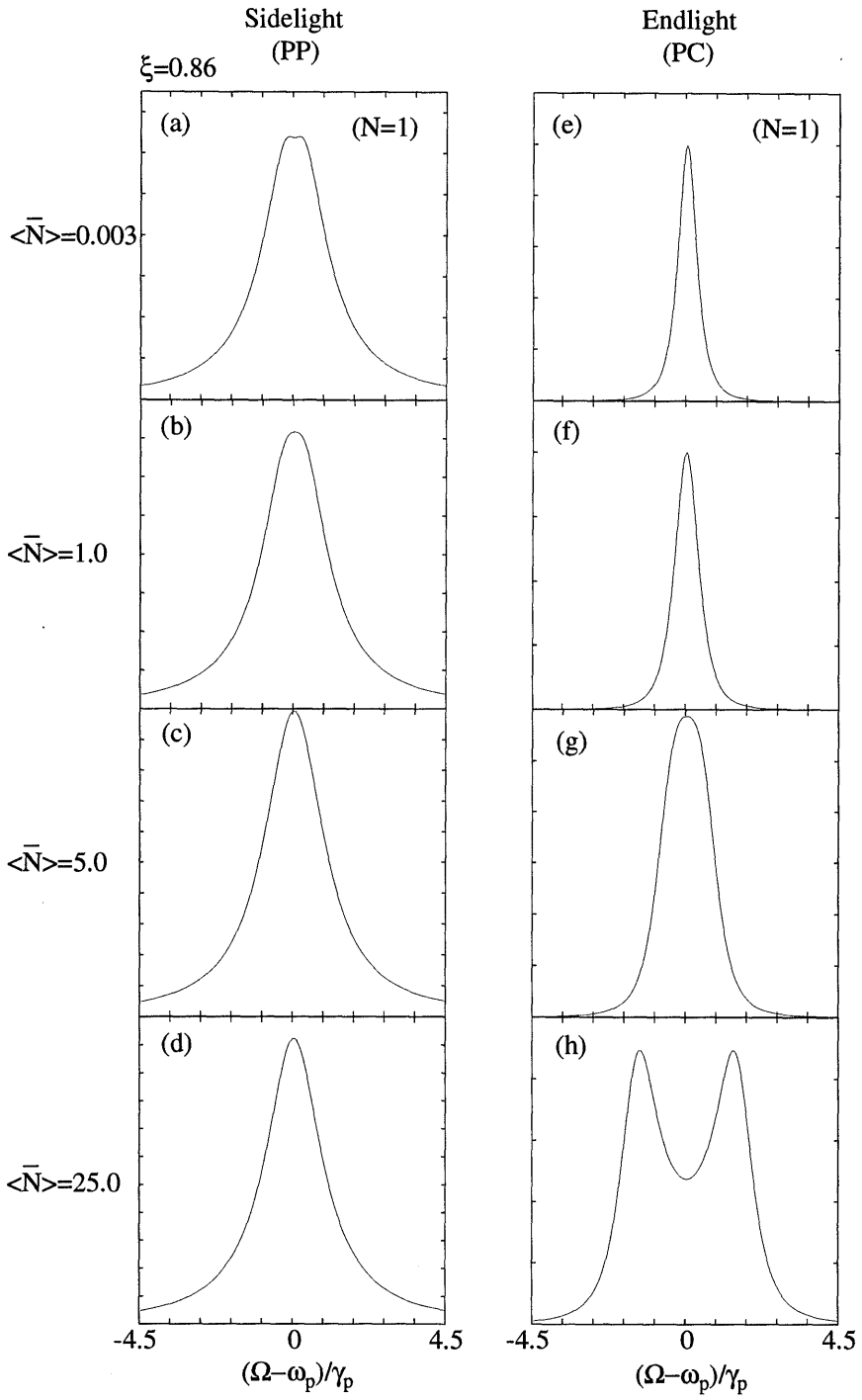

Figure 3-8: Intermediate coupling ($\xi = 0.86$) lineshapes for driven-atom case ($\epsilon = p$) in the narrow cavity limit for several values of $\langle \overline{N} \rangle$.

regard to a fixed atom. It arises from the fact that the atom undergoes enhanced emission into the resonator mode within the cavity's bandwidth. With this enhanced emission, the excited state population decreases (in comparison to the free atom case) and the sidelight, which is a measure of this population, also decreases. Note, however, that the corresponding total spontaneous emission rate is only slightly enhanced ($= \frac{(g_0/\gamma_p)^2}{1+(\gamma_c/\gamma_p)} \approx 7\%$ increase). A related interpretation was given in Sec. 2.3.2: The intra-cavity field is out of phase with the driving field so that as it builds up, the total field at the atom is reduced with subsequent suppression of the atomic radiation out the side.

The density for the curves in (a) and (e) of Fig. 3-8 corresponds to the situation in which no more than one atom is in the mode at a time ($N = 1$ or $N = 0$), and the atom's position over the active volume is randomly varying. Trace (a) exhibits a significantly reduced splitting in comparison with the sidelight trace of Fig. 2-5 for the single fixed-atom case. The diminished, or lack of, splitting in traces (a-d), however, occur because the contribution of free atoms to the sidelight is significant, and washes out the two-peaked lineshapes arising from the coupled atoms (see Eq. 3.32). Trace (b), with a much larger atomic beam density so that there is now one *intra-cavity* atom, $\langle \overline{N} \rangle = 1$, exhibits no splitting. Similarly, traces (e-g) do not exhibit splitting but, as the intra-cavity atomic number increases, the "effective coupling", $\sqrt{\langle \overline{N} \rangle} g_0$, becomes larger and the system eventually becomes strongly coupled. Therefore, the cavity lineshape in trace (h) exhibits splitting as expected. The lack of splitting in traces (e-f) is consistent with the lack of oscillatory energy exchange. The equation for the cavity lineshape in the driven atom case has no Lorentzian factor in the numerator and any splitting arises only as a result of nondegenerate normal mode frequencies (Eq. 3.31).

We now consider the following values for the system parameters: $F = 5.8 \times 10^3$, $R = 10$ cm, $L = 240$ μm, and $\lambda = 553.5$ nm. These parameters give $g_0/\gamma_p = 1.75$ and $\gamma_c/\gamma_p = 5.7$ and correspond to the broad cavity, $\epsilon = c$ case which should also exhibit lineshape splitting with degenerate normal mode frequencies (compare with the above narrow cavity, $\epsilon = p$ case). Shown in Fig. 3-9 are the resulting lineshapes.

An experiment to demonstrate these effects is performed for these parameters in which the *cavity mode* is excited in the intermediate, *broad cavity* regime, and is described in Chapter 4. Similar to the discussion in the driven atom case, above, lineshape splitting in the CP scheme indicates oscillatory energy exchange whereas the splitting in the CC scheme, trace (f), arises only from the "blocking" action of the atoms in the cavity mode. With increasing atomic beam density enough atoms will eventually be coupled to the mode to place the system in the strong coupling regime so that splitting appears in both the CC and CP lineshapes (traces (h) and (d), respectively).

3.2.4 Strong Coupling Regime

In the strong coupling regime, the sidelight and transmission lineshapes for the $\epsilon = c$ scheme, are shown in traces (a-d) and (e-h), respectively, of Fig. 3-10, for several values of $\rho_0 \propto \langle \overline{N} \rangle$. We choose the values $g_0/\gamma_p = 1.28$ and $\gamma_c/\gamma_p = 0.36$, corresponding to those in the experiment performed by Thompson *et al.* [21]. Note that only cavity transmission was measured in this study. The two-peaked lineshapes in transmission are evidence for oscillatory energy exchange. (Note that the notation $\overline{N}$ in that work corresponds to $\langle \overline{N} \rangle$ used here.) In light of the splitting described in the previous paragraph for intermediate coupling, this interpretation is unambiguously confirmed by the two similar peaks in the sidelight, traces (b-d). Note that as $\langle \overline{N} \rangle \rightarrow 0$, the lineshape splitting is seen to reduce. Furthermore, the lineshapes for $\langle \overline{N} \rangle = 1$, traces (b) and (f), exhibit a reduced splitting when compared with the corresponding lineshapes derived from Eqs. 2.96 and 2.87, respectively, for the single fixed-atom case. In order to explain this, refer again to Fig. 3-7. For $\langle \overline{N} \rangle \approx 1$, trace (a) exhibits the probability that a given $\overline{N}$ occurs. The *effective* coupling parameter that determines the lineshape is $\overline{N} g_0^2$. For small $\overline{N}$ the system is weakly coupled with a single lineshape and for large $\overline{N}$ it is strongly coupled with a two-peaked lineshape. Averaging these possible outcomes together can reduce the magnitude of the splitting, as seen in traces (e-g) of Fig 3-10. Again, curves (a-d) exhibit less splitting than the corresponding curves (e-h) of this figure because of the Lorentzian

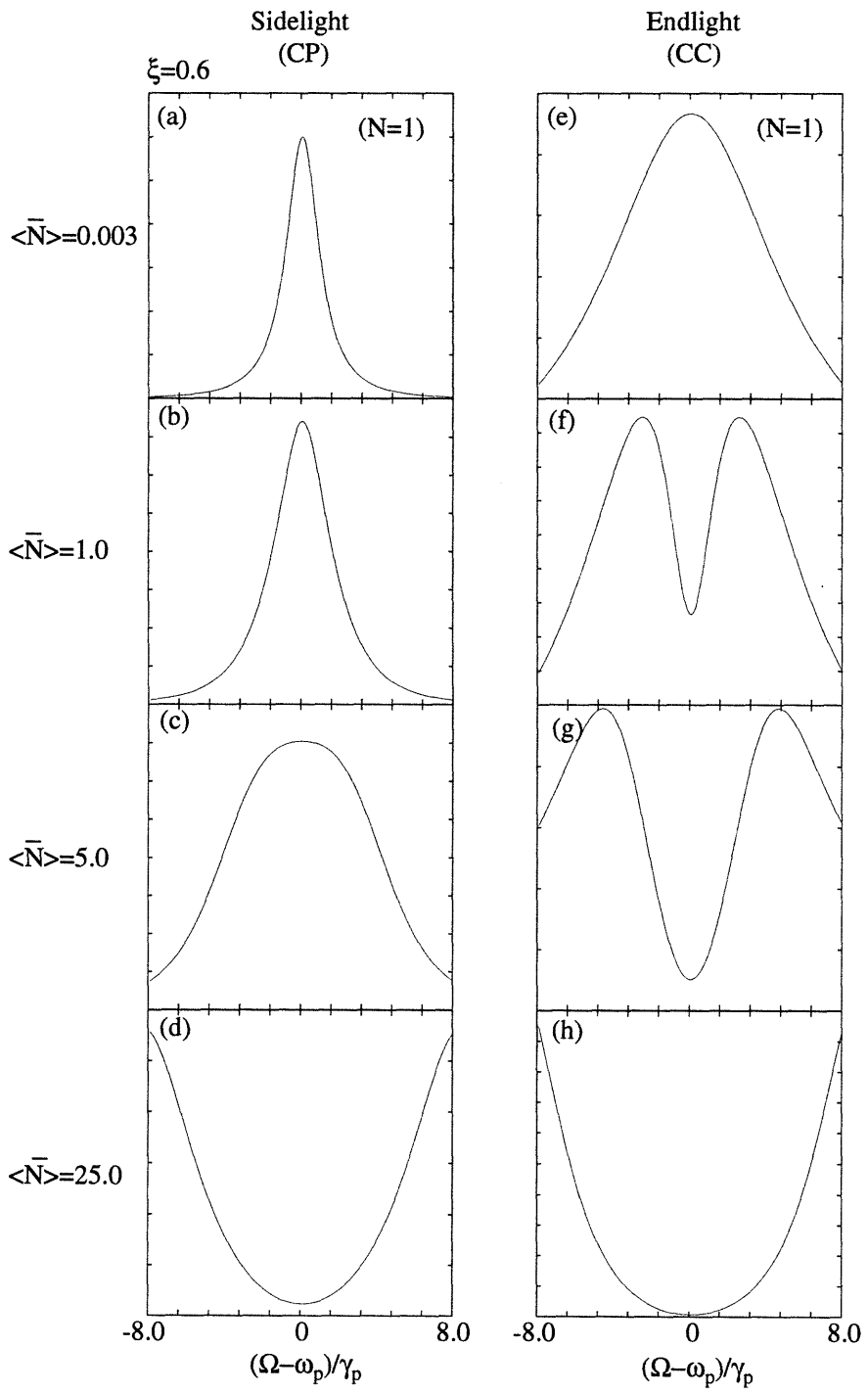

Figure 3-9: Intermediate coupling ($\xi = 0.6$) lineshapes for driven-cavity case ($\epsilon = c$) in the broad cavity limit for several values of $\langle \overline{N} \rangle$.

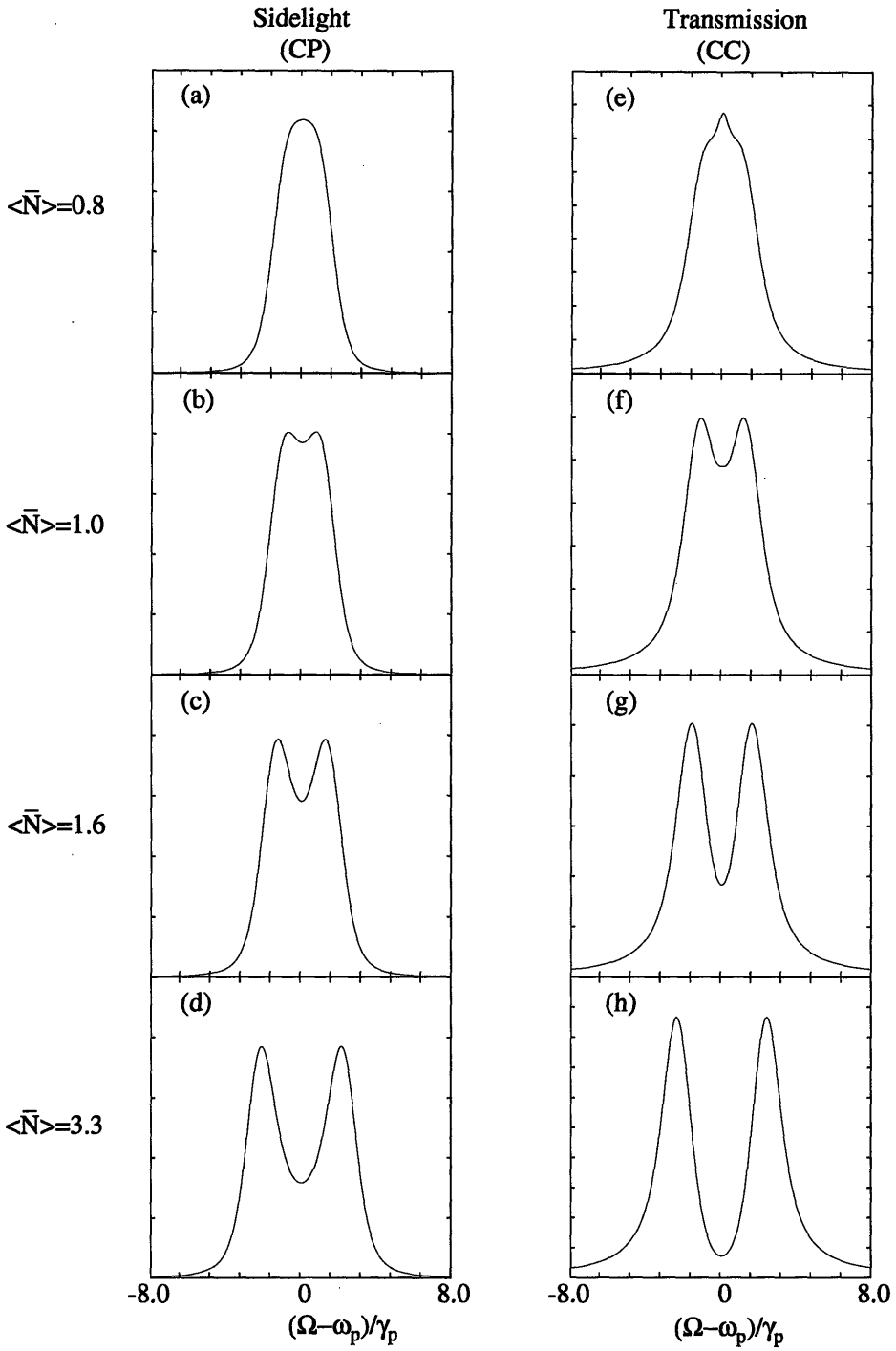

Figure 3-10: Strong coupling ($\xi = 17.3$) sidelight and transmission lineshapes for several values of $\langle \overline{N} \rangle$.

factor in the numerator, as discussed in Sec. 2.3.2.

3.2.5 Single Atom Regime

An important consequence of the standing wave nature of the resonator mode, when used in atomic beam experiments, is the inherent fluctuations induced in the intracavity atomic number, $\overline{N}$. As discussed above, $\langle\overline{N}\rangle \approx 1$ is a regime in which the fluctuations are as large as the mean value and resulting lineshapes can be dramatically altered. These fluctuations can arise from a single atom whose position is allowed to change or from several atoms that are also allowed to change positions. The lineshapes associated with these two cases are dramatically different, as will be shown below.

In fact, the purpose of this section is to demonstrate that *several* atoms interacting appreciably with the resonator mode are required, on average, to obtain $\langle\overline{N}\rangle \approx 1$. To demonstrate this, consider the total number of atoms in a given volume, V, within both the atomic beam and the cavity mode:

$$N = \int\int\int \rho_0 dx dy dz = \int_0^r \int_0^{2\pi} \int_0^l \rho_0 r' dr' d\phi dz = \pi r^2 l \rho_0, \tag{3.42}$$

with ρ_0 the atomic beam density, assumed uniform, and where l extends over many SW mode wavelengths along the optical axis of the cavity ($\equiv z$ axis). The number of intra-cavity atoms in this volume at any instant is given by

$$\overline{N} = \int_0^r \int_0^{2\pi} \int_0^l \rho_0 \psi^2(r', z) r' dr' d\phi dz. \tag{3.43}$$

Therefore, the ratio $\overline{N}/N$ of the number of intracavity atoms to total number of atoms is

$$\frac{\overline{N}}{N} \approx (1 - e^{-2u^2})/(2u)^2, \tag{3.44}$$

with $u = r/\omega_0$. Choosing $u = 1$, $N \approx 4.6$ atoms are required to obtain $\overline{N} \approx 1$. One must therefore conclude that $\langle\overline{N}\rangle \approx 1$ does not constitute the true single atom regime. Furthermore, models based on extensions of the Jaynes Cummings

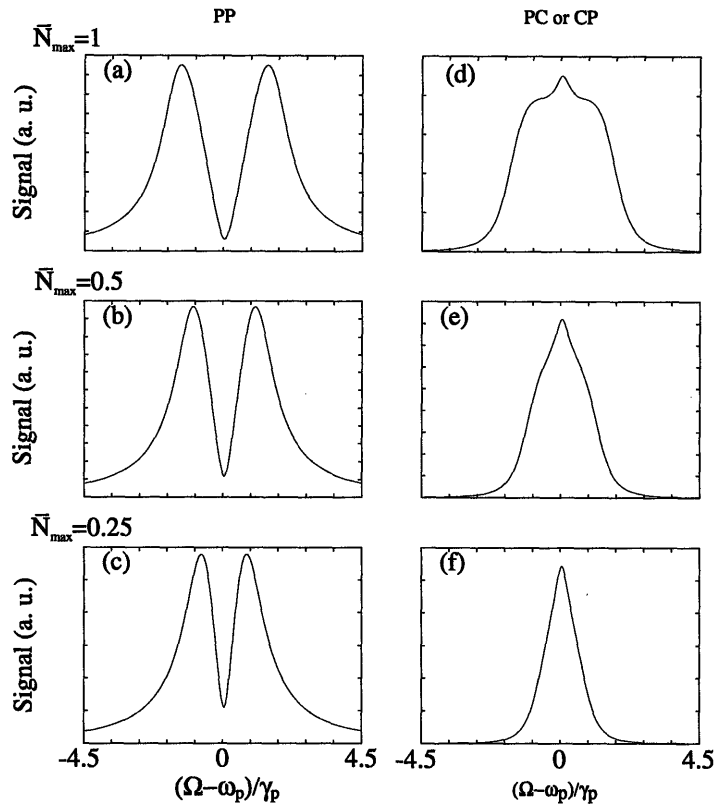

Figure 3-11: Single atom lineshapes for the parameters of the previous figure. In traces (a) and (d) the upper limit for the integral is $\overline{N}_{MAX} = 1$.

theory to many atoms assume a uniform mode function [44, 40] and do not strictly apply to experiments of this type. In the true single atom regime, the atom samples all positions within the volume specified above, and $\langle\overline{N}\rangle \longrightarrow 0.2$. The resulting lineshapes would not exhibit splitting for our parameters, as the trend in Fig. 3-10 suggests.

To realize the true single atom lineshapes experimentally, the atomic beam density should be decreased to a value low enough that never more than one atom is in the atomic beam at a time. In this case, *no* atoms will interact appreciably with the resonator for a significant part of the signal acquisition time. Note, however, that the CC scheme always gives a lineshape even with no atom at all in the resonator (the empty cavity Lorentzian), whereas the other schemes give signals *only* when atoms are present (signals $\propto \overline{N}$). Therefore, for the CP, PC, and PP lineshapes, the averaging procedure only needs to include those cases in which a single atom is present, and

the resulting experimental lineshapes may be calculated by simply integrating the appropriate fixed-atom lineshapes over $\overline{N}$. Since a single atom may be positioned anywhere within the mode volume with equal probability, we have:

$$\langle L(\Omega,\overline{N})\rangle_{ave} = \int_0^1 L(\Omega,\overline{N})P(\overline{N})d\overline{N}, \tag{3.45}$$

where $L(\Omega,\overline{N})$ is the appropriate term of Eq. 3.31, 3.32, or 3.24 (PC, PP, or CP, respectively), where $P(\overline{N})$ is an appropriate distribution function. If the cavity mode function were simply a standing plane-wave mode with no radial gaussian function, then $P(\overline{N}) = 1$ for all $\overline{N}$. With a radial gaussian mode function, however, the probability that the atom is in the tails of the gaussian function (with small $\overline{N}$) is larger than that for which the atom is optimally coupled at the mode center ($\overline{N} = 1$). (The atom is equally likely to be anywhere in the atomic beam so that the probability for a given $\overline{N}$ scales as the ratio of the area for which $\overline{N}$ has the specified value to the total atomic beam area.) Note that for PP, $\langle N\rangle = 1$, and only the second term in Eq. 3.32 is needed. (We assume a probe waist much larger than the cavity and atomic beam waists so that $\phi(\vec{r}_j) = 1$.)

This averaging procedure will apply to the CC scheme only if the atomic beam density is large enough so that there is one, and only one, atom within the mode during the course of the experiment, a situation impossible to realize. As the atomic beam density is reduced further, zero-atom signals dominate and the limiting signal becomes simply the empty cavity lineshape. The above integrals are performed for the pane-wave case ($P(\overline{N}) = 1$) and the resulting single-atom lineshapes for the PC, PP, and CP schemes are shown in traces (a) and (d) of Fig. 3-11. The lack of splitting in trace (d) for the PC or CP schemes (both give the same result) is not surprising. However, the splitting in trace (a) may be explained by noting that the strength of the signal for a given lineshape (for a given $\overline{N}$) is proportional to $\overline{N}$. For smaller values of $\overline{N}$ the single-peaked lineshapes do not contribute much to the overall signal. To approximate the gaussian mode case, the upper limit in the integral over $\overline{N}$ is reduced to simulate the modification in $P(\overline{N})$ in traces (b,e,c,f).

Lineshapes obtained in the CC scheme for $\langle\overline{N}\rangle = 1$, eg., curve (f) of Fig. 3-10, when compared with the fixed-atom lineshapes for various values of $\overline{N}$, see (b) of Fig. 3-7 (note the different scan widths), suggest that their dominant contribution arises from the $\overline{N} = 1$ fixed-atom lineshape. This is also demonstrated by $P(\overline{N})$ in Fig. 3-7. Furthermore, these fixed-atom lineshapes depend *only* on $\overline{N}$ and do not discriminate between the various ways that $\overline{N} = 1$ can arise. Therefore, it may be argued that the results of this type of experiment can be interpreted as arising from a single atom optimally coupled to the cavity mode. However, as we have argued above $\overline{N} = 1$ can occur in many ways which involve several atoms coupled to the cavity mode. An experiment which can definitively discriminate between the situation in which a single atom is optimally coupled and the situation in which several atoms are all coupled in such a way that $\overline{N} = 1$, is the PP scheme. In this case, the true single atom optimally coupled lineshape would exhibit the anticipated two peaks. The alternative case with several atoms, however, can exhibit only a single peak lineshape, as can be seen in Eq. 3.32 (if, for example, $\langle N_{exc}\rangle = 4$ and $\langle\overline{N}\rangle = 1$; for a related discussion see also Eq. 3.36). Experiments have been performed to demonstrate this and are discussed in the next chapter.

3.3 Saturation

An important issue to address is the effect of the atom-cavity interaction on atomic level populations. In previous sections, the atomic level population equation was neglected and all atoms were assumed to remain essentially in their ground states. In this section this assumption is relaxed.

We seek the condition for which the atomic population is perturbed to first order. For simplicity, we assume a single atom located at a fixed position, $\vec{r}_j$, in the SW resonator mode. The results of the previous chapter then apply with $N = 1$. Neglecting the driving terms, Eqs. 3.11–3.13 may be solved for the inversion in the steady state to obtain

$$\mathcal{N} = \frac{\mathcal{N}_0}{1+\epsilon}, \tag{3.46}$$

where

$$\epsilon = \frac{1}{2}\left(\frac{g_0}{\gamma_p}\right)^2 \frac{|E_0\psi(\vec{r}_j)\mathcal{E}|^2}{|E_0|^2}. \tag{3.47}$$

Note that $|\mathcal{E}|^2$ depends on the square of the inversion. However, since we desire effects only to first order, we assume $\mathcal{N} \approx \mathcal{N}_0 = -1$ in the expression for $|\mathcal{E}|^2$ and demand that $|\epsilon| \ll 1$. The number of photons, ν, in the cavity mode at the driving frequency is given by

$$\nu\hbar\omega = 2\frac{\int |E_0\psi(r)\mathcal{E}|^2 dV}{8\pi} = \frac{|E_0\mathcal{E}|^2 V}{4\pi}. \tag{3.48}$$

Therefore

$$\epsilon = \left(\frac{g_0\psi(\vec{r}_j)}{\gamma_p}\right)^2 \nu, \tag{3.49}$$

so Eq. 3.46 may be rewritten as

$$\mathcal{N} = \frac{\mathcal{N}_0}{1+\nu/\nu_s}, \tag{3.50}$$

with the *saturation parameter*, ν_s, given by

$$\nu_s = \left(\frac{\gamma_p}{g_0\psi(\vec{r}_j)}\right)^2. \tag{3.51}$$

The saturation parameter is a measure of the number of photons required in the resonator mode to effect the atomic population. As is easily seen, an atom more strongly coupled to the mode with larger $\psi(\vec{r}_j)$ has a smaller saturation parameter than an atom closer to the cavity nodes. An optimally coupled atom therefore exhibits saturation effects before a weakly coupled atom.

3.4 Optical Resonators

Several different kinds of resonators are being used to study various aspects of cavity QED; (1) closed, low order (the superconducting boxes of Kleppner's and Walther's groups), (2) open, low order (the micro-cavities and Fabry-Perots of Haroche, DeMartini, Yamamoto, etc.), (3) open, high order, degenerate (the concentric and confocal

cavities of Mossberg's and our groups), and (4) open, high-order, nondegenerate cavities (of Kimble's and our groups). In open or closed resonators, the atom can or cannot, respectively, spontaneously decay to free space modes. High or low order refers to the size of the axial quantum number of the participating mode. Degeneracy means that more than one mode of the resonator field, described by a suitably chosen mathematical basis, interact with the atom. For the cavity used in this work the atom interacts with the TEM_{00} mode only and is considered nondegenerate. This type of resonator is spherically symmetric with the mirror separation much smaller than the mirror radius of curvature (for a discussion of such resonators see [63, 64]). In the concentric and confocal cavity, the atom interacts with many spherical harmonic modes simultaneously, and is thus degenerate (see below). Interestingly, one study utilizes the confocal cavity geometry, but excites only a single TEM_{00} mode in a transmission (absorption) experiment [20]. In this setup, an intra-cavity aperture may be employed to restrict atom-field interaction to this mode only. If no aperture is used, the atom can interact with all the degenerate modes of the cavity to which it couples. Used with a restricting, intra-cavity aperture, the degenerate, confocal resonator becomes equivalent to a nondegenerate cavity similar to our's, but with a much shorter free spectral range (FSR=$c/2L$) and much smaller coupling constant. Note that FSR=$c/4L$ for the confocal cavity with no restricting aperture (i.e., allowing for interaction with all degenerate modes). To overcome the smaller coupling, many atoms are required to observe normal mode splitting.

An illustration of this situation can be given by comparing our nondegenerate supercavity with the confocal or concentric resonators. The coupling constant may be written as

$$g_0^2 = 2f \times \mathrm{FSR} \times \gamma_p, \tag{3.52}$$

with the free spectral range $\mathrm{FSR} = \frac{c}{2L}$ for the nondegenerate and degenerate cavities (TEM_{00} mode only), and $\mathrm{FSR} = \frac{c}{4L}$ for the confocal cavity without the aperture, and with

$$f = 3\theta^2, \tag{3.53}$$

where

$$\theta = \frac{b}{L} \qquad \text{(concentric or confocal)} \tag{3.54}$$

and

$$\theta = \frac{\lambda}{\pi\omega_0}, \qquad \text{(nondegenerate or degenerate with aperture)}, \tag{3.55}$$

with $2b$ the open aperture diameter of the degenerate cavity mirrors, L the mirror spacing, and ω_0 the TEM_{00} cavity mode waist. In terms of the mirror parameters,

$$\omega_0^2 = \frac{\lambda}{\pi}\sqrt{\left(\frac{L}{2}\right)\left(R - \frac{L}{2}\right)}, \tag{3.56}$$

with R the mirror radius of curvature and λ the atomic transition wavelength (resonant with the mode). For the confocal cavity $R = L$ but for the nondegenerate cavity $L \ll R$, so that the TEM_{00} mode waist is

$$\omega_0^2 = \frac{\lambda}{\pi}\frac{L}{2}, \tag{3.57}$$

for the degenerate confocal resonator with intra-cavity aperture and

$$\omega_0^2 = \frac{\lambda}{\pi}\sqrt{\frac{RL}{2}}, \tag{3.58}$$

for the nondegenerate cavity.

We compare the confocal cavity with (TEM_{00} mode) and without the intra-cavity aperture. The ratio of the two coupling constants (squared) is therefore

$$\frac{g^2_{\mathrm{conf}}}{g^2_{\mathrm{TEM}_{00}}} = \frac{f_{conf}}{f_{\mathrm{TEM}_{00}}}. \tag{3.59}$$

Assuming $b = 0.5$ cm, $R = 2.5$ cm, $L = 2.5$ cm, and $\lambda = 553.5 \times 10^{-7}$ cm, we obtain $f_{conf} = 0.12$ and $f_{\mathrm{TEM}_{00}} = 4 \times 10^{-5}$ so that the ratio is 3×10^3.

Initial attempts to realize a strong coupling resonator naturally involved the concentric resonator which had been successfully used to demonstrate enhanced and

suppressed spontaneous emission in our laboratory. The coupling constant is large, thanks to the large f factor. Recall that this factor is a measure of the solid angle subtended by that part of the mirror which bounds the diffraction limited mode with which the atom interacts. To achieve the required conditions of strong coupling (the atom chosen was sodium, explained below, with $2\gamma_p = 10$ MHz), a finesse of only $F \approx 120$ is required. However, this large solid angle factor has two disadvantages; (1) doppler broadening and (2) low finesse.

(1) Atoms in an atomic beam moving through the resonator mode will emit light into the mode at angles which significantly deviate from 90^o relative to their direction of motion. The resulting Doppler shift of the emitted or scattered light is a source of Doppler broadening which would obscure the normal mode splitting we wished to observe. In parallel with a search for the desired mirrors, therefore, a slowing and cooling apparatus, with an atomic beam of sodium, was built. We employed a scheme similar to that introduced by Prentiss et al. [65] and succeeded in slowing the atoms to $\approx 5\%$ of thermal velocity, which was sufficient to eliminate the Doppler effect.

(2) The concentric resonator mirrors, on the other hand, proved to be very expensive to manufacture, with only a guaranteed minimum finesse of 60! Although the value of the required finesse is by no means extraordinary for conventional Fabry Perots, it is very difficult to realize for the concentric and confocal resonators when used in this type of experiment. The overall finesse is determined by two factors, mirror reflectivity and surface quality. (For a general discussion of spherical mirror Fabry-Perot interferometers, see [66].) Existing technologies for surface coatings, with multi-layered dielectric materials, can provide the required reflectivities for very low-loss resonators. The serious problems, however, arise with surface quality. Roughly speaking, the surface quality may be divided into two regimes scaled by the dimensions over which the surface irregularities occur, surface roughness and surface figure. For the concentric and confocal cavities, which use a very large portion of the mirror surface ($1 - 3$ cm^2), the overall surface figure quality is limiting.

For the nondegenerate cavities with length much smaller than the mirror radius of curvature, however, surface roughness is limiting. In this case, the spot size of

the participating portion of the mirror is on the order of 10^{-3} mm^2 and overall surface figure deviations from the desired figure are negligible over this spot size. Super-polishing techniques which minimize surface roughness have been successfully developed, and extremely smooth surfaces are possible with RMS deviations on the order of Angstroms ($\lambda/1000$). In this case, the resonator finesse becomes reflectivity limited.

In Sec. 3.1, we described how the coupling constant depends on the atom's location in the mode of a nondegenerate cavity. Furthermore, we mentioned that several atoms within the mode communicate their presence to one another via the cavity field (recall the macroscopic dipole of Eq. 3.15). In a concentric resonator, on the other hand, both of these situations are altered: (1) All atoms within the "interaction" volume, see below, are equally coupled to the mode, regardless of their positions, and (2) all atoms act independently.

Recall, from earlier results, the ray picture of atom-cavity interaction in a concentric resonator [67]. In this picure, the interaction volume is defined by that region within which a radiating atom will constructively interfere with its own radiated fields that are reflected back by the mirrors, and is much larger than the diffraction-limited mode volume used to calculate the interaction strength. A brief argument for the plausibilty of (1) invokes the boundary value solution to the complete spherical resonator using spherical harmonics, described in [67]. In this work, it was shown that the atom interacts simultaneously with many, degenerate spherical harmonic modes, each proportional to mode functions given by

$$\xi_l = \sqrt{2l+1} j_l(x), \tag{3.60}$$

where $j_l(x)$ is the spherical Bessel function of order l and x is the position of the atom. These modes include the many high-order transverse mode functions resonant with the atom. The zeroes for these functions occur in varying positions so that, for any position within the interaction volume, the atom is *always* coupled to some modes. Hence no anti-nodes exist since the atoms are always coupled to the resonator

via some, possibly high-order transverse, spherical harmonic modes. We may loosely ascribe all these degenerate spherical harmonic modes to a single diffraction-limited mode whose waist remains at the location of the radiating atom during its passage through the interaction volume. All positions within this volume of degeneracy may be viewed as identical from the point of view of the overall coupling to the resonator.

An argument for the plausibility of (2) relies on the above mentioned approximation: An atom interacts with a diffraction-limited field mode (which may be described as a sum over the above mentioned spherical harmonics) whose waist is on the order of a micron. All other atoms within the (much larger) interaction volume generate their own "modes" and only those atoms located within this mode waist, or at its mirror image, (a very unlikely occurrence, given the low atomic beam density) can know of that atom's presence and act cooperatively.

Following this argument, the only way to inhibit spontaneous emission into a concentric resonator mode is to detune the cavity. In this case, all positions within the volume of degeneracy are essentially at a "node" (destructive interference of reflected waves). In the nondegenerate cavity, on the other hand, one can inhibit spontaneous emission into the mode by placing the atom at a node or by detuning the cavity. To study true single atom effects, therefore, the degenerate resonator would be ideal if the required finesse could be met.

To summarize, we have presented a comparison between degenerate and nondegenerate resonators and demonstrated that true single atom effects could be realized in the degenerate cavity. This resonator is more stable against vibrations and thermal drifts, but the large solid angle demands a slowing and cooling scheme for the atoms in the atomic beam due to the doppler shifts. Furthermore, attaining the required surface figure quality is quite challenging but may be possible. Note that with the required finesse, the interaction volume's diameter (which is dependent upon finesse) is ≈ 10 μm with the diffraction limited mode waist ≈ 1 μm. Therefore, atoms would still interact independently for atomic beam densities in which, on average, one atom is in the interaction volume at a time.

Chapter 4

Experimental Studies

This chapter describes the setup and results of several experiments that study the atom-cavity system. Section 4.1 discusses the schemes used to study the normal mode structure of the atom-cavity system. Section 4.2 provides details of the experimental apparatus and atomic system, the optical layout, and instrumentation. Section 4.3 describes the results for the strong coupling and Sec. 4.4 describes the intermediate coupling results. Section 4.5 presents lineshape data taken with probe powers exceeding saturation.

4.1 Schemes

The experimental investigation of strong and intermediate coupling in the atom-cavity system may be performed with two excitation arrangements. The cavity mode may be excited by a laser beam coupled directly into the cavity mode or the atoms may be excited directly by a laser beam incident from the side of the resonator (Fig. 4-1). In both excitation schemes, the probe polarization is carefully chosen to be parallel with the direction of the atomic beam.

As depicted in Fig. 4-2, photon counts are simultaneously collected out the sides (sidelight scattered by the atom) and end of the cavity (transmission), as functions of the excitation laser frequency, with a photon counter, (SR400, Stanford Research), and photomultiplier tubes, (Hamamatsu, R1635).

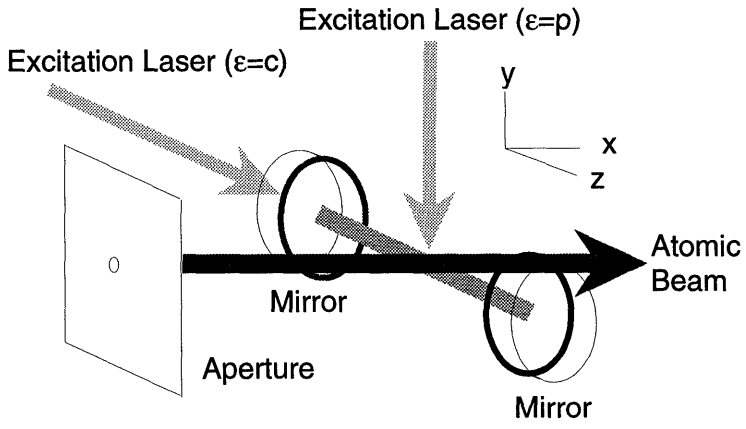

Figure 4-1: Diagram of atomic beam intersecting cavity mode and the two possible excitation schemes.

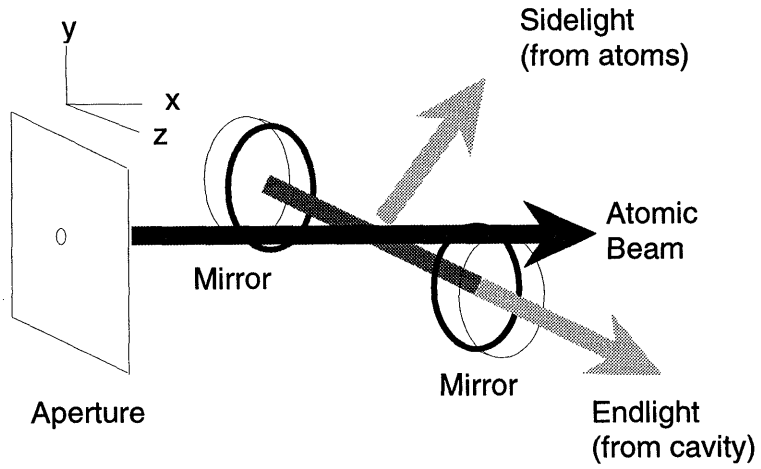

Figure 4-2: Diagram of the two signals simultaneously observed in all experiments.

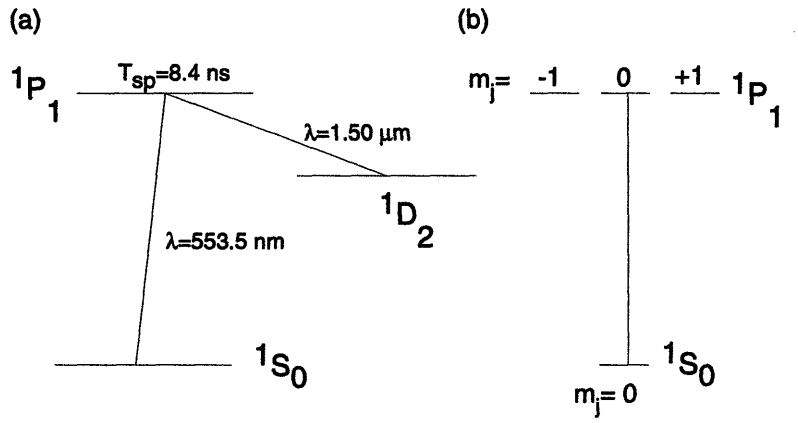

Figure 4-3: (a) ^{138}Ba Level Structure. (b) Ideal two-level system, Δm=0 transition.

4.2 Experimental Setup and Apparatus

4.2.1 Ba Level Structure

In choosing the ideal atomic system for study, several requirements had to be satisfied: (1) Only a single, two-level transition can interact with the cavity mode, (2) the excited state lifetime and transition wavelength should be consistent with technically possible cavity geometries and mirror finesse to satisfy the various coupling strength requirements (*i.e.*, $g_0 > \gamma_c, \gamma_p$ for strong and $g_0 \approx (|\gamma_c - \gamma_p|/2)$ for intermediate coupling, and (3) the atomic transition's (as well as cavity's) linewidth should be broader than the excitation laser linewidth.

Consistent with these requirements, the lowest lying electronic level structure of ^{138}Ba ($^1S_0 \rightarrow ^1P_1$, Δm=0, λ = 553.5 nm), shown in Fig. 4-3, was selected as the two-level atomic system. The nearest transition is the $^1S_0$ (F=3/2)$\rightarrow ^1P_1$ (F=5/2) component of the ^{137}Ba isotope, approximately 65 MHz away (higher frequency). Its contribution to the signals is less than 1% and has a negligible effect on the lineshapes. Finally, the branching ratio for the $^1D_2$ state is quite large ($\approx$ 400) so that the selected transition makes an ideal two-level system. With a lifetime of 8.4 ns, the transition linewidth is $2\gamma_p \approx$19 MHz (FWHM).

4.2.2 Atomic Beam

An effusive atomic beam is generated inside a vacuum chamber ($\approx 10^{-6} - 10^{-7}$ Torr using a 4 inch diffusion pump) by passing $\approx 150 - 200$ Amps through an SS-304 metal tube with ≈4-5 grams of Barium (isotopic purity≈ 72% for ^{138}Ba). The tube's dimensions are typically 6.75"x.5"x.024"(LxDxw) with a resistance of a few hundred milliohms. Current through the tube is controlled by a 10 Amp variac through a step-up transformer arrangement. This provides for oven temperature and, therefore, atomic beam density control. Barium vapor escapes through a pinhole ($\approx$ 1 mm in diameter) in the side of the oven. The oven assembly is mounted in the oven vacuum chamber via a bellows system so that the oven pinhole position can be controlled. Three apertures are placed downstream to collimate the beam to $\pm$1.5 mrad, with the final aperture a 25 μm pinhole. This pinhole is located $\approx$ 30 cm from the oven pinhole and $\approx$ 1.7 cm from the cavity mode waist. It is mounted on two translation stages which are manually adjustable via vacuum feedthroughs so that precise positioning (within a few microns) of the pinhole along the y and z axis is possible (Fig. 4-1). With this arrangement, the atomic beam can be aligned to intersect the cavity mode at $90^o \pm 0.5$ mrad. At this point, the beam diameter is < 100 μm. The maximum beam density attainable at the cavity mode is $\rho_0 < 10^8$ cm^{-3} so that the maximum number of atoms possible in the interaction region (defined by the intersection of the cavity mode with the atomic beam) is $N \approx 10$.

4.2.3 Optical Layout

Several laser beams are required for the following tasks; (1) a frequency reference beam to stabilize the laser frequency, (2) an independently tunable reference beam to stabilize the cavity frequency and also allow for adjustable atom-cavity detunings, and (3) an independently tunable probe for exciting either the atoms from the side or the cavity mode. Figure 4-4 shows how all these tasks are accomplished with a single CR-699 (Coherent) dye laser ($\approx$ 550 mW of single-mode power with frequency bandwidth $\approx$ 3 MHz at λ=553.5 nm) and several Isomet acoustooptic modulators

(AOM).

All AOM's except #5 and #6 are used in a double-pass configuration. In this arrangement the input laser beam is focussed to $\approx$ 50 μm waist at which the AOM crystal is centered. This size waist is chosen so that the acoustic wave's transit time across the laser beam ($\approx$ 30 ns) is well outside the bandwidths of relevant interest (e.g., the 1 kHz frequency correction bandwidth of AOM #1). In addition to time response, small waist sizes are necessary to preserve the laser beam's mode quality. The first-order diffracted beam is then reflected by a mirror (M) directly back upon itself, through a second lens which is placed at a distance equal to its geometrical focal length from the AOM. The back-reflecting mirror is then placed at the focus of the beam so that the return beam, after being split-off from the input beam by a 50:50 beamsplitter, is collimated with the same diameter as the input beam. The double-pass configuration serves two purposes: (1) Laser beam motion due to RF frequency changes is minimized, and (2) the tuning range of the exiting laser beam is doubled from 45 MHz to 90 MHz. Note that a first order diffracted beam is selected in AOM #1. This results in a 220 MHz ($= 2 \times 110$ MHz) shift in frequency relative to the output laser frequency. This beam is then split off several times to AOM's #2-5. The *opposite* diffracted order of these AOM arrangements are selected so that the exiting beams have $\approx$ 0 MHz net shift relative to the laser output frequency. Note that SBC in Fig. 4-4, which consists of a cross polarizer followed by a Soleil Babinet Compensator, serves as an optical isolator.

Frequency Stabilization

Acoustooptic modulator #1 (Isomet 1206C, center frequency of 110 MHz with 50 MHz RF bandwidth), the first in the optical circuit, is used for both frequency and power stabilization. The RF amplitude and frequency applied to the crystal are controlled by two analog voltages to the ports of an Isomet driver (D323B-788). These voltages are derived from two feedback circuits, a frequency correction circuit and a laser power correction circuit. Laser frequency correction is accomplished with saturation spectroscopy in a Ba cell. In this Lamb dip setup, the pump beam is frequency

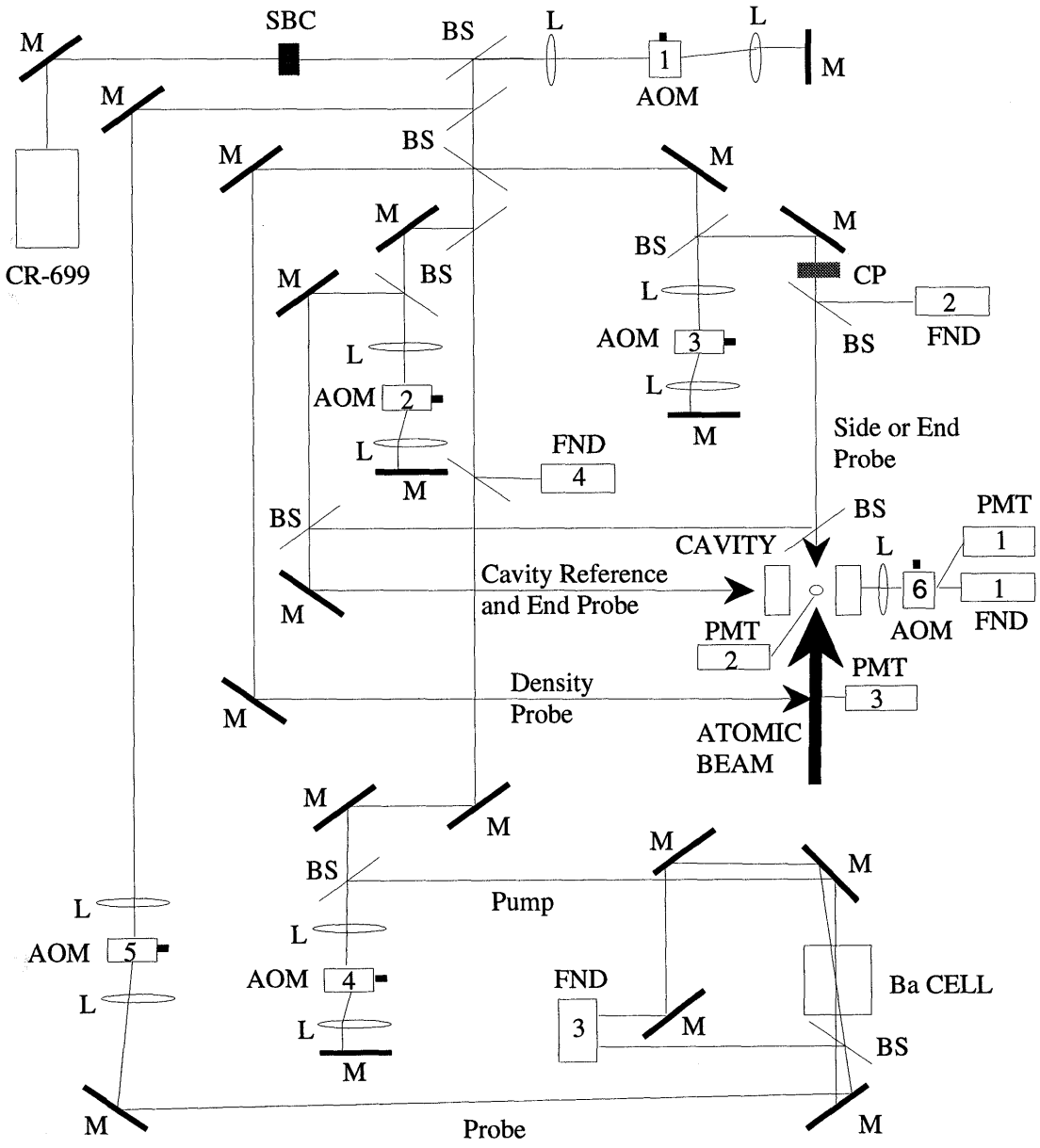

Figure 4-4: Optical layout.

modulated (excursion $\approx \pm 9$ MHz at 100 kHz) by a signal generator applied to the RF driver (Isomet D302) of AOM #4 (Isomet 1206C). The probe beam traverses, in a single pass, AOM #5 (Isomet 1250C, center frequency 200 MHz with 100 MHz RF bandwidth) which is driven at 220 MHz by an RF circuit. This RF circuit uses an Isomet 223A-1 driver (center frequency 110 MHz) as the RF source. The generated RF signal is sent to a double balanced mixer (DBM-25) for frequency doubling, followed by an amplifier before being sent to the crystal. The analog signal from a balanced diode arrangement (FND #3), which monitors both the probe transmission signal as well as incident probe power (thereby subtracting out power fluctuations), is sent to a lock-in amplifier where it is mixed with the signal generator output for phase-sensitive detection. Output of the lock-in, which is a measure of the excursion of the laser frequency from the atomic transition frequency, is then fed to an integrator circuit whose output is, in turn, sent to the frequency controlling port of AOM #1's driver. The resulting laser frequency uncertainty is reduced from 3-4 MHz to ≈ 0.75 MHz within a 1 kHz bandwidth.

Power Stabilization

Power stabilization is accomplished by monitoring laser power with an FND-100 diode detector (FND #4) and subtracting the resulting voltage from an adjustable, stable reference voltage. The difference signal is then fed to an integrator whose output is fed back to the RF amplitude controlling port of AOM #1's driver. With this arrangement, power fluctuations are reduced from 15% to 2%. Most of the power fluctuations monitored here arise from laser power fluctuations. However, two additional sources of power modulation arise due to the nature of the acoustooptic modulator. The first occurs because the Bragg diffraction angle changes with AOM frequency. Since the crystal is not rotated to compensate for this, the diffraction efficiency also changes (by as much as 40% over the entire bandwidth) giving rise to a variation in power. The second source of power modulation ($\approx 15\%$), also coupled to RF frequency, arises from the fact that the crystal acts as an etalon to the incident acoustic wave. Since either end of the crystal normal to the direction of propagation of the acoustic wave

is not perfectly damped, multiply reflected interfering waves occur. The crystal then acts as a lossy etalon with slighty larger intra-crystal acoustic power with RF frequency resonant with the etalon than when it is not. A measurement of the period (in frequency) of these power modulations is performed by scanning the RF frequency and monitoring the laser power modulations. The result agrees very well with the expected value $\delta\nu = v/2L \approx 180$ kHz with $v = 3.63$ mm/μs, the sound velocity and $L \approx 1$ cm the length of the crystal. Note that the amount of laser power modulations in a single-pass arrangement is doubled in a double-pass configuration since the optical beam interacts with the acoustic wave twice. Since these effects are most important in AOM #3, (this is the source for the probe beam), an additional power stabilization circuit, which monitors laser power at FND #2, is required. Correction signals are applied to the driver of AOM #3 (also an Isomet D323B-788) and power modulations are kept below 5% over the entire tuning range.

Cavity Stabilization

Acoustooptic modulator AOM #2 is used to control the cavity reference beam. The cavity frequency is locked to this beam using an FM modulation technique similar to that used in stabilizing laser frequency. In addition, the reference beam is chopped off and on by TTL signals applied to AOM #2 at a 50 Hz rate, alternating between data taking and cavity locking, respectively, with a 30% duty cycle. The same TTL signals (derived from LM555 oscillators with supporting circuitry) are also inverted (using an inverter chip) and applied to AOM #6. This causes AOM #6 to diffract the cavity emission signal into the first diffracted order beam which is focussed onto PMT #1 while the cavity reference (locking) beam is turned off (see Fig. 4-5). Following the data collection period, AOM #6 is turned off and the cavity reference beam, now on, is monitored by FND #1 as it travels undiffracted through the crystal.

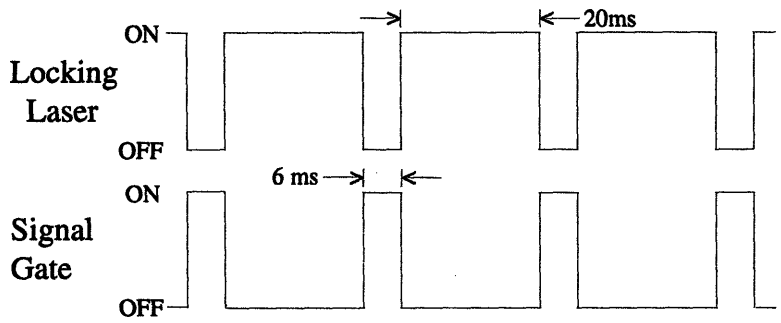

Figure 4-5: Timing sequence used for data taking and cavity locking.

4.2.4 Resonators and Mount

Two cavities, which differ only in finesse and throughput, were constructed to investigate the strong and intermediate coupling regimes. Each cavity consists of two "supercavity" mirrors, all with radius of curvature 10 cm, separated by $L = 247$ μm and 240 μm, respectively. The mirrors were specially fabricated to the required specifications with multi-layered dielectric coatings on a superpolished substrate [68]. The substrate of the strong coupling mirrors is fused silica with dimensions 5.5 mm diameter and 8 mm thickness. The substrate of the intermediate coupling mirrors is BK-7 with dimensions of 7.5 mm diameter and 4 mm thickness. This cavity geometry gives a TEM_{00} mode with waist $w_0 \approx 25$ μm. In addition, $g_0/2\pi = (16.6 \pm 0.5)$ MHz for the coupling constant and $2\gamma_c/2\pi = (2.4 \pm 0.2)$ MHz ($F = 2.5 \times 10^5$) for strong coupling, and $2\gamma_c/2\pi = (108 \pm 4)$ MHz ($F = 5.8 \times 10^3$) for intermediate coupling. The throughputs are $\eta \approx 0.31$ and $\eta \approx 0.9$ for the strong and intermediate coupling cavities, respectively.

The specifications for the optical cavities required in the experiments are very demanding. In attempting to obtain the largest coupling possible, the shortest cavity length was chosen consistent with the technical challenges of the highest finesse obtainable and the abilities of the experimenter to fit and align beams at the center of the cavity mode. Note that curvature in the mirrors imply edge separations smaller than the cavity lengths. In fact, the mirror separation at the edges are 170 μm and 100 μm for the strong and intermediate coupling cavities, respectively. These dimensions are only slightly larger than the atomic and laser beams, so care must be

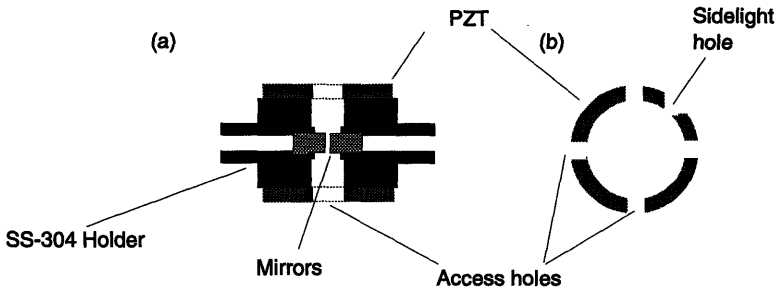

Figure 4-6: Cavity design: (a) Side view of cavity and (b) end view of PZT.

exercised to prevent the beams from scattering off the mirror edges. Furthermore, additional challenges with the shorter cavity lengths must be met. The cavity frequency should be quite stable, but adjustable, and not significantly effected by either thermal drifts or mechanical vibrations. To prevent a change in cavity frequency of 1 MHz, for example, the length cannot change by more than $\delta L = L\delta\nu/\nu \approx 5 \times 10^{-13}$ m! Neglecting external influences, thermal vibrations at room temperature of the mirror substrates and coating surface could easily cause the mirror surface to vibrate with amplitudes exceeding this value. However, the surface modes which are excited are of high order (many nodes) so that no net *global* motion of the cavity occurs. Global in this sense means net motion of an entire portion of the mirror surface, the active spot, whose size is twice the TEM_{00} mode waist at the mirrors (≈ 50 μm).

To meet these requirements, a series of studies were conducted to determine the most stable mounts possible. The best cavity design, shown in Fig. 4-6, is to simply cement (with Torr Seal) the mirror holders (to which the mirrors are carefully cemented) to each end of a cylindrical piezoelectric transducer (PZT), which has 5 holes drilled in its side for beam access [69]. Two pair of diametrically opposite holes are drilled at 90^o relative to each other for laser and atomic beam entrance and exit. A fifth hole, drilled along a line 30^o from vertical (see (b) of Fig. 4-6), is for the collection of sidelight scattered by the atoms. The vertical pair of holes is for the side excitation laser probe and the horizontal pair is for the atomic beam. With this design, voltages applied across the PZT control mirror spacing (≈ 1 MHz/mV). To minimize mechanical and thermal coupling to the environment, the cavity is bolted

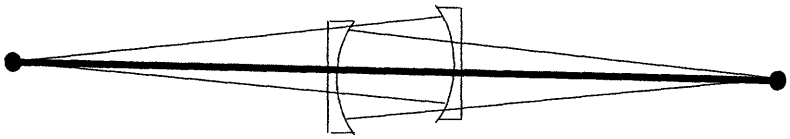

Figure 4-7: Cavity alignment.

to the top of a massive SS-304 block ($\approx$ 75 lbs). However, the cavity is supported by two Viton O-rings so that it does not come into contact with any metal. The block is placed on top of Viton O-rings inside the main vacuum chamber. Necessary optics and aperture support assemblies are then mounted on top of the block. The resulting stabilized cavity frequency, $\delta\nu_c \leq \pm 0.5$ MHz, is locked to the cavity reference laser beam to prevent slow drift that is always present. During the data taking intervals the cavity drift is less than 0.5 MHz so that atom-cavity detuning, $\Delta = 0 \pm 0.5$ MHz. This drift is measured by monitoring transmission by an unchopped probe, which was initially resonant with the cavity, during the unlocked periods.

In the construction of the cavities, all metal pieces were machined with 5 mil tolerances so that the mirror substrates fit snugly in their holder and the holders fit snugly within the PZT cylinder. The tilt of the mirrors is not too critical. So long as the center of curvature of the two mirror surfaces are reasonably close to the axis of the PZT cylinder, an optical axis can be found which supports a TEM_{00} mode of the required finesse. Figure 4-7 demonstrates why this is so. The thick line joining the two centers of curvature (large black dots) intersects the mirror surfaces. This line defines the optical axis of the cavity and will be centered on the TEM_{00} mode. The only requirement is that it meet the mirror surfaces somewhat near the mirror centers, where the coating and surface quality are as specified by the manufacturer [68]. The most challenging aspect of the mirror alignment procedure is to obtain the desired mirror spacing. Using specially built mounts, the cavity can be held together without cementing. While coupling laser light into the TEM_{00} cavity mode and measuring the transmitted fringes with the laser scanning, the beam is purposely misaligned slightly to excite transverse modes of the same order. Identification of the modes is simplified

by the fact that they can easily be seen on a piece of paper. For $L = 245$ μm, for example, $\delta\nu_{trans} \approx 13.6$ GHz and we adjusted the cavity length with micron screws until this transverse mode spacing was obtained. Once the length was set, one end of the mount could be unbolted and torr seal applied to the mirror holder. (The other mirror holder was already cemented in place to the PZT.) The mount was then bolted back in place. The mirror spacing was checked and adjusted, if necessary, before the cement hardened (≈ 1 hour).

Birefringence

An important consideration when placing the mirrors in their SS-304 holders is the minimization of mechanically induced stresses in the substrate and dielectric coatings. Such stresses give rise to distorted surface figures and can lead to birefringence. Indeed, the strong coupling resonator exhibits a two-peaked empty cavity lineshape for certain input beam polarization orientations, attributable to birefringence, as shown in the empty-cavity transmission lineshapes of Fig. 4-8. This probably arises from the strain induced by the cured cement even though care was exercised in the construction procedure by placing the cement symmetrically in the holder. However, the effect of this birefringence may be minimized, since the c-axis (defined by that direction along which the light wave should be polarized so that the polarization state of the multiply reflected waves within the cavity is not changed) can be made parallel to the atomic beam to within 10^o. Note that for the cavity driven ($\epsilon = c$) experiments, the incident beam is polarized exactly along the c-axis, so that birefringence is eliminated. For the atom driven experiments ($\epsilon = p$), however, the laser probe polarization is approximately parallel to the atomic beam so that the atomic polarization is within the above mentioned 10^o of the c-axis. Shown in Fig. 4-9 is the empty cavity transmission for the typical orientation used in the strong coupling experiment. Note that the finesse measurements are consistent with transmission and throughput measurements: We obtained $T = 5 \pm .4$ ppm and $\eta = .31$ which gives $F \approx 2 \times 10^5$ for the strong coupling mirrors and $T = 560 \pm 40$ ppm and $\eta = .9$ which gives $F \approx 5 \times 10^3$ for the intermediate coupling mirrors. The slightly higher finesse measured in the cavity

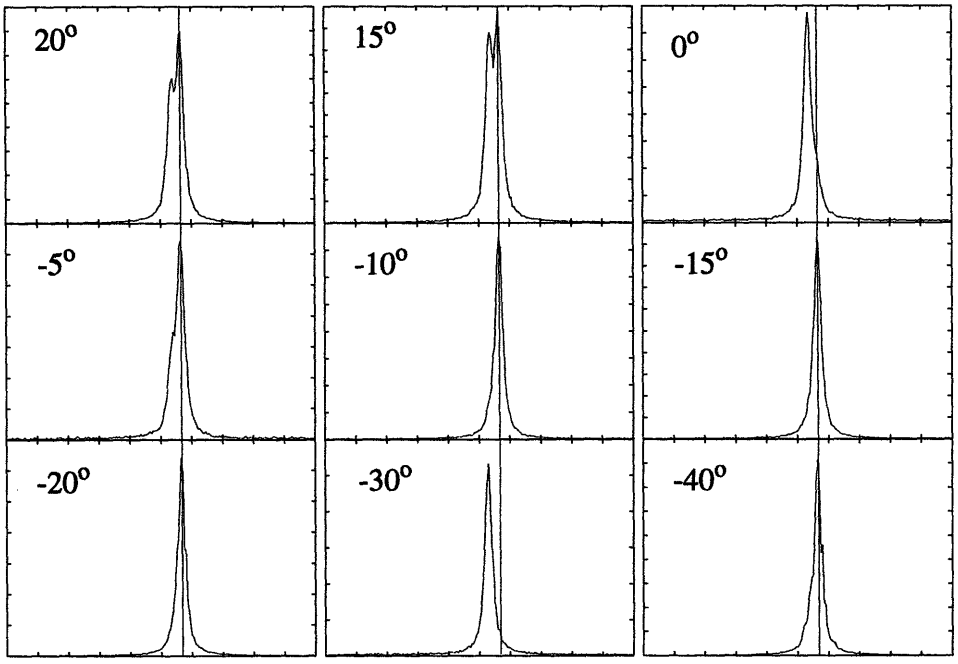

Figure 4-8: Empty cavity transmission for the TEM_{00} mode with incident polarization orientated at the specified angle relative to horizontal. The vertical lines mark the peak at higher frquency for reference with the two peaks separated by ≈ 2.2 MHz.

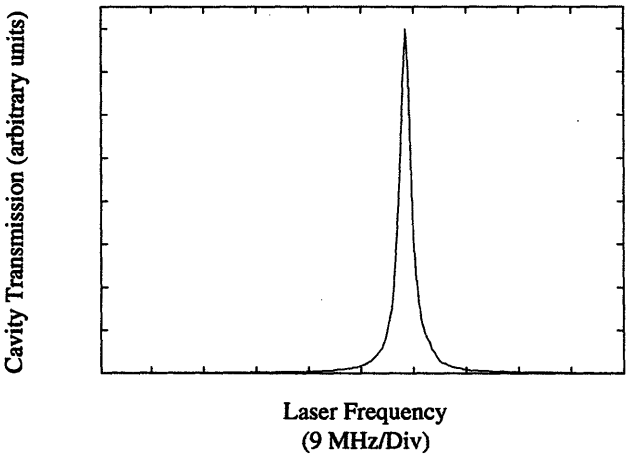

Figure 4-9: Empty cavity transmission with incident polarization along the c-axis. Cavity linewidth (FWHM), $2\gamma_c/2\pi = 2.4$ MHz, $L = 247$ μm, $F = 2.5 \times 10^5$

linewidth measurements is not inconsistent with the throughput measurements. In fact, the throughput is slightly larger than the value quoted because the laser was not optimally coupled into the cavity mode when the measurements were performed. Rough estimates imply that $\approx 10\%$ of the incident laser power was not coupled into the TEM_{00} mode although the total incident laser power was used in the estimate.

Alignment Procedure

Excitation of the cavity mode is accomplished with a 30 cm lens mounted on x-y-z translation stages. The lens focusses the probe and cavity reference beams to a waist size less than the cavity mode waist for optimum coupling. Since the cavity mode divergence angle is very small ($\theta = \lambda/\pi\omega_0 \approx 7$ mrad) any change in the angle between probe beam and cavity mode during frequency scanning would result in variations of the power coupled into the cavity mode. The double pass arrangement for the AOM's, however, minimize angular movement of the probe and reference beams so that this systematic variation in input power does not exceed 10%.

The optical arrangement for sidelight collection (with an image magnification factor of 4) is also used to visually check alignment of the atomic beam, cavity mode, and side probe. After locking the cavity to the atomic resonance, the atomic beam position is varied, using the pinhole stages, until fluorescence is seen. This fluorescence arises from the atomic beam interacting with the cavity mode which is excited by the resonant reference beam. Excitation of the atom directly from the side is accomplished by focussing the probe beam with a 25 cm lens which is located on top of the vacuum chamber. The lens is mounted on x-y-z translation stages so that the focus (having a waist approximately equal to the cavity mode waist) can be adjusted in the x-z plane of Fig. 3-1 as well as positioned along the z axis. The sidelight probe is positioned until it intersects the atomic beam (fluorescence seen) and then moved along the atomic beam until the fluorescent spot overlaps that of the cavity mode which is still excited.

The final alignment procedure is to make all beams perpendicular to one another. The cavity mode and atomic beam are made perpendicular by essentially performing

the transmission experiment (CC scheme) and optimizing the lineshapes. Once this tedious procedure is accomplished, the side probe is introduced and its angle adjusted for optimum lineshapes in the PC scheme.

4.2.5 Instrumentation

Data acquisition and control is automated using GPIB (PC-2A) and data translation (DT-2701) cards in an IBM PC-XT computer, together with an SR-400 photon counter and an assortment of analog and digital circuits built to suit various special needs. Hamamatsu photomultiplier tubes (R1635) are used for photon counting the side and end emission signals, as well as the atomic fluorescence signal for density calibration. They all were measured to have an efficiency of $\approx$ 7%. The density calibration PMT is used with a 10kΩ load, generating analog signals, since the fluorescence signal is very large. Two lock-in amplifiers and several FND-100 detectors, together with several circuits built in the lab, provided the feedback control circuits for laser power and frequency, as well as the cavity frequency control. In addition, vendor supplied software packages (ASYST) allowed for quick and easy programming for data acquisition. All data analyses were performed on Sun and NeXT (rest its soul) workstations.

As mentioned above, we can obtain length changes $\approx$ 1 MHz/mV with the PZTs used in the cavities. In order to initially place a TEM_{00} mode in resonance with the atomic transition, it is necessary to have the capability of scanning the cavity length over a free spectral range ($c/2L \approx 612$ GHz). This is accomplished with a 3 kV DC Kepco power supply. However, the small increments in voltage required for frequency correction can not be obtained from such a supply. We therefore applied a frequency correction voltage (from the cavity locking circuit) to one side of the PZT and the Kepco voltage to the other side. The entire PZT assembly is electrically floating, since it is isolated from the environment by O-rings. An additional problem of several millivolts of noise on the Kepco output required the connection of a large capacitor across its output. Since the only available capacitors had a maximum rating of 200 volts, a power supply was built which allowed switching to a backup battery supply

when necessary. This supply is extremely noise-free but gives rise to a uniform drift of the cavity resonance ($\approx$ 10 MHz/s) due to the slow discharging of the batteries. This drift is not a problem, however, since frequency changes during the data taking period (= 6 ms) do not exceed $\approx$ 0.5 MHz. Careful shielding of the cables leading from the power supplies to the PZT is essential in preventing ground loop and other external sources of noise from disturbing the cavity length.

4.3 Strong Coupling Results

To connect the theory of the previous chapter with the following experimental results, the expressions for the power out the side and ends of the cavity, $P_{side}(\Omega)$ and $P_{end}(\Omega)$, must be multiplied by appropriate attenuation factors and constants. The recorded photon count rates out the side is:

$$\dot{\nu}_{side} = \eta_{PMT} F_{side}^{opt} f_{side} \frac{P_{side}(\Omega)}{\hbar\omega}, \tag{4.1}$$

with η_{PMT} the photomultiplier tube efficiency, F_{side}^{opt} the total loss of all optical elements, and f_{side} the fraction of free-space radiated power into the solid angle of the sidelight optical collection system to the total power radiated in all space. Similarly, the expression for the count rate out the cavity is

$$\dot{\nu}_{end} = \eta_{PMT} \eta_{AOM} F_{end}^{opt} \frac{P_{end}(\Omega)}{\hbar\omega}, \tag{4.2}$$

with η_{AOM} the diffraction efficiency of the AOM. $P_{side}(\Omega)$ and $P_{end}(\Omega)$ are the appropriate expressions for the power from the previous chapter. Values for these parameters are given in Table 4.1.

An estimate for the expected signal strengths is based on the above parameters and the saturation photon number, ν_s, calculated in Sec. 3.3. If ν_s photons are in the cavity mode, then Eq. 4.2 may be written as

$$\dot{\nu}_{end} = \eta_{PMT} \eta_{cav} \eta_{AOM} F_{end}^{opt} \gamma_c \nu_s. \tag{4.3}$$

parameter	*value*
η_{PMT}	7%
f_{side}	7.0×10^{-3}
F_{side}^{opt}	70%
F_{end}^{opt}	75%
η_{cav}	0.31
η_{AOM}	80%

Table 4.1: Measured parameters for the strong coupling experiment.

In the strong coupling cavity, $\nu_s \approx 0.3$ and, therefore, $\dot{\nu}_{end} \approx 6 \times 10^4$ cps. End signals in the CC and CP schemes are kept below this value to ensure that the atom is not saturated. The peak sidelight signal with $\nu = \nu_s$ photons in the cavity and one atom optimally coupled can be calculated using Eq. 4.1 to give $\dot{\nu}_{side} \approx 10^4$ cps. Typically, the end signals are on the order of $0.1\nu_s$ so that $\dot{\nu}_{side} \approx 10^3$ cps. For the PP and PC schemes, the side probe power is adjusted so that the intensity at the laser beam's waist is less than the free space saturation intensity of the atom ($I_s \approx 15$ mW/cm^2). With a probe laser waist of ≈ 30 μm, the laser power for saturating a free space atom is 0.4 μW. If a free space atom is excited on resonance by a probe with intensity $I_L = 0.1I_s$, the estimated signal out the side is $\approx 10^3$ cps. This signal provides a reasonable estimate of the coupled atom signal. However, as the atom becomes more strongly coupled, by moving away from the node, the peak signal decreases slightly, as demonstrated in the curves for $\overline{N} = 0.01$, $\overline{N} = 0.5$, and $\overline{N} = 1$ of Fig. 3-7(e). The end signal exhibits similar behavior but with a larger change in the peak signal as $\overline{N}$ gets small (see Fig. 3-7(d)): Not only does the peak signal first start to grow as $\overline{N}$ gets small, but the linewidth (for the single-peaked lineshapes) also decreases. However, as $\overline{N}$ continues to decrease and approach zero, the peak signal stops increasing and eventually decreases to zero with the linewidth remaining at the empty cavity linewidth: An uncoupled atom cannot radiate into the cavity. Note that the strongly coupled atom has a larger saturation intensity than it does when uncoupled because of the enhanced (reversible) spontaneous emission into the cavity mode.

4.3.1 Cavity Excitation

Lineshapes obtained for both sidelight and cavity transmission ($\epsilon = c$) are shown in Fig. 4-10 in the strong coupling regime ($\xi \approx 16$) for various values of $\langle \overline{N} \rangle$. Note that the excitation laser beam, labeled "density reference" in Fig. 4-4, and controlled by AOM #3, also excites the atomic beam in a region before it enters the cavity and the resulting (free-atom) fluorescence is collected by photomultiplier tube PMT #3 to monitor the atomic beam density. This free-atom fluorescence signal determines $\langle \overline{N} \rangle$ as the atomic beam density, ρ_0, is varied. However, uncertainties in overall collection efficiency limit the accuracy of these estimates to $\approx 50\%$. A more accurate calibration is obtained by a fit (in which $\langle \overline{N} \rangle$ is the only free parameter) to one experimental data trace using the model described in the previous chapter which incorporates fluctuations in atomic number and position. The resulting uncertainty in $\langle \overline{N} \rangle$ is $\pm 10\%$.

Considering the $\langle \overline{N} \rangle = 1$ case, the transmission lineshape, trace (g), exhibits the two peaks expected with oscillatory energy exchange. This interpretation is unambiguously confirmed by the two similar peaks in the sidelight, trace (c). Interestingly, a central third peak is also present in the transmission lineshape. Its origin can be understood by considering Fig. 3-7 in Sec. 3.2.2. As discussed in that section, the expected experimental lineshape can be calculated as a weighted average of the fixed-atom lineshapes (from chapter 2) with the appropriate $P(\overline{N})$ distribution (curve (a) of Fig. 3-7). The two outside peaks in trace (g) of Fig. 4-10 are present because the probability for the value $\overline{N} \approx 1$ is largest. The third peak arises because: (1) Although the probability for small $\overline{N}$ is low, the empty-cavity transmission signal is large compared to the $\overline{N} \approx 1$ lineshapes; and (2) the cavity resonance is narrow. Note that the importance of the cavity resonance's width compared with that of the atomic resonance, as well as the strength of the coupling, is emphasized by comparing the results in Fig. 4-10 with those of Fig. 3-10. The third peak *is* present in that figure although not prominent enough to see in the data: The disparity between the widths is not great enough for the given coupling strength. There is no third peak

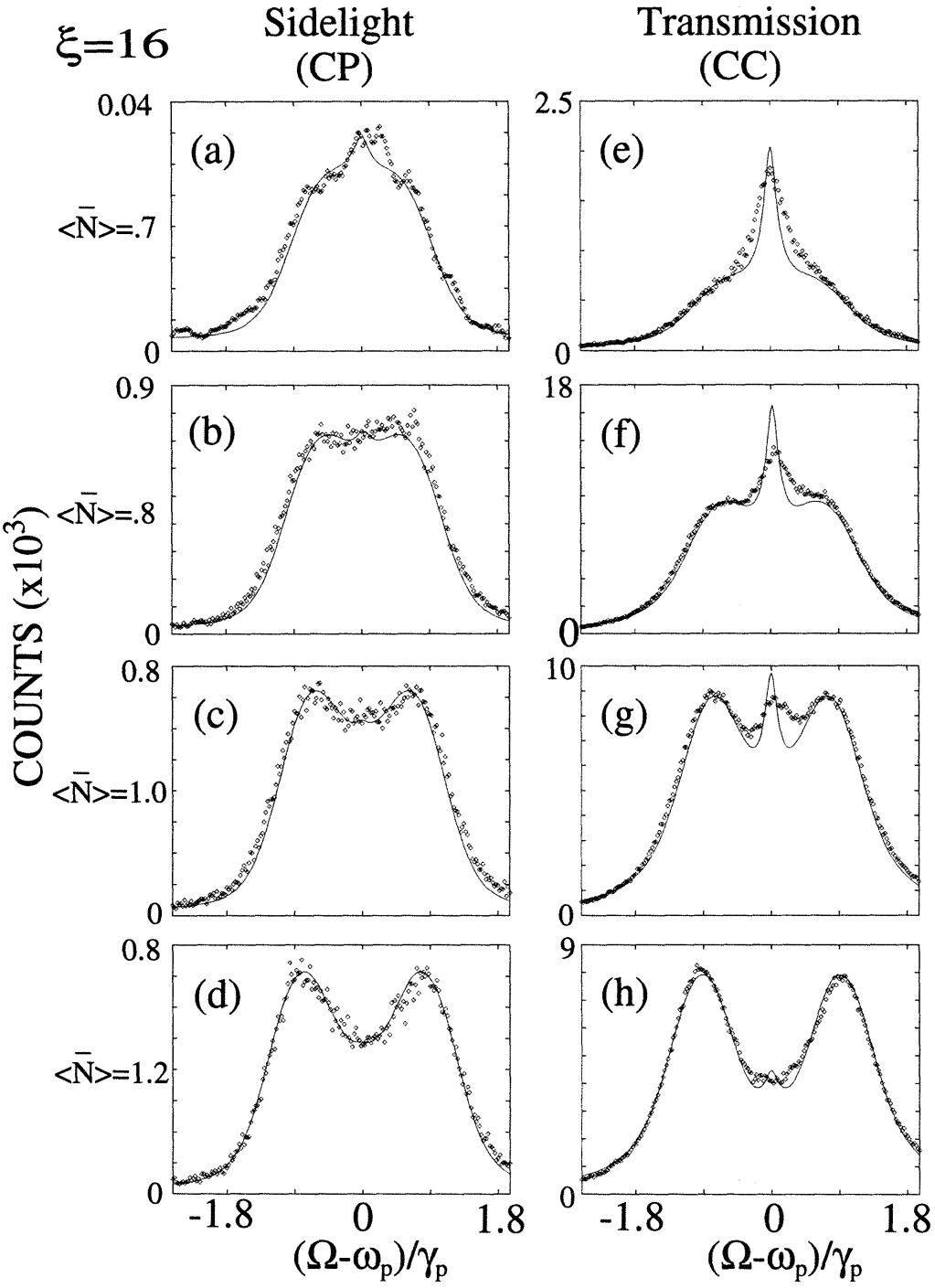

Figure 4-10: Strong coupling ($\xi = 16$) sidelight and transmission data with theoretical fits (solid lines). Data was collected at 120 ms/point for traces (a) and (e) and at 300 ms/point for all other traces.

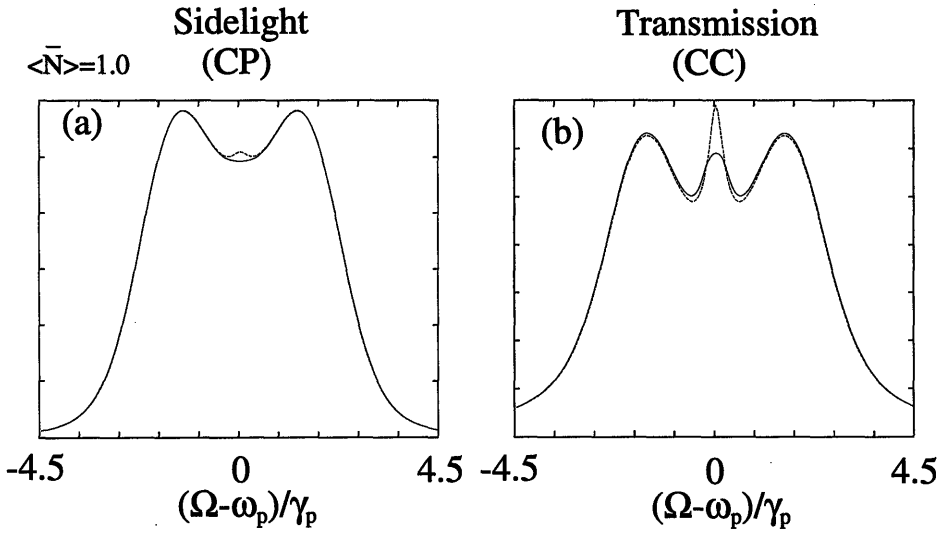

Figure 4-11: Comparison of lineshapes averaged over a range of detunings, $-0.25 < \Delta < 0.25$ (solid curve) with the lineshape for $\Delta = 0$ (dotted curve). The same strong coupling parameters are assumed as in the experiment ($\xi = 16$).

in the sidelight signal, trace (c) of Fig. 4-10, because empty cavity signals out the side of the resonator are absent: An atom not coupled to the cavity mode will not be excited.

Note the extreme sensitivity of the lineshapes (particularly the cavity transmission lineshapes in traces (e–h)) to small changes in $\langle \overline{N} \rangle$. As the atomic beam density is increased, the probability for small $\overline{N}$ decreases and the "empty" cavity resonance disappears, as in trace (h). The empty cavity effect dominates at the other extreme of low atomic beam density, however, and washes out the normal mode splitting in trace (e). The broadened pedestal of trace (e) arises, in fact, from the presence of splitting due to the $\overline{N} \approx 1$ case. Note that traces (a) and (e) were taken after adjustments in alignment, probe power, and count period were made. To compare with the other traces, trace (e) counts should be multiplied by ≈ 14 ($= 2.5 \times 5.7$ corresponding to the count period and power adjustments, respectively), and trace (a) should be multiplied by ≈ 28 (twice the endlight factor because the sidelight alignment had changed). The splitting is seen to be slightly larger in traces (g) and (h) than in (c) and (d) for the cavity and atomic oscillators, respectively. This is a particular example of a general result that reflects the sensitivity of lineshapes to geometry:

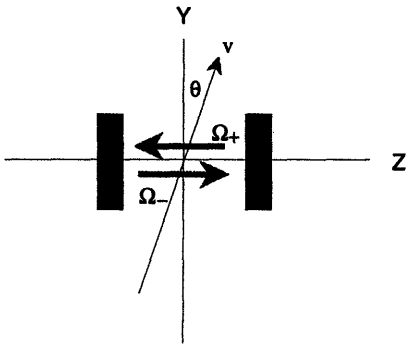

Figure 4-12: Atom with velocity, v, moving through the cavity mode at angle, θ, no longer interacts with a standing wave. The atomic frequency is shifted by $\Omega_{\pm} = \omega_p \pm \mathrm{kv}\theta$.

Lineshape splitting measured by observing the oscillator which is not being driven (atom) is smaller than that which is (cavity mode), but splitting in the former always implies normal mode oscillation (Sec. 2.3.2).

The agreement between the data and computed lineshapes is quite good. The discrepancies are due to atomic beam misalignment, atom-cavity detuning uncertainty, and Doppler broadening. In order to demonstrate this, Fig. 4-11 compares a cavity lineshape, obtained by performing an averaging of several, atom-cavity detuned lineshapes, with the single lineshape for zero atom-cavity detuning, $\Delta = 0$. Each of the detuned lineshapes is computed using the model of the previous chapter with a specified Δ. The range chosen satisfies $-0.25 < \Delta/\gamma_p < 0.25$. The central peak is reduced and broadened in both lineshapes. Note that an atom traversing the cavity mode at an angle $\frac{\pi}{2} - \theta$ relative to the optical axis is Doppler-shifted out of resonance with the SW cavity field by an amount $\mathrm{kv}\theta$ with k the wavenumber and v the atom's velocity. In the situation depicted in Fig. 4-12, for example, the atomic frequency, in the resonator's frame, is shifted by $\mathrm{kv}\theta$ for the field traveling to the left and by $-\mathrm{kv}\theta$ for the field traveling to the right. For an atom moving at the thermal velocity, this gives rise to ≈ 0.5 MHz/mrad shift in frequency. Neglecting homogeneous broadening and cavity damping, the cavity may be tuned such that one of the traveling waves is resonant with the atom. The coupling constant is reduced relative to the SW case,

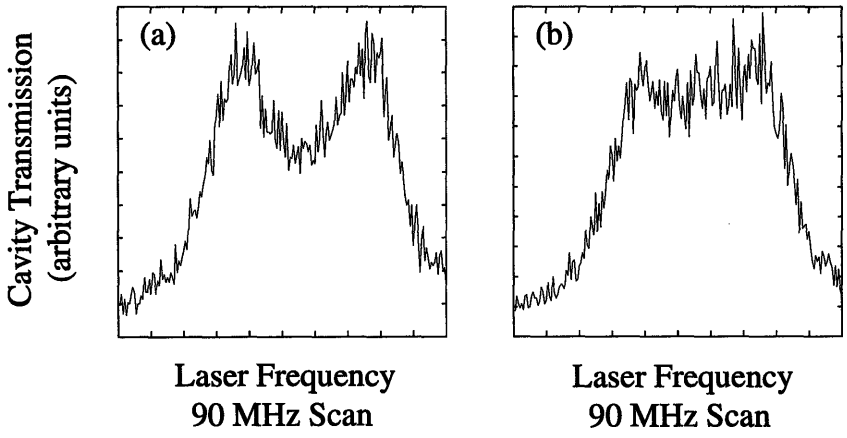

Figure 4-13: Demonstration of atomic beam misalignment for $\langle \overline{N} \rangle \approx 1.2$. (a) Cavity transmission for optimum (90 degrees) atomic beam and cavity mode alignment. (b) Same as (a) but with atomic beam-cavity mode angle changed by $\approx .2$ mrad. This misalignment corresponds to a Doppler frequency shift of ≈ 0.1 MHz for atoms with mean thermal velocity ($\approx 2.5 \times 10^4$ cm/s).

but it is spatially more uniform since their are no nodes and anti-nodes along the cavity axis. This fact is exploited in future single-atom laser studies. Although the above mentioned averaging performed over various detunings does not account for this reduction in coupling, it nonetheless provides a qualtitative explanation of the discrepancies.

Figure 4-13 demonstrates the lineshape's sensitivity to alignment of the relative angle between the atomic beam and cavity mode axis. The final 25 μm pinhole is translated horizontally by ≈ 50 μm to induce an $\approx .2$ mrad (50 μm/30 cm) change in atomic beam angle with all other parameters held fixed.

Similarly, sensitivity to atom-cavity detuning is demonstrated in Figure 4-14. Again, all other parameters are held fixed during these two scans. The atomic side-light signals behave similarly.

Transmission lineshapes for various atom-cavity detunings, Δ, are shown in Figure 4-15. The corresponding normal mode frequencies are plotted in Fig. 4-16 together with the theoretical curves. The theoretical curves for the normal mode frequencies are taken from the fixed atom model, Eqs. 2.29, with $|\mathcal{N}| \rightarrow \overline{N} \approx 1.2$. These frequency shifts were measured comparing the frequency location of each peak in the data to the

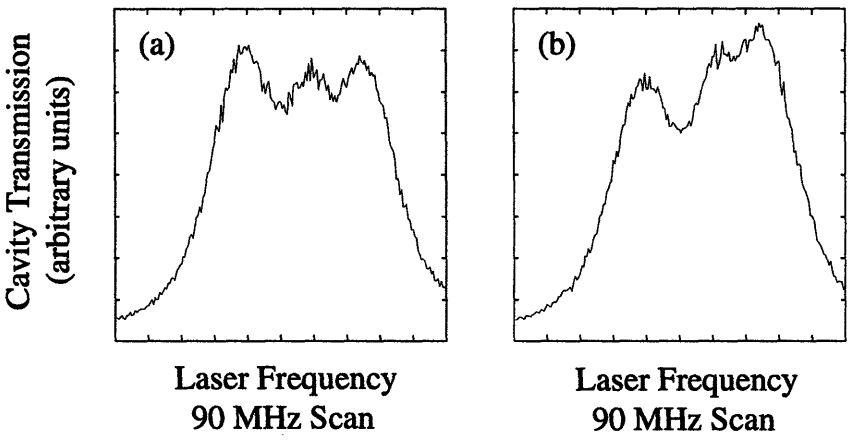

Figure 4-14: Sensitivity to atom-cavity detuning, Δ. The data are cavity transmission lineshapes for (a)$\Delta \approx 0$ MHz, (b) $\Delta \approx 2$ MHz.

position of the atomic free-space resonance frequency. This is a somewhat inaccurate method to determine the normal mode frequencies due to "shoulder" effects (the influence of one normal mode resonance on another due to its proximity) as well as the numerator Lorentzian factor in the CC scheme, discussed in Sec. 2.3.2. The normal mode frequencies may also be taken from the fits (not shown) which were performed on each lineshape. The actual normal mode frequencies obtained from the fits are in better agreement with the theoretical curve than Fig. 4-16 suggests.

4.3.2 Atom Excitation

We now turn to the scheme in which we excite the atoms directly from the side of the strong coupling resonator. The probe waist was chosen to be approximately the same size as the atomic beam and cavity mode waists. In Fig. 4-17, the first demonstration of normal mode splitting using this scheme is shown. As we have seen in Sec 2.3.2, the lineshape splitting of trace (a) is indicative of normal mode oscillatory energy exchange. The lack of splitting in trace (b) results from the contribution of uncoupled atoms to the sidelight signal, dominating the two-peaked lineshapes which arise from the coupled atoms (see Eq. 3.32). The coupled atom's presence may be inferred from the non-Lorentzian character of trace (b) (i.e., a broadening of the base). Note that

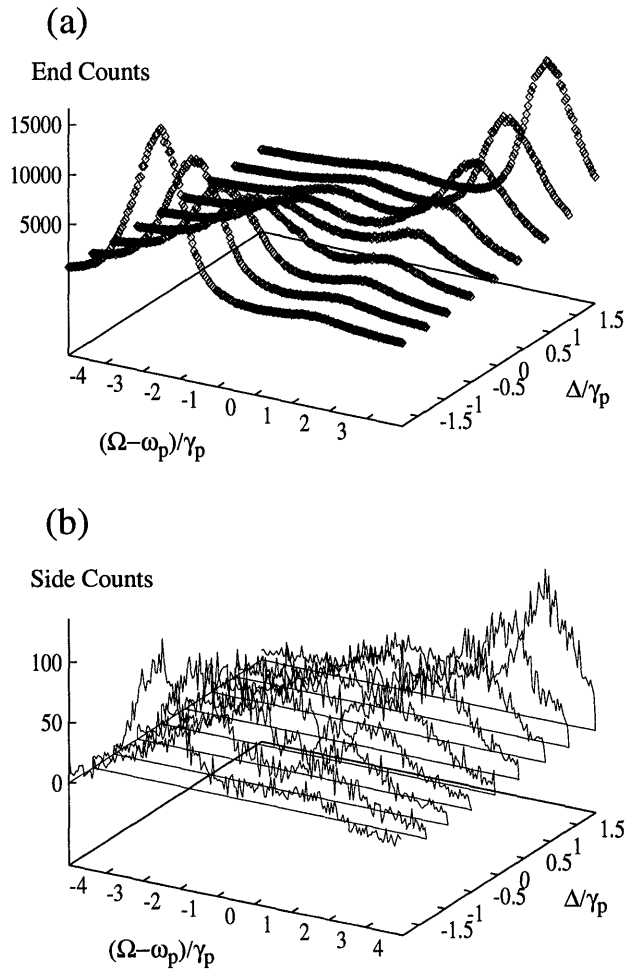

Figure 4-15: (a) Cavity transmission lineshapes in CC scheme for various detunings and (b) Atomic lineshapes in CP scheme. In these plots, $\langle \overline{N} \rangle = 1.2$, and $\xi = 16$.

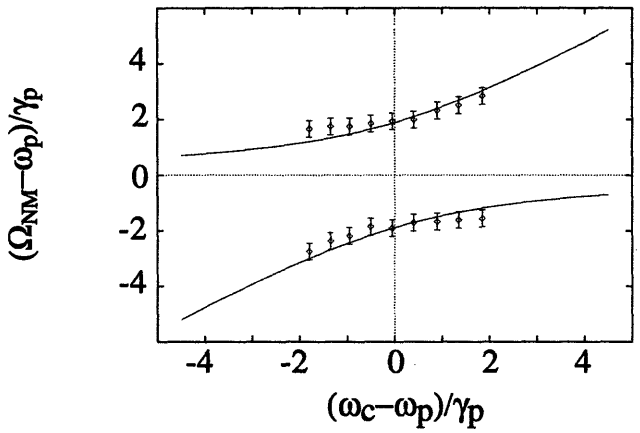

Figure 4-16: (a) Normal mode frequencies, Ω_{NM}, for the lineshapes of the previous figure with $\langle \overline{N} \rangle = 1.2$, and $\xi = 16$.

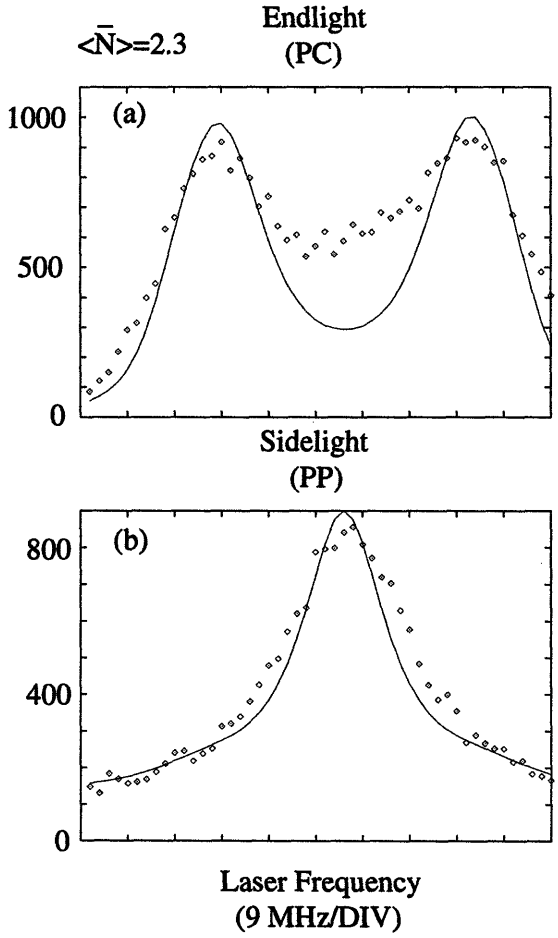

Figure 4-17: (a) Cavity signal (PC scheme) and (b) Side signal (PP) with $\langle \overline{N} \rangle = 2.3$ and zero atom-cavity detuning.

the addition of the side probe gives rise to another source of misalginment broadening which is responsible for the quality of fit with the theoretical curve, particularly in trace (a). All sidelight lineshapes resembled that of trace (b) and will thus not be shown in the remainder of this section.

To demonstrate the influence of the number of interacting atoms on lineshapes for the PC scheme, several scans were performed at various oven temperatures (or, equivalently, atomic beam densities). The results are plotted in Fig. 4-18 together with the theoretical curves for the designated values of $\langle \overline{N} \rangle$ (dotted lines). Note the gradual increase in the linewidth, and the emergence of two peaks in traces (e-f) as a result of strong coupling. The two theoretical curves shown in trace (f) demonstrate the effect of slight changes in atomic beam density.

Trace (a) exhibits a lineshape which is closest to the true single atom regime, discussed in Sec. 3.2.5, above. Comparison of this trace with trace (f) of Fig. 3-11 demonstrates that the rough approximation for $P(\overline{N})$ assumed in the calculation of trace (f) is fairly accurate. Unfortunately, limitations in the signal-to-noise ratio of the present setup prohibits study of the PP lineshape (trace (a), for example, of Fig. 3-11) in this regime. Nonetheless, the lineshape in Fig. 4-17(b) (which appears in all PP scans) demonstrates that indeed the main contribution to the experimental lineshapes arise from the situation in which several atoms are coupled to the mode, as argued in Sec. 3.2.5. (The probe power is less during acquisition of traces (e) and (f) in Fig. 4-18, by approximately a factor of 10, than that for traces (a-d). This accounts for the reduction in the counts for these traces).

In Figure 4-19 we compare CC and PC schemes with consecutive data scans. In the data shown, a CC lineshape scan is taken and immediately followed by a PC scan. Trace (c) for the CC lineshape is fit with $\langle \overline{N} \rangle = 1.7$. Following the scan for this trace, the atomic beam density dropped by 10%, resulting in a value for the intracavity atomic number, $\langle \overline{N} \rangle = 1.5$. The first fit shown for PC in trace (f) assumes this density. The second value of beam density gives a closer fit. In most of the PC lineshapes taken, a similar, slight, reduction in $\langle \overline{N} \rangle$ below that expected on the basis of the CC fits is required to obtain a better looking fit. Again, misalignment

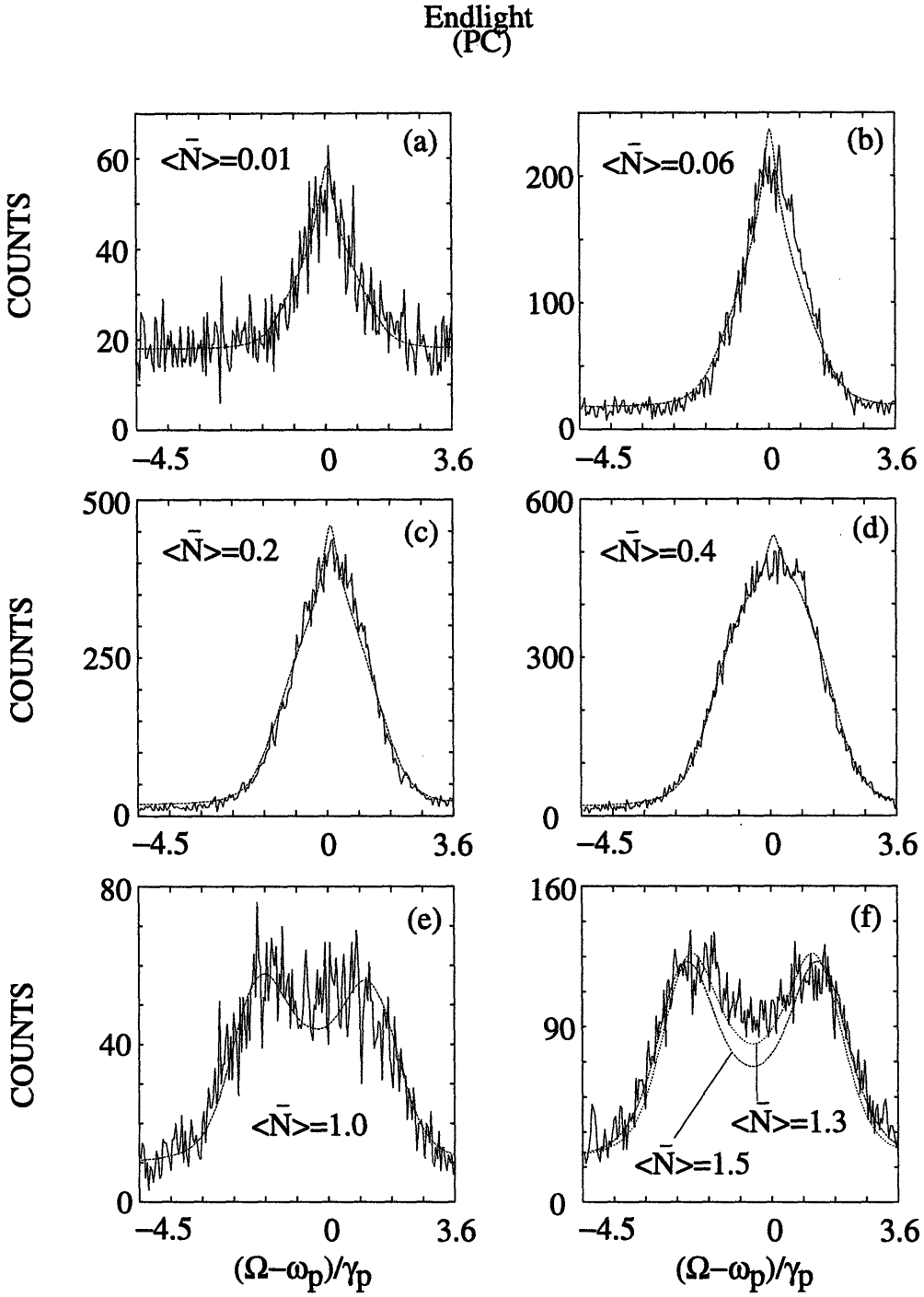

Figure 4-18: Cavity signal for atomic excitation (PC scheme) for various atomic beam densities.

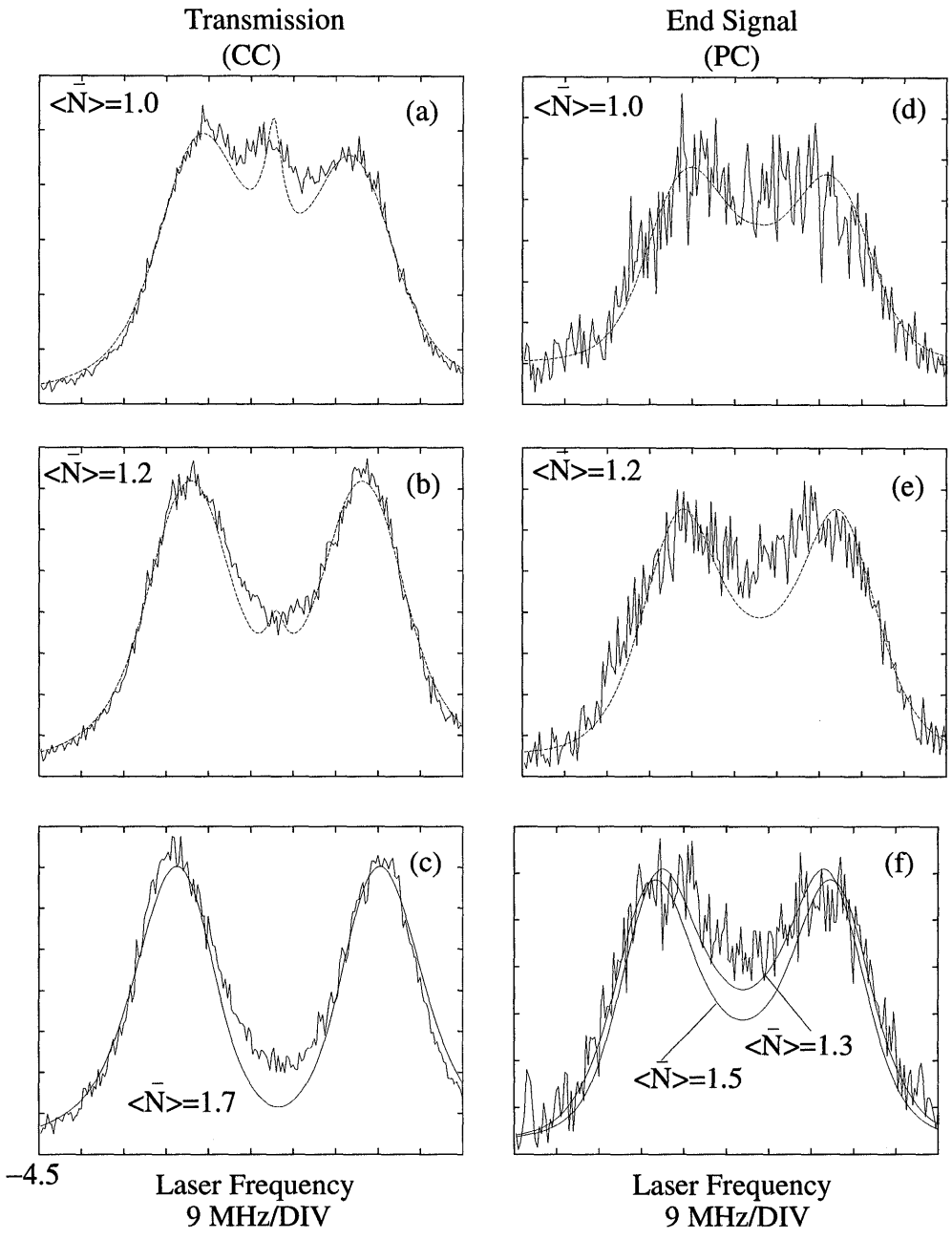

Figure 4-19: Comparison of CC scans with PC scans.

broadening of the side probe is the most likely cause. Nonetheless, the corresponding CP lineshapes of Fig. 4-10 (traces (c) and (d)) are similar to the PC lineshapes for the same values of $\langle \overline{N} \rangle$ shown in Fig. 4-19, as expected.

4.4 Intermediate Coupling Results

In this section, the experimental results for the intermediate coupling resonator are presented. Both cavity excitation and atom excitation schemes are performed. The experimental arrangement is identical to the strong coupling arrangement, with the only exception the cavity finesse, as discussed at the beginning of this chapter. Note that the empty cavity linewidth is $2\gamma_c/2\pi = 108$ MHz. However, the maximum tuning range for the experimental probe is 90 MHz. This range is sufficient for the CP, PP, and PC lineshapes since their linewidths are of the same order as the atomic linewidth and, hence, do not exceed ≈ 50 MHz (FWHM). The CC lineshape, however, exceeds the available tuning range. Below, we present one CC lineshape for a scan which is ≈ 190 MHz. This is accomplished by detuning the AOMs appropriately above, at, and below the atomic and cavity resonances and performing the 90 MHz scan for each detuning. The three resulting 90 MHz scans, which overlap each other, are then pasted together. Since the cavity lineshape is only altered in the vicinity of the atomic resonance, only a single 90 MHz scan is shown in the rest of the data.

Estimates for the expected signals are similar to those in the strong coupling case of Sec. 4.3 with only the cavity finesse different. This effects only the end signal which may be estimated with Eq. 4.3 using the correct finesse in γ_c. Since the coupling is independent of finesse, $\nu_s \approx 0.3$ (same as the strong coupling cavity), and the end signal is $\dot{\nu} \approx 3 \times 10^6$ cps for ν_s photons in the cavity mode.

4.4.1 Cavity Excitation

In Fig. 4-20, lineshapes for CC and CP schemes in the intermediate coupling regime are shown. For comparison, strong coupling lineshapes for the corresponding schemes are presented with approximately the same atomic beam density. The intermediate coupling sidelight, trace (a), exhibits a 45 MHz linewidth (FWHM, with ≈ 3 MHz Doppler and transit time broadening), twice the free-space value, providing a dramatic demonstration of line broadening. In view of the single-peaked lineshape observed out the resonator side, trace (a), the two peaks in trace (b) cannot be attributed to

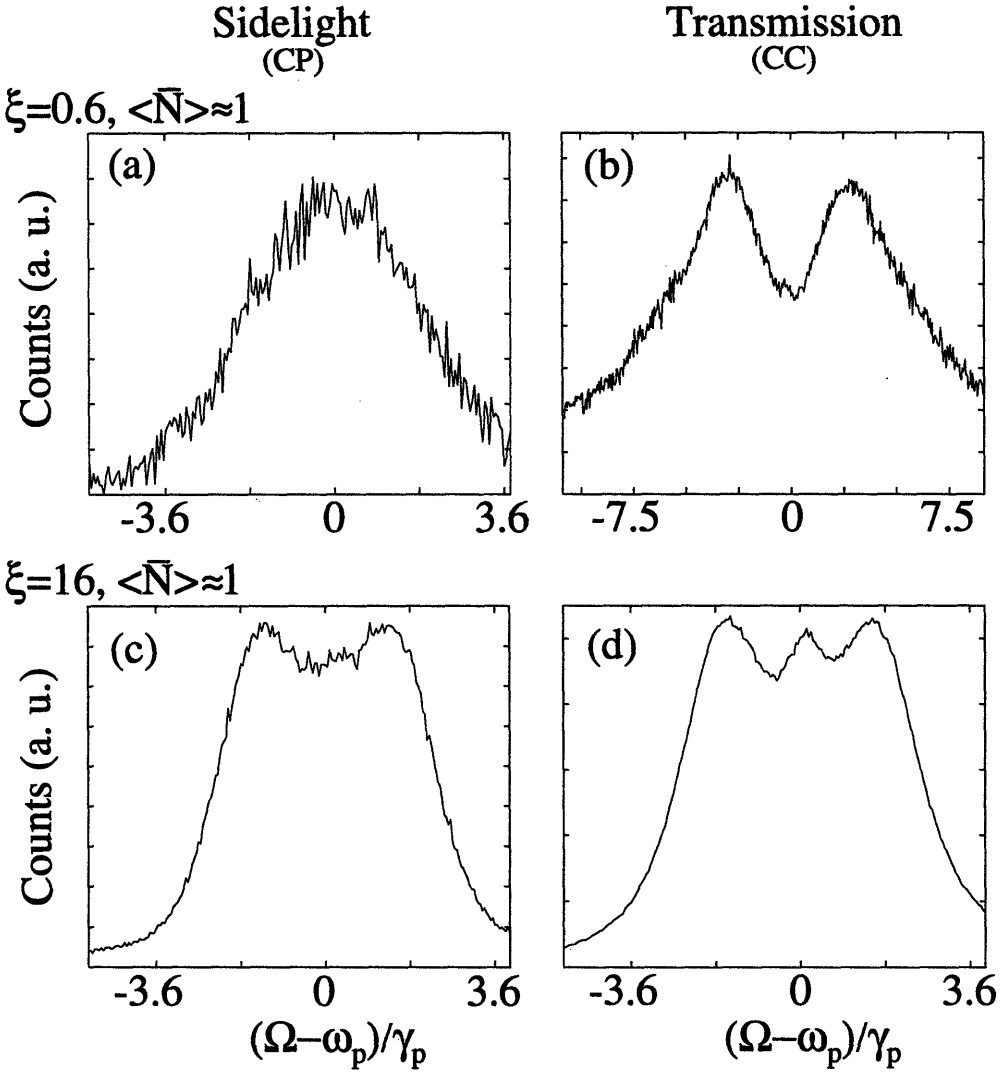

Figure 4-20: Atomic (a) and cavity (b) lineshapes for intermediate coupling with $\langle \overline{N} \rangle \approx 1$. For comparison, traces (c) and (d) show the corresponding lineshapes for strong coupling and $\langle \overline{N} \rangle \approx 1$. Lineshape splitting does not necessarily imply oscillatory energy exchange.

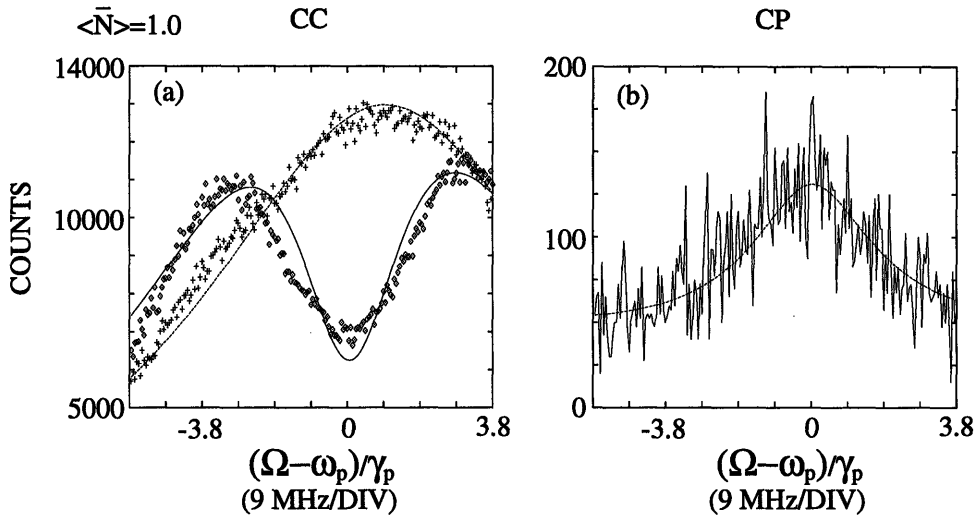

Figure 4-21: Cavity (a) and atomic (b) lineshape data with fits (solid curves) for intermediate coupling and $\langle \overline{N} \rangle \approx 1$. For comparison, the two traces in (a) are with and without atoms (empty cavity). Note that the cavity is detuned ≈ 9 MHz higher than the atomic transition frequency ($\Delta/\gamma_p \approx 1$).

oscillatory energy exchange. Furthermore, $\xi \approx 0.6$, which excludes the possibility of two distinct normal mode frequencies. This splitting, instead, can be explained by noting that when the excitation laser is near resonant with the atom, light is scattered out the resonator side and, since $\gamma_p < \gamma_c$, a dip results in the cavity transmission lineshape. A similar result is reported in [70].

Figure 4-21 displays typical CC and CP scans simultaneously collected, together with fits based on our model. The parameters for the fits include the atomic and cavity linewidths ($2\gamma_p$ and $2\gamma_c$), the end and side signal attenuation factors due to collection efficiencies, incident probe power, atom-cavity detuning (Δ), atomic center frequency location within the scan, atomic beam density ($\rho_0 \propto \langle \overline{N} \rangle$), and end and side background signal strengths. Values for these parameters are given in Table 4.2. They are determined in the following way (note that similar procedures were applied in the strong coupling experiment): Atom and cavity linewidths are independently measured by laser scans. The atomic width is compared with independent measurements in the literature and the cavity linewidth is checked for consistency with the cavity throughput measurements. All the collection efficiency factors, such as PMT

parameter	*value*
η_{PMT}	7%
f_{side}	7.0×10^{-3}
F_{side}^{opt}	70%
F_{end}^{opt}	75%
η_{cav}	0.9
η_{AOM}	80%

Table 4.2: Measured parameters for the intermediate coupling experiment.

efficiency, loss via scattering off intermediate optical components, AOM efficiency, and cavity throughtput are independently measured. For the sidelight signal, the solid angle collection factor is estimated. Correction factors for both end and side signals are introduced to correct for slight deviations (particularly for the sidelight signal solid angle estimate). They are adjusted in a best fit to a single scan for both the end and side signals and thereafter left fixed. Incident probe power is determined by measuring the CC signal for empty cavity scans, as in Fig. 4-21(a). Atom-cavity detuning, Δ, is adjusted by the controlling voltage to the cavity reference AOM and is measured by performing an empty cavity scan (CC scheme) as in Fig. 4-21(a). The location of the peak of this scan is compared with the location of the peak of the free-atom fluorescence signal (not shown), which is adjusted for any offsets due to Doppler shifts caused by beam misalignment. (Location of the atomic center frequency within the 90 MHz scan is fixed from scan to scan.)

Estimated uncertainty in the atom-cavity detuning is somewhat large, ± 5 MHz, because of the low finesse cavity. The atomic beam density is measured via the free-space fluorescence signal for all scans. It is calibrated in a fit performed on CC and CP lineshapes for a single scan in which all other parameters are known, as was done in the strong coupling experiments. Estimated uncertainty for this measurement is $\pm 10\%$. The sidelight signal for the empty cavity scan, CP (not shown), is also used as a measure of the background signal out the side. The background signal out the end is essentially zero in all CC scans. Also, the CC data is taken with a 1% filter before the PMT and all counts displayed are actual counts. Therefore, to obtain the actual signal strength, one should multiply the displayed counts by 10^2. In this scan,

the total counting time per point is 120 milliseconds.

In Fig. 4-22, CC and CP lineshapes for various atom-cavity detunings are shown. The fits are reasonable in view of the various broadening mechanisms discussed above. Slight probe power variations, particularly at the ends of the scan, also contribute to the degradation in fit quality. This power variation is not the result of actual laser power changes but, instead, is due to the fact that the probe alignment changes slightly during the frequency scan. The divergence angle of the TEM_{00} mode of the cavity is $\theta \approx 7$ mrad, as mentioned in the alignment procedure discussion of Sec. 4.2.4, so that very small changes in the probe angle can effect the coupling of the probe into the mode. These variations are on the order of 10% and occur only near the ends of the scans. Their effect on the lineshapes with widths smaller than that of the scan is negligible (eg., in the strong coupling experiment). Note that the scan for traces (d) and (i) was performed on a different day with slightly larger laser and, therefore, probe power.

In Sec. 3.4, we compare the degenerate resonators used in previous studies of enhanced and suppressed spontaneous emission [67] with the high finesse resonators of the present work. In Fig. 4-23, CP lineshapes are presented for two cases: (a) $\Delta = 0$ and (b) $\Delta = 50\gamma_p$. The probe power is increased by a factor of 10^2 in trace (a) to improve signal-to-noise. Note that this large power will not saturate the system since the detuning is very large. The linewidth increases dramatically, from ≈ 25 MHz (natural width plus broadening) to ≈ 43 MHz, as does the peak height. This is attributable to the enhanced spontaneous emission the atoms undergo when in the resonator at or near anti-nodes. As a rough estimate, we calculate the enhanced emission linewidth using Γ_- of Eq. 2.120. For the case of a single optimally coupled atom, $\Gamma_-/\gamma_p \approx 1.84$, so the full width is $2\Gamma_- \approx 35$ MHz. This value is smaller than the measured linewidth. There is therefore a significant contribution of spontaneous emission by several atoms simultaneously coupled to the resonator mode, all driven coherently by the cavity field (note that $\langle \overline{N} \rangle = 1.4$). This situation should not be confused with superradiance since only one quanta of energy excites the system (at most one atom is excited) and, more importantly, since the atoms must be treated

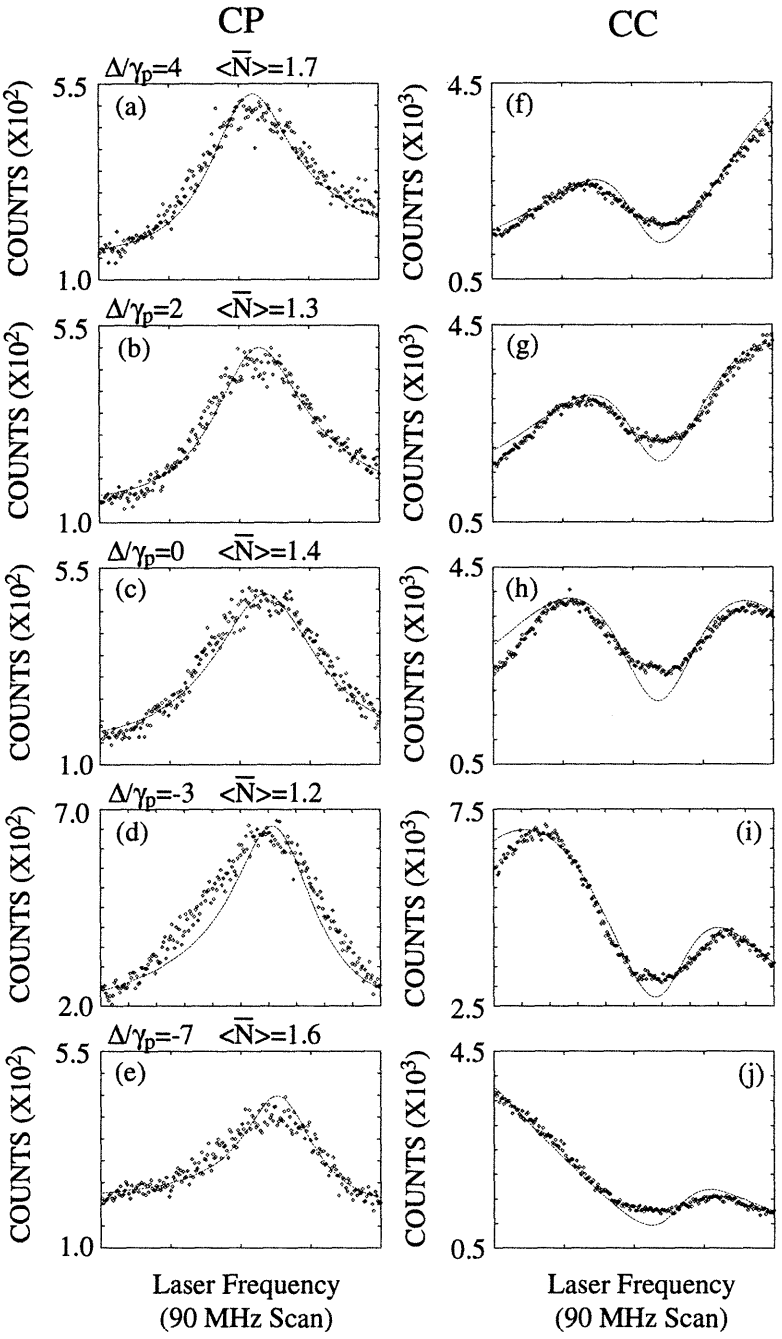

Figure 4-22: Cavity (a-d) and atomic (e-h) lineshape data with fits (solid curves) for intermediate coupling at various atom-cavity detunings. The time per data point is 300 ms.

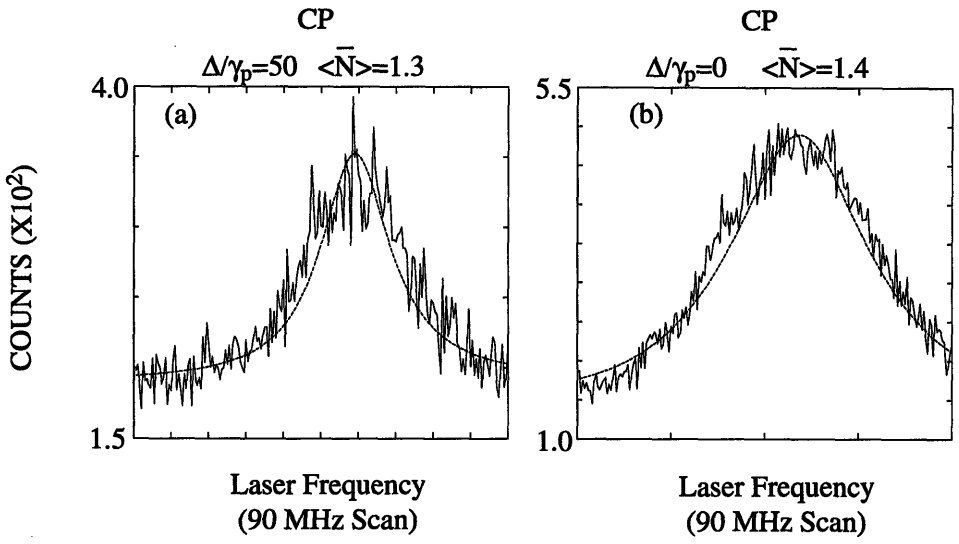

Figure 4-23: Two scans for CP with (a) $\Delta = 50\gamma_p$ and (b) $\Delta = 0$ together with fits (solid curves) for intermediate coupling.

as distinguishable. This explanation also applies to the results shown in Fig. 4-18 for the PC scheme in strong coupling. In comparison with the concentric cavity, in which atoms cannot "communicate" their presence to one another, the expected linewidth would be 35 MHz since all atoms act independently. For the detuned case, each atom in the supercavity resonator, in effect, becomes weakly coupled to the resonator and behaves as though it were in free space. Since the solid angle factor is very small, no suppression of spontaneous emission (i.e., reduction in the linewidth below the natural linewidth) is seen.

4.4.2 Atom Excitation

Excitation of the atoms via a probe from the side of the cavity is performed as in the strong coupling experiment. The probe is focussed to a waist approximately the same size as the cavity mode waist, with polarization parallel to the atomic beam direction. The separation of the mirrors at their edges (≈ 90 μm), however, is smaller than that for the strong coupling resonator (≈ 170 μm). Although the cavity lengths and radii of curvature are the same, the mirror diameters are not. With the increased scattering of the probe off the mirror edges, the signal-to-noise ratio for the sidelight is reduced

and systematic background drifts arise as the probe is scanned. Consequently, the sidelight signals are not very reliable but they do exhibit the same qualitative features observed in the strong coupling experiments, i.e., the dominant contribution is from the uncoupled atoms. Shown in Fig. 4-24 are the PC and PP lineshapes for various detunings. Fits from the model are also shown with the data and are in reasonable agreement.

As another demonstration of the cooperative nature of the atom-cavity interaction in the SW resonator, Fig. 4-25 shows PC and PP lineshapes obtained for two different atomic beam densities at fixed detuning. All other parameters are the same. Note that the linewidth increases with density. (A similar effect was observed in the strong coupling experiment for the PC scheme in Fig. 4-18 of Sec. 4.3.2.) If the atoms interacted with the cavity mode independently, as in the degenerate resonators, only the signal strength would increase in proportion to the number of atoms. The linewidth would not increase.

4.5 Saturation Study

The study of saturation in the SW mode experiment is complicated by the fact that atoms at different locations have different saturation parameters. We have observed three-peaked lineshapes in the strong coupling CC scheme (trace (g) of Fig. 4-10) and identified various features of the lineshape with different coupling strengths. More precisely, the central third peak of this lineshape arises due to weakly coupled atoms and the outside two peaks arise from the strongly coupled atoms. Therefore, we may expect that the two outside peaks will exhibit saturation before the central peak, i.e., deviate from linearity with laser probe power. This would give rise to a single peaked lineshape as the laser power is increased for both the end and side signals. If, on the other hand, the lineshapes do not change with increasing power but only increase in size linearly, then we may conclude that this constitutes a demonstration that these powers are not saturating the system. In Fig. 4-26 we demonstrate that the powers used for obtaining data in the driven cavity scheme do not exhibit saturation effects.

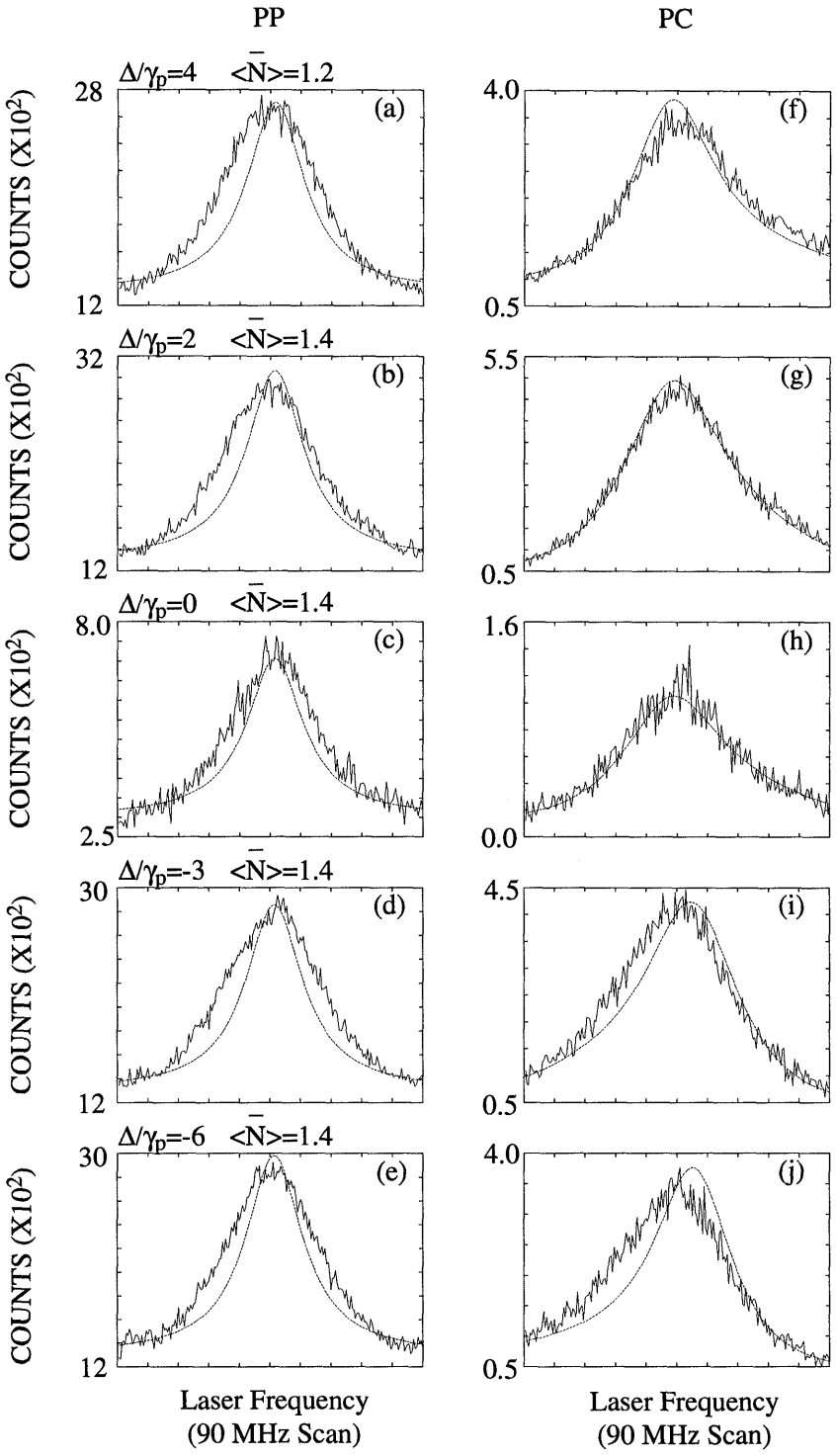

Figure 4-24: PC and PP lineshapes for various detunings.

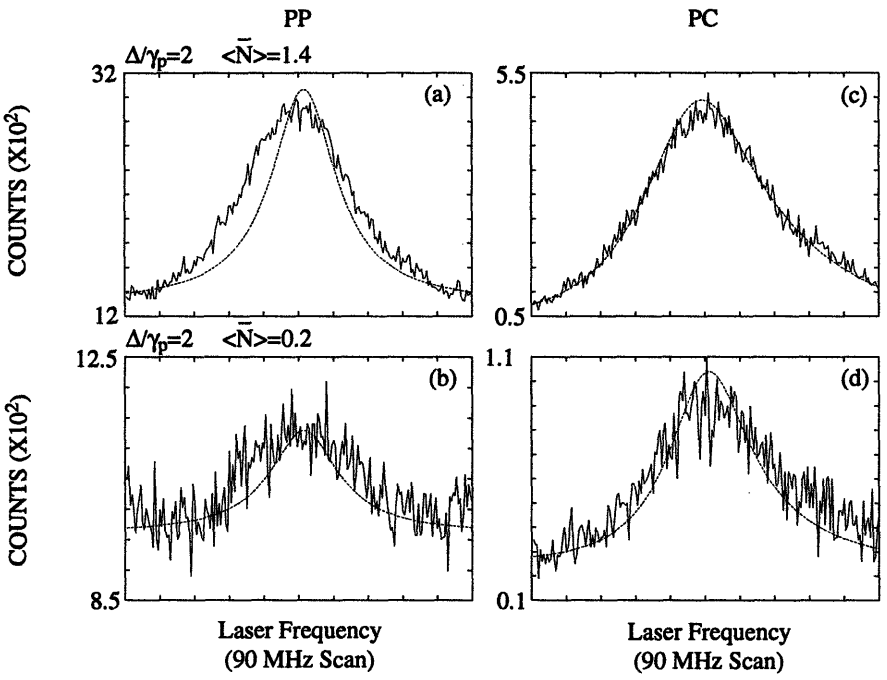

Figure 4-25: PC and PP lineshapes for two densities at fixed detuning.

In this figure, as in all previous data shown, the sidelight (CP) and cavity endlight (CC) lineshape data are collected simultaneously (eg., traces (a) and (e) are simultaneously recorded). The probe power is then increased and the laser scan repeated. Note that trace (d) suggests that saturation is beginning to occur (a deviation in the lineshape), but in this scan the atomic beam density dropped, as seen in comparing the values for $\langle \overline{N} \rangle$ (as discussed previously, the atomic beam density is monitored via measuring the free-space lineshapes from a region of the atomic beam before the cavity). The solid curves are fits to the data. These fits do *not* include the effects of saturation as they are simply the solutions obtained by assuming the inversion is constant (i.e., the model of Chapter 3 is used). The count period for this data is 120 ms per point.

Finally, we increase the laser probe power by large amounts to demonstrate saturation effects. Figure 4-27 is a plot of the CC and CP lineshapes in the strong coupling regime demonstrating the variation in lineshapes as input probe laser power is increased above saturation. Traces (a) and (e) were taken at probe powers close to saturation. For very large powers, note the broadening in the pedestal of the

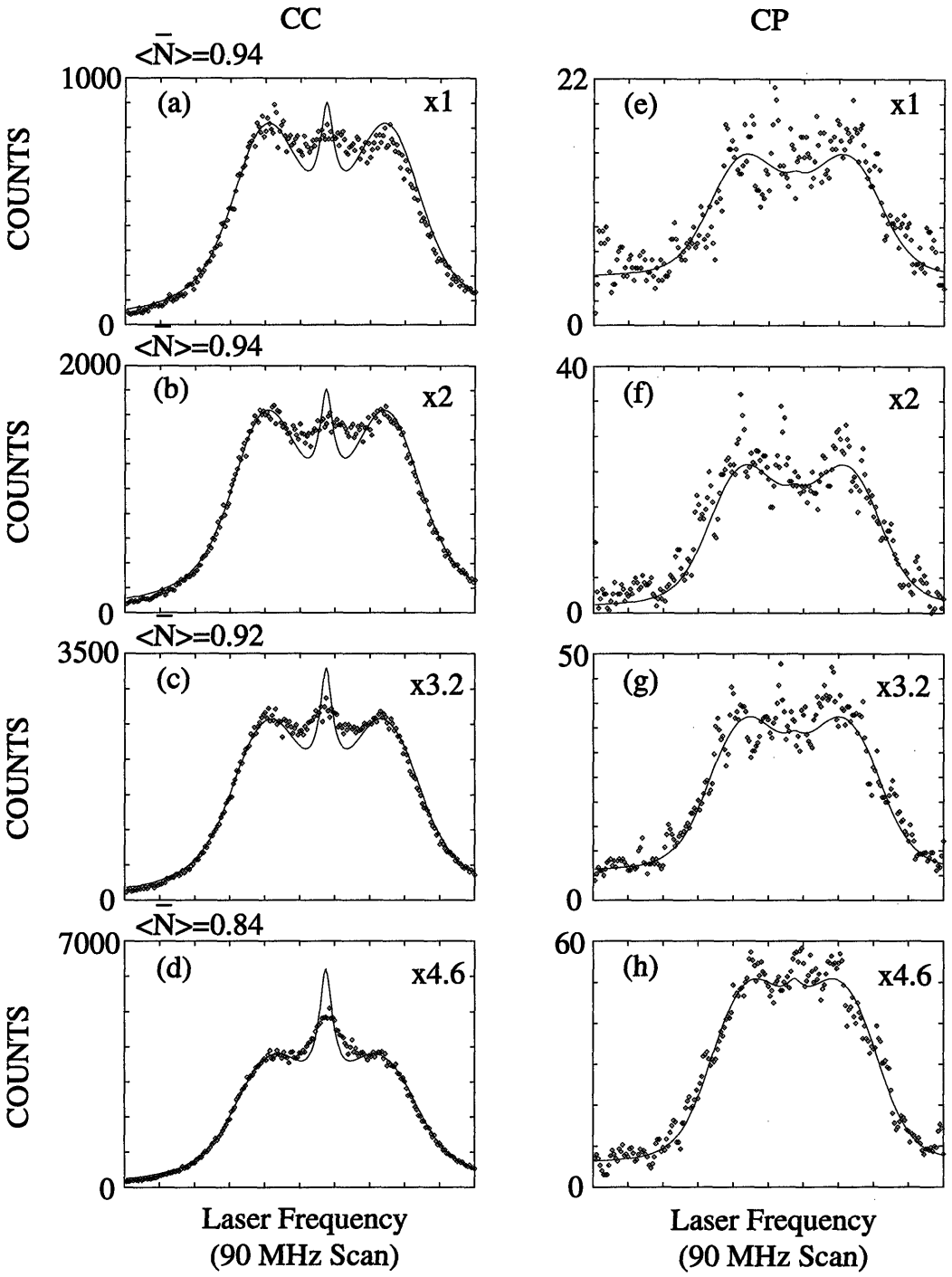

Figure 4-26: Cavity transmission and sidelight lineshapes for various probe laser powers. The $\times 1$ factor in the upper right corner of each scan refers to the relative probe power.

sidelight lineshape, trace (d) (compare with trace (b)). Such broadening is probably attributable to excitation of the so-called Jaynes Cummings ladder-state transitions.

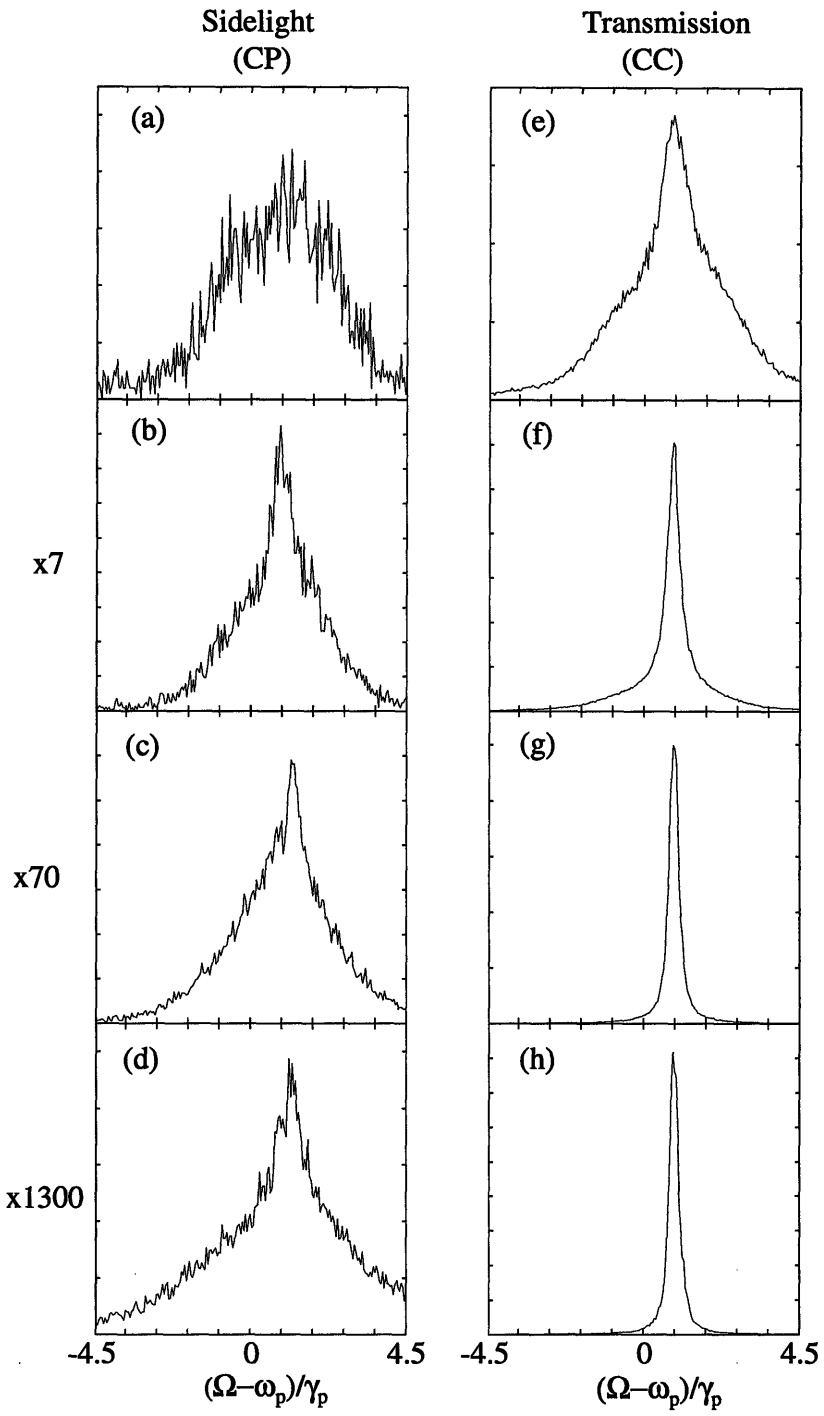

Figure 4-27: Strong coupling cavity transmission and sidelight lineshapes for various probe laser powers with $\langle \overline{N} \rangle \approx 1$.

Chapter 5

Conclusion

5.1 Summary

A spectral lineshape study of the normal mode structure of an atom-cavity system has been presented. This atom-cavity system consists of atoms in an atomic beam interacting with a single standing-wave mode of a spherically symmetric optical cavity. Two cavities were used, each with a different finesse so that both the strong and intermediate coupling regimes could be investigated: All other essential dimensions of the cavities were the same. The atomic beam density was chosen so that the number of intra-cavity atoms was approximately one. Dramatic modifications of spontaneous emission is inferred from the measured lineshape structures. Three-peaked, two-peaked, and broadened single-peaked lineshapes arise in the strong coupling regime, depending on the excitation scheme chosen. The two-peaked lineshapes arise because of the reversible spontaneous emission (much greater than the free-space rate) and the three-peaked lineshapes arise for an additional reason: Large fluctuations in intra-cavity atomic number cause the atom-cavity system to fluctuate between a strongly coupled system and a weakly coupled system. Similarly, one and two-peaked lineshapes have also been observed in the intermediate coupling regime. Sidelight (or atomic) linewidths, as well as endlight (or cavity) linewidths, exceeding the natural linewidth have been attributed to enhanced spontaneous emission rates twice that in free space.

The role of fluctuations in the intra-cavity atomic number has been demonstrated in the various lineshapes. These fluctuations are attributable to the standing-wave cavity mode and to the changes in the atomic positions. As mentioned above, the number of intra-cavity atoms was kept near unity. Several atoms, on average, are required to achieve this limit. This regime, therefore, does not constitute a true single atom regime. The role of single atom effects in such a system has been described. For the parameters of the strong coupling cavity (strong coupling, narrow cavity limit), lineshape splitting which is attributable to oscillatory energy exchange could not possibly occur for a single atom. Nonetheless, lineshape splitting in this regime could be observed for the scheme in which the atom is excited and the sidelight (or atomic) lineshape is measured. This splitting owes its existence to suppression of fluorescence due to interference between cavity and probe fields at the position of the atom. With modest improvements in the signal-to-noise ratio, these lineshapes could also be measured.

The relationship between lineshape splitting and oscillatory exchange of energy has been clarified. Reversible (and enhanced) spontaneous emission has been demonstrated in the strong coupling regime via lineshape splitting, leading to oscillatory exchange of energy between the atom and the cavity mode, in a scheme which cannot exhibit splitting otherwise, i.e., measuring the spectral lineshape of the oscillator which is not being probed. Also, conditions for which no oscillations can occur but lineshape splitting nontheless is observed (intermediate coupling, CC scheme) were realized and explained.

A brief study of saturation effects attributable to cavity photons has been presented. In such a system, these effects are quite complicated because of fluctuations in intracavity atomic number: Atoms at different positions have different saturation intensities. In the driven atom scheme, account must be taken of the probe field as well. In this case, an optimally coupled atom is more difficult to saturate than a weakly coupled or free atom because of its larger total spontaneous emission rate, A_{tot}. In fact, we have

$$\frac{A_{tot}}{A_{free}} = \frac{2\gamma_p + A_{cav}}{A_{free}} \approx \frac{1}{1-\beta}, \tag{5.1}$$

where the approximation assumes $f \ll 1$. For the optimally coupled atom in the intermediate coupling cavity, $\beta \approx 0.31$ so that $A_{tot} \approx 1.45 \times A_{free}$.

Finally, we briefly considered the possibility of exciting a single normal mode of the strong coupling system, but this cannot be realized with the present setup. Several atoms interacting with the mode are at different positions in the cavity field as well as the side excitation field. They therefore see different relative phases of the two excitation fields: The relative phases of the two fields is position dependent. Therefore, the net effect would be to average over these relative phases, violating the required condition that the relative phase for each atom should be fixed and the same. Planes of constant relative phase can be found but the required confinement of the atoms to these planes is technically difficult.

Appendix A

Calculation of Cavity-Probe Coupling

In this appendix we calculate α for the case $\epsilon = c$. From Eq. 2.81, if we assume no atoms are present ($g_0 \to 0$), we get for the cavity field:

$$E_c = \frac{\alpha E_L}{2i\Omega L_c}. \tag{A.1}$$

The intensity transmitted through the resonator, I_T is:

$$I_T = \eta_{cav} \frac{1}{2} \left(\frac{2\gamma_c V |E_c|^2}{8\pi a} \right), \tag{A.2}$$

where $a = V/L$ and η_{cav} is the cavity output coupling factor:

$$\eta_{cav} = \frac{T}{T + A_L}, \tag{A.3}$$

where T is the transmission and A_L is the loss of the cavity. Substituting gives

$$I_T = \eta_{cav} \frac{1}{2} \left(\frac{2\gamma_c V}{8\pi a} \right) \left(\frac{8\pi I_L \alpha^2}{c|L_c|^2 4\Omega^2} \right). \tag{A.4}$$

We calculate α in the following way. From simple interference arguments for calculating the transmitted intensity, I_T, through an empty Fabry Perot resonator [71], we

get:

$$\frac{I_T}{I_L} = \eta_{cav}^2 \left(\frac{\gamma_c^2}{(\Omega - \omega_c)^2 + \gamma_c^2} \right), \tag{A.5}$$

where $I_L = c|E_L|^2/8\pi$. This expression must agree with Eq. (A.4). Setting the two equal gives:

$$\frac{\alpha^2}{4\Omega^2} = 2 \left(\frac{c}{2L} \right) \gamma_c \eta_{cav}. \tag{A.6}$$

Appendix B

Broadband Excitation

In this appendix we consider the use of broadband excitation to study emission. This source of excitation destroys the phase coherence of the scattering process and enables the excited state population to be measured in an emission process. Consider, therefore, an atom-cavity system in which the atom is excited by a weak, broadband light source with intensity per unit bandwidth, $i_L(\Omega)$. We assume that each spectral component is statistically independent, and that the bandwidth of the source is much broader than any other linewidth of the system. Using the expressions in the scattering section for $N_u^{\epsilon=p}(\Omega)$, $P_{ends}^{\epsilon=p}(\Omega)$, and $P_{side}^{\epsilon=p}(\Omega)$, Eqs. 2.98, 2.86, and 2.95, respectively, we can then write

$$N_u = \int_0^\infty N_u^{\epsilon=p}(\Omega)\frac{i_L(\Omega)}{I_L}d\Omega \cong \frac{i_L(\omega_p)}{I_L}\int_0^\infty N_u^{\epsilon=p}(\Omega)d\Omega, \tag{B.1}$$

$$P_{ends} = \int_0^\infty P_{ends}^{\epsilon=p}(\Omega)\frac{i_L(\Omega)}{I_L}d\Omega \cong \frac{i_L(\omega_p)}{I_L}\int_0^\infty P_{ends}^{\epsilon=p}(\Omega)d\Omega, \tag{B.2}$$

and

$$P_{side} = \int_0^\infty P_{side}^{\epsilon=p}(\Omega)\frac{i_L(\Omega)}{I_L}d\Omega \cong \frac{i_L(\omega_p)}{I_L}\int_0^\infty P_{side}^{\epsilon=p}(\Omega)d\Omega, \tag{B.3}$$

where

$$\int_0^\infty i_L(\Omega)d\Omega = I_L. \tag{B.4}$$

We can evaluate the integrals by the method of residues to obtain:

$$P_{ends} = \eta_{cav}\left[\frac{\pi\gamma_p i_L(\omega_p)}{2I_s}\right]\hbar\omega 2\gamma_p\left(\frac{\sigma c}{2\gamma_c V}\right)\left(\frac{\gamma_c}{\gamma_c+\gamma_p}\right)\frac{1}{1-G'}, \tag{B.5}$$

$$P_{side} = N_u\hbar\omega 2\gamma_p, \tag{B.6}$$

with

$$N_u = \left[\frac{\pi\gamma_p i(\omega_p)}{2I_s}\right]\left[1+\left(\frac{\gamma_c}{\gamma_c+\gamma_p}\right)\frac{G'}{1-G'}\right]. \tag{B.7}$$

Comparing Eqs. B.5 and B.7 with Eqs. 2.69 and 2.66 respectively, it is clear that the same results are obtained.

An experiment in the broad cavity limit with weak coupling was performed by Heinzen *et al.*, [12] with single ^{174}Yb atoms weakly excited by a broadband laser field ($\gamma_c \approx 11$ MHz, $\gamma_p \approx 0.09$ MHz, and $g_0 \approx 0.46$ MHz). In this regime Eqs. B.5–B.7 may be used to obtain the emission rate out the cavity mirrors with $\mathcal{N} \approx -1$ and $\gamma_c \gg \gamma_p$:

$$P_{ends} \approx N_u^0\hbar\omega_p\frac{g_0^2}{\gamma_c}\frac{\gamma_c^2}{(\omega_c-\omega_p)^2+\gamma_c^2}. \tag{B.8}$$

with

$$N_u^0 \approx \frac{\pi\gamma_p i(\omega_p)}{2I_s}. \tag{B.9}$$

Again note that Eqs. B.8 and B.9 are single mode results which give the correct inhibition rate (when $(\omega_c-\omega_p) \approx c/4L$) so long as $F \gg 1$. In the experiment $F \approx 70$, so that this assumption is justified and the experimental results are found to be in good agreement with these results.

Appendix C

Stimulated Emission and Linewidth Narrowing

We wish to consider the conditions under which atom-cavity emission is narrowed by stimulated emission. First notice that the smaller linewidth exhibits gain narrowing for positive inversion and broadening for negative inversion, as seen in Eqs. 2.105 and 2.115, when compared with the corresponding uncoupled linewidths, γ_p and γ_c, respectively. If, however, the normal mode frequencies are not degenerate (i.e., if splitting occurs), the system cannot be characterized by a single linewidth. As seen in Eqs. 2.28–2.36, the normal mode frequencies become equal when

$$\omega_- = 0 \qquad \text{and} \qquad \mathcal{N} > -\left(\frac{\gamma_-}{g_0}\right)^2, \tag{C.1}$$

or

$$\gamma_- = 0 \qquad \text{and} \qquad \mathcal{N} > \left(\frac{\omega_-}{g_0}\right)^2. \tag{C.2}$$

In order to discuss the broadening/narrowing of the lineshape, the linewidth has to be compared to that of uncoupled atom and cavity oscillators ($g_0 = 0$). Furthermore, if the atom-cavity detuning is not zero, there will be no well-defined single linewidth for the uncoupled oscillators (although the coupled system can exhibit a single linewidth if Eq. C.2 is satisfied). Therefore, we specialize to the case in which Eq. C.1 is

satisfied. The linewidth formulae then take on simple forms (2.140):

$$\Gamma_- = \gamma_+ - \gamma_- \sqrt{1 + \frac{\mathcal{N} g_0^2}{\gamma_-^2}}, \tag{C.3}$$

$$\Gamma_+ = \gamma_+ + \gamma_- \sqrt{1 + \frac{\mathcal{N} g_0^2}{\gamma_-^2}}. \tag{C.4}$$

However, the narrower of Γ_+ is not the true linewidth of the atom-cavity emitter. The true FWHM of the emission lineshape, Γ, is obtained from

$$\frac{1}{2} = \frac{\Gamma_+^2}{\Gamma_+^2 + \Gamma^2} \frac{\Gamma_-^2}{\Gamma_-^2 + \Gamma^2}, \tag{C.5}$$

which gives

$$\Gamma^2 = \sqrt{2(\gamma_+^4 + \gamma_-^4 + \mathcal{N}^2 g_0^2) + 4\gamma_-^2 \mathcal{N} g_0^2} - (\gamma_+^2 + \gamma_-^2 + \mathcal{N} g_0^2). \tag{C.6}$$

This linewidth can be compared to that of an uncoupled atom-cavity emitter, Γ_0:

$$\Gamma_0^2 = \sqrt{2(\gamma_+^4 + \gamma_-^4)} - (\gamma_+^2 + \gamma_-^2). \tag{C.7}$$

We define a function, $h(\mathcal{N}) = \Gamma^2 - \Gamma_0^2$ and examine its asymptotic behavior:

$$h \overset{\mathcal{N} \to \pm\infty}{\longrightarrow} (\pm\sqrt{2} - 1)\mathcal{N} g_0^2, \tag{C.8}$$

$$h \overset{\mathcal{N} \to 0}{\longrightarrow} \left(\frac{\sqrt{2}\gamma_-^2}{\sqrt{\gamma_+^4 + \gamma_-^4}} - 1 \right) \mathcal{N} g_0^2, \tag{C.9}$$

where

$$\frac{\sqrt{2}\gamma_-^2}{\sqrt{\gamma_+^4 + \gamma_-^4}} - 1 = \frac{\gamma_-^4 - \gamma_+^4}{\sqrt{\gamma_+^4 + \gamma_-^4}\left(\sqrt{2\gamma_-^4} + \sqrt{\gamma_+^4 + \gamma_-^4}\right)} < 0, \tag{C.10}$$

always. Actually, the steady-state inversion can not take on arbitrary positive values. It is always limited by an upper bound

$$\mathcal{N} < \frac{\gamma_c \gamma_p}{g_0^2} \equiv \mathcal{N}_{th}, \tag{C.11}$$

or equivalently

$$G' = \frac{\mathcal{N}}{F}\frac{\sigma_0 L}{1-R}\left(\frac{\gamma_p}{\gamma_c+\gamma_p}\right) = \frac{\text{(single pass gain)}}{\text{(single pass loss)}} < \frac{\mathcal{N} g_0^2}{\gamma_c \gamma_p} < 1. \tag{C.12}$$

In other words, the saturated single-pass gain is always smaller than the single-pass loss. (This is also true for a laser operating above threshold.) Therefore, the range of inversion for a well-defined linewidth is

$$-\left(\frac{\gamma_c}{g_0}\right)^2 < \mathcal{N} < \mathcal{N}_{th}. \tag{C.13}$$

In this range, we find

$$\begin{aligned} \Gamma &< \Gamma_0 \qquad (\mathcal{N} > 0), \\ \Gamma &> \Gamma_0 \qquad (\mathcal{N} < 0). \end{aligned} \tag{C.14}$$

Therefore, the emission linewidth of the atom-cavity system, whenever it can be defined unambiguously, is broader than that of the uncoupled system if the inversion is negative and narrower if the inversion is positive.

Appendix D

PRL Manuscript

Normal Mode Lineshapes for Atoms in Standing-Wave Optical Resonators

J. J. Childs, K. An, M. S. Otteson, R. R. Dasari, and M. S. Feld

Abstract

A high finesse standing-wave cavity mode resonantly interacting with a beam of two-level ^{138}Ba atoms is weakly driven by a tunable laser. Transmitted and side-light scattered lineshapes are recorded. With mean intra-cavity atomic number, $\langle \overline{N} \rangle \approx 1$, we observe one, two, and three-peaked lineshapes for strong coupling. In addition, two-peaked spectra observed in intermediate coupling demonstrate that lineshape splitting is not necessarily indicative of oscillatory atom-cavity energy exchange. Several atoms are required for $\langle \overline{N} \rangle \approx 1$, so this is not a true single atom regime.

The study of an atom coupled to a single mode of a resonator, known as cavity quantum electrodynamics (QED), has undergone significant advances since Purcell first pointed out that a resonator could alter the atomic spontaneous emission rate [7]. For the case of a weakly coupled atom-cavity system, enhanced and suppressed spontaneous emission have been demonstrated in several experiments. Recent improvements in resonator design, however, have led to larger atom-cavity coupling strengths, and several experiments have demonstrated single intra-cavity atom Rabi oscillations [17], normal mode splitting [21], optical bistability [23] and single-atom

maser and laser oscillation [19, 25]. Most of the above experiments employed atomic beams, but enhanced spontaneous emission [26] as well as normal mode splitting [27] have also been observed in semiconductor devices, where practical as well as fundamental issues of cavity QED are studied [28, 29].

All of the above studies utilized standing-wave (SW) mode resonators, in which the coupling of the radiator to the cavity mode is position dependent. The effect of such mode structure on atom-cavity dynamics has both fundamental and practical significance. For example, single-atom laser operation is critically dependent on the location of successive atoms within the cavity mode volume [33]. Similarly, in microcavities the spontaneous emission coefficient, β, is position dependent. The larger the β parameter, the lower the threshold for laser oscillation. In the limit $\beta \rightarrow 1$ thresholdless lasing occurs [28]. Low-threshold and, therefore, more efficient microcavities have been demonstrated recently [32].

Many of the above mentioned phenomena are manifested in spectral lineshapes. For example, two-peaked lineshapes result from oscillatory exchange of energy between the atom and cavity mode (normal-mode splitting), multi-resonance lineshapes are predicted to arise from atomic motion through the cavity mode [34, 35], and broadened and narrowed Lorentzians demonstrate enhanced and suppressed spontaneous emission, respectively. These lineshapes are sensitive not only to the particular kind of resonator (standing/travelling wave, open/closed and degenerate/nondegenerate) and radiator (moving atoms in a beam or fixed excitons), but also to the particular excitation and observation geometry. In particular, normal-mode lineshapes in an atom-cavity system with an open optical resonator may be obtained either by exciting the atom from the side of the resonator, or the cavity mode through the mirrors. In either case one may observe light scattered by the atom out the resonator side (sidelight) or transmitted out the resonator ends. As shown below, the various geometries can exhibit dramatically different lineshapes.

A single, two-level atom coupled to a cavity mode may be treated as two coupled, damped harmonic oscillators when weakly excited. The atomic and cavity oscillator's spectral lineshapes can be calculated in fully quantized or semiclassical

treatments, with both giving the same results [47, 52]. Three regimes may be defined by the parameter $\xi = 4g_0^2/(\gamma_c - \gamma_p)^2$ where the atom-cavity coupling constant, $g_0 = (\mu/\hbar)\sqrt{2\pi\hbar\omega_p/V}$, with μ and ω_p the atomic dipole moment and frequency, respectively, V the cavity mode volume, $2\gamma_c$ the cavity decay rate, and $2\gamma_p$ the atomic spontaneous emission rate to modes other than the cavity mode: (1) strong coupling ($\xi \gg 1$); (2) intermediate coupling ($\xi \approx 1$) and (3) weak coupling ($\xi \ll 1$). For strong coupling, energy exchange implies two-peaked spectra for both oscillators. For weakly coupled systems, on the other hand, exponential decay leads to single-peaked Lorentzian spectra.

We present a study of lineshape splitting in an atom-cavity system comprised of an atomic beam interacting with an SW mode resonator in intermediate and strong coupling regimes. We are particularly interested in the case with mean intra-cavity atom, $\langle \overline{N} \rangle \approx 1$. Normal mode splitting for $\langle \overline{N} \rangle \approx 1$ in the strong coupling regime has been reported in a cavity transmission experiment [21]. We demonstrate that: (1) lineshape splitting in the cavity transmission spectrum alone does not necessarily imply normal-mode oscillations, but two peaks observed in both the sidelight and transmission lineshapes do, (2) lineshape distortions can be dramatic and very sensitive to fluctuations in the intra-cavity atomic number when $\langle \overline{N} \rangle \approx 1$, (3) details of the lineshapes arising from these fluctuations are critically dependent on the choice of the excitation/observation geometry . In addition, we wish to clarify the connection between such experiments and the true single-atom Jaynes Cummings model [37].

In the present series of experiments, the cavity mode is weakly excited by frequency stabilized, tunable light ($\delta\nu \approx 0.5$ MHz) from a dye laser (Coherent CR-699). Photon counts are simultaneously collected out the sides (a measure of atomic excitation) and end of the cavity (transmission), as functions of the excitation laser frequency, with a photon counter, (SR400, Stanford Research), and photomultiplier tubes, (Hamamatsu, R1635). An effusive atomic beam of ^{138}Ba with collimation ± 1.5 mrad and beam diameter $\approx 25\mu$m, intersects the optical axis of a high finesse cavity at $90^o \pm 0.5$ mrad. The first resonance transition $^1S_0 \rightarrow ^1P_1$, $\lambda = 553.5$ nm, $2\gamma_p/2\pi \approx 19$ MHz (FWHM), interacts with a single, SW field mode whose mode func-

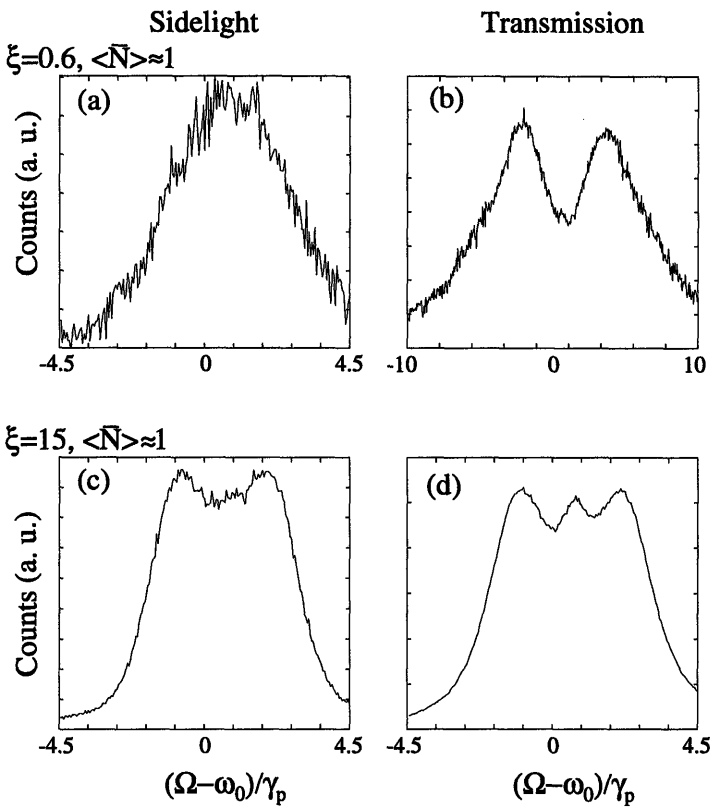

Figure D-1: Sidelight and transmission lineshapes for $\Delta = 0$.

tion is $\psi(r,z) = e^{-(\frac{r}{w_0})^2} \sin kz$ and mode volume $V = \frac{1}{4}\pi w_0^2 L$, with w_0 the cavity mode waist and L the mirror separation. The optical axis defines the z axis. The stabilized cavity frequency, $\delta\nu_c \leq \pm 0.5$ MHz, is locked to a reference laser beam to prevent slow drift. The laser is, in turn, locked with an accuracy $\delta\nu \leq \pm 0.5$ MHz within a 1 kHz bandwidth to the atomic resonance using a Lamb dip cell and a frequency modulation technique. The reference beam is chopped off and on by an acousto-optic modulator (110 MHz Isomet) at 50 Hz, alternating between data taking and cavity locking, respectively, with a 30% duty cycle. During the data taking intervals the cavity drift is less than 0.5 MHz so that atom-cavity detuning, $\Delta = 0 \pm 0.5$ MHz. Part of the excitation laser beam interacts with the atomic beam before it enters the cavity, and the resulting (free-atom) fluorescence is collected to monitor the atomic beam density, ρ_0.

Two cavities, which differ only in finesse, F, and throughput, η ($= TF/\pi$ with T the mirror transmission), are used to investigate the strong and intermediate cou-

pling regimes. Each cavity consists of two "supercavity" mirrors, each with radius of curvature 10 cm, with $L = 247\mu$m and 240μm, respectively ($w_0 \approx 25\mu$m). This gives $g_0/2\pi = 16.6 \pm 0.5$ MHz for the coupling constant and $2\gamma_c/2\pi = 2.4 \pm 0.2$ MHz ($F = 2.5 \times 10^5$, $\eta \approx 0.31$) for strong coupling ($\xi \approx 16$), and $2\gamma_c/2\pi = 108 \pm 4$ MHz ($F = 5.8 \times 10^3$, $\eta \approx 0.9$) for intermediate coupling ($\xi \approx 0.6$). The spontaneous emission coefficient $\beta = 0.73/0.31$ for the strong/intermediate coupling resonators, respectively.

Lineshapes obtained for both sidelight and cavity transmission are shown in Fig. D-1 for the intermediate (a,b) and strong (c,d) coupling regimes with $\langle \overline{N} \rangle \approx 1$. The free-atom fluorescence signal determines $\langle \overline{N} \rangle$ as ρ_0 is varied. However, uncertainties in overall collection efficiency limit the accuracy of these estimates to $\approx 50\%$. A more accurate calibration is obtained by a fit (in which $\langle \overline{N} \rangle$ is the only free parameter) to one experimental data trace using an extension to our previous model [52] which incorporates fluctuations in atomic number and position [72]. The resulting uncertainty in $\langle \overline{N} \rangle$ is 10%.

The intermediate coupling sidelight, trace (a), exhibits a single-peaked lineshape of width 45 MHz (FWHM, with ≈ 3 MHz Doppler and transit time broadening), twice the free-space value, providing a dramatic demonstration of cavity QED line broadening. In view of this single-peaked sidelight, the two peaks observed in transmission (b) cannot be attributed to oscillatory energy exchange. Furthermore, $\xi \approx 0.6$, which excludes the possibility of two distinct normal mode frequencies. This splitting, instead, can be explained by noting that when the excitation laser is near resonant with the atom, light is scattered out the resonator side and, since $\gamma_p < \gamma_c$, a dip results in the cavity transmission lineshape. A similar result has recently been reported [70].

In the strong coupling regime, the transmission lineshape, trace (d), exhibits the two peaks expected with oscillatory energy exchange. This interpretation is unambiguously confirmed by the two similar peaks in the sidelight, trace (c). Interestingly, a central third peak is also present in (d). Its origin can be understood by considering Fig. D-2. Lineshapes depend upon fluctuations in intra-cavity atomic number, defined by $\overline{N} = \sum_{j=1}^{N} \psi^2(r_j, z_j)$ with N the total number of atoms interacting with the

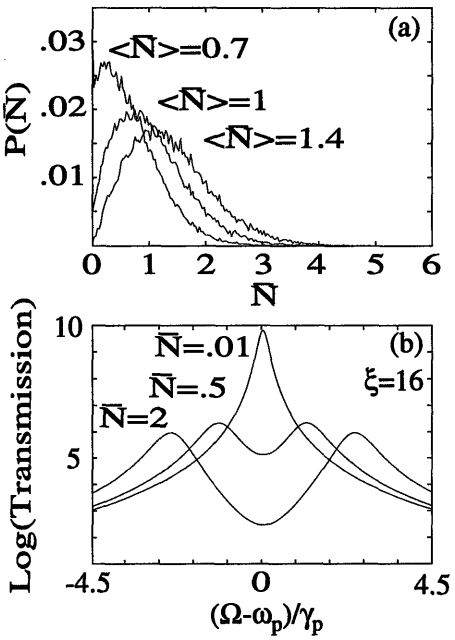

Figure D-2: (a) Probability distribution, $P(\overline{N})$. (b) Transmission lineshapes.

cavity mode and r_j/z_j the radial/axial position of the j^{th} atom, respectively. During the data taking intervals both the number of atoms and their positions fluctuate. These fluctuations may be characterized by a distribution function P($\overline{N}$), shown for several values of $\rho_0 \propto \langle\overline{N}\rangle$ in the computer generated curves (a). They are the result of repeated random placements of a large but fixed number of atoms ($\propto \rho_0$) in a large volume defined by the atomic beam. Only those atoms, N, falling within a fraction of the atomic beam, centered on the cavity mode axis, are used to estimate $\overline{N}$. The volume of this fraction is chosen large enough so that all atoms outside, if included, would make a negligible contribution to $\overline{N}$. The curves in (b) are lineshapes for specific values of $\overline{N}$ (no fluctuations), obtained from the single-atom model [52] by replacing $g^2 \rightarrow \overline{N}g_0^2$. For a given $\langle\overline{N}\rangle$, theoretical fits are calculated by a weighted average of these lineshapes with the appropriate P($\overline{N}$) distribution in (a). The two outside peaks in trace (d) of Fig. D-1 are present because the probability for the value $\overline{N} \approx 1$ is largest. The third peak arises because: (1) Although the probability for small $\overline{N}$ is low, the empty cavity transmission signal is large compared to the $\overline{N} \approx 1$ lineshapes (note the log scale in (b)) and (2) the cavity resonance is narrow. There is

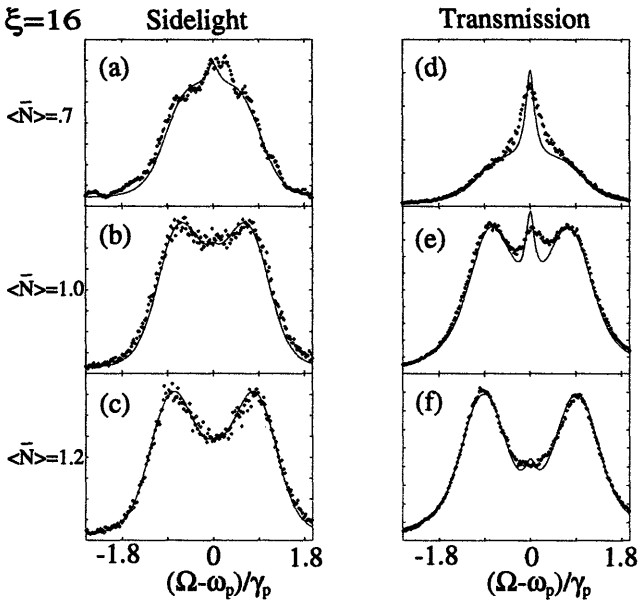

Figure D-3: Strong coupling ($\xi = 16$) sidelight and transmission data and theoretical fits (solid lines).

no third peak in trace (c), because empty cavity sidelight signals are absent; an atom not coupled to the cavity mode will not be excited.

Experimental lineshapes for various values of $\langle \overline{N} \rangle$ are shown in Fig. D-3 together with theoretical fits. Note the extreme sensitivity (particularly the cavity transmission lineshapes in traces (d–f)) to small changes in $\langle \overline{N} \rangle$. As ρ_0 is increased, the probability for small $\overline{N}$ decreases and the empty cavity resonance disappears, as in trace (f). The empty cavity effect dominates at the other extreme of low atomic beam density, and washes out the normal mode splitting in trace (d). The splitting is seen to be slightly larger for the cavity oscillator, trace (f), than for the atomic oscillator, trace (c). This is a particular example of a general result that reflects the sensitivity of lineshapes to geometry: Lineshape splitting measured by observing the oscillator which is not being driven (atom) is smaller than that which is (cavity mode), but splitting in the former always implies normal mode oscillation [52]. The agreement between data and fits is quite good. The discrepancies are due to atomic beam misalignment, atom-cavity detuning, and Doppler broadening.

None of the features in the data are attributable to saturation. The lineshapes did not change over a large range of excitation laser intensities ($\approx$ two orders of magni-

tude), even with intra-cavity photon number, n, somewhat larger than the saturation parameter, n_0. For the case of a single atom located at (r_j, z_j), $n_0 = [\gamma_p/(\psi(r_j, z_j)g_0)]^2$ and is position dependent. In the cavities studied here, $n_0 = 0.33$ for an optimally coupled atom. However, a single saturation parameter cannot be ascribed to the lineshapes when fluctuations are important ($\langle\overline{N}\rangle \approx 1$); optimally coupled atoms saturate before weakly coupled atoms. In the data presented here n never exceeded n_0. Multi-resonance lineshapes have been predicted to arise from atomic motion through the cavity mode [34, 35]. However, the three-peaked lineshapes observed here are not attributable to this effect, since the maximum Doppler shift is $\delta\nu_{max} \approx 1$ MHz$< 2\gamma_c/2\pi \ll g_0/2\pi$.

Normal-mode splitting for a single intra-cavity atom, $\langle\overline{N}\rangle \approx 1$, requires, on average, the simultaneous presence of several atoms interacting with the cavity mode. To demonstrate this, consider the total number of atoms in a given volume, $N = \int_0^l \int_0^r \rho_0 dV = \pi r^2 l \rho_0$, with ρ_0 assumed uniform and where l extends over many SW mode wavelengths. The number of intra-cavity atoms in this volume at any instant is given by $\overline{N} = \int_0^l \int_0^r \rho_0 \psi^2(r,z) dV$. Therefore, the ratio $\overline{N}/N$ of the number of intracavity atoms to total number of atoms is $\approx (1 - e^{-2u^2})/(2u)^2$, with $u = r/\omega_0$. Choosing $u = 1$, $N \approx 4.6$ atoms are required to obtain $\overline{N} \approx 1$. One must therefore conclude that $\langle\overline{N}\rangle \approx 1$ does not constitute the true single atom regime. Furthermore, models based on extensions of the Jaynes Cummings theory to many atoms assume a uniform mode function [44, 40] and do not strictly apply to experiments of this type. For a true single atom which samples all positions within the volume specified above, $\langle\overline{N}\rangle \longrightarrow 0.2$. The resulting lineshapes would not exhibit splitting for our parameters, as the trend in Fig. D-3 suggests.

In conclusion, these results demonstrate that care in interpreting the lineshapes must be taken in order to extract information about the fundamental coupling mechanism. We have demonstrated (1) lineshape splitting without normal mode oscillations, (2) spectral lineshape features which are dependent on experimental geometry, and (3) dramatic manifestations of intra-cavity atomic number fluctuations for $\langle\overline{N}\rangle \approx 1$. We have described the role that these fluctuations play in studying atom and cavity

lineshapes for various values of $\langle \overline{N} \rangle$. Furthermore, we have shown that splitting in one lineshape only is not necessarily an indication of oscillatory energy exchange. We have also demonstrated that normal mode splitting for $\langle \overline{N} \rangle \approx 1$ requires several atoms to be present in the cavity mode, and thus is not a true single atom effect. Finally, the trend in our data suggests that lineshapes in the true single atom limit would not exhibit splitting.

This work is supported by NSF Grant No. PHY-9112421 and No. CHE-9304251.

Bibliography

[1] D. ter Haar. *The Old Quantum Theory.* Pergamon Press, London, 1984.

[2] V. S. Weisskopf and E. Wigner. Berechnung der natürlichen linienbreite auf grund der Diracschen lichttheorie. *Z. Physik*, 63:54, 1930.

[3] H. A. Bethe. The electromagnetic shift of energy levels. *Physical Review*, 72:339, 1947.

[4] K. H. Drexhage. Interaction of light with monomolecular dye layers. In Emil Wolf, editor, *Progress in Optics*, volume 12, page 165. North-Holland, Amsterdam, 1974.

[5] G. Gabrielse and H. Dehmelt. Observation of inhibited spontaneous emission. *Physical Review Letters*, 55:67, 1985.

[6] J. J. Sanchez-Mondragon, N. B. Narozhny, and J. H. Eberly. Theory of spontaneous emission lineshape in an ideal cavity. *Physical Review Letters*, 51:550, 1983.

[7] E. M. Purcell. Spontaneous emission probabilities at radio frequencies. *Physical Review*, 69:681, 1946.

[8] P. Goy, J. M. Raimond, M. Gross, and S. Haroche. Observation of cavity-enhanced single-atom spontaneous emission by a Rydberg atom. *Physical Review Letters*, 50:1903, 1983.

[9] R. G. Hulet, E. S. Hilfer, and D. Kleppner. Inhibited spontaneous emission by a Rydberg atom. *Physical Review Letters*, 55:2137, 1985.

[10] D. Kleppner. Inhibited spontaneous emission. *Physical Review Letters*, 47(4):233, 1981.

[11] W. Jhe, A. Anderson, E. A. Hinds, D. Meschede, L. Moi, and S. Haroche. Suppression of spontaneous decay at optical frequencies: test of vacuum-field anisotropy in confined space. *Physical Review Letters*, 58:666, 1987.

[12] D. J. Heinzen, J. J. Childs, J. E. Thompson, and M. S. Feld. Enhanced and inhibited visible spontaneous emission by atoms in a confocal resonator. *Physical Review Letters*, 58:1320, 1987.

[13] D. J. Heinzen and M. S. Feld. Vacuum radiative level shifts and spontaneous emission linewidth of an atom in an optical resonator. *Physical Review Letters*, 59:2623, 1987.

[14] D. J. Heinzen, J. J. Childs, and M. S. Feld. Spectroscopic measurements of single atom emission in an optical resonator. *Spectrochimica Acta*, 45A:75, 1989.

[15] S. E. Morin, C. C. Yu, and T. W. Mossberg. Strong atom-cavity coupling over large volumes and observation of subnatural intra-cavity atomic linewidths. *Physical Review Letters*, 73:1489, 1994.

[16] G. Rempe and H. Walther. Experiments with the single-atom maser. *Physical Review Letters*, 58:353, 1987.

[17] G. Rempe, H. Walther, and N. Klein. Observation of quantum collapse and revival in a one-atom maser. *Physical Review Letters*, 58:353, 1987.

[18] G. Rempe, F. Schmidt-Kaler, and H. Walther. Observation of sub-poissonian photon statistics in a micromaser. *Physical Review Letters*, 64:2783, 1990.

[19] D. Meschede, H. Walther, and G. Muller. One-atom maser. *Physical Review Letters*, 54:551, 1985.

[20] Yifu Zhu, D. J. Gauthier, S. E. Morin, Qilin Wu, H. J. Carmichael, and T. W. Mossberg. Vacuum Rabi splitting as a feature of linear-dispersion theory: analysis and experimental observations. *Physical Review Letters*, 64:2499, 1990.

[21] R. J. Thompson, G. Rempe, and H. J. Kimble. Observation of normal-mode splitting for an atom in an optical cavity. *Physical Review Letters*, 68:1132, 1992.

[22] M. G. Raizen, L. A. Orozco, Min Xiao, T. L. Boyd, and H. J. Kimble. Squeezed-state generation by the normal modes of a coupled system. *Physical Review Letters*, 59(2):198, 1987.

[23] G. Rempe, R. J. Thompson, R. J. Brecha, W. D. Lee, and H. J. Kimble. Optical bistability and photon statistics in cavity quantum electrodynamics. *Physical Review Letters*, 67(13):1727, 1991.

[24] Kyungwon An. *The Microlaser: Study of Laser Oscillation with One Atom in an Optical Resonator.* PhD thesis, Massachusetts Institute of Technology, 1995.

[25] K. An, J. J. Childs, R. R. Dasari, and M. S. Feld. The microlaser: Observation of laser oscillation with a few atoms in a single-mode resonator. *Physical Review Letters*, 73:3375, 1994.

[26] Y. Yamamoto and S. Machida. Microcavity semiconductor laser with enhanced spontaneous emission. *Physical Review A*, 44(1):657, 1991.

[27] C. Weisbuch, M. Nishioka, A. Ishikawa, and Y. Arakawa. Observation of the coupled exciton-photon mode splitting in a semiconductor quantum microcavity. *Physical Review Letters*, 69(23):3314, 1992.

[28] H. Yokoyama and S. D. Brorson. Rate equation analysis of microcavity lasers. *Journal of Applied Physics*, 66(10):4801, 1989.

[29] Y. Yamamoto and R. Slusher. Optical processes in microcavities. *Physics Today*, page 66, June 1993.

[30] R. Houdré, R. P. Stanley, U. Oesterle, M. Ilegems, and C. Weisbuch. Room-temperature cavity polaritons in a semiconductor microcavity. *Physical Review B*, 49(23):16761, 1994.

[31] H. Cao, J. Jacobson, G. Björk, S. Pau, and Y. Yamamoto. Observation of dressed-exciton oscillating emission over a wide wavelength range in a semiconductor microcavity. *Applied Physics Letters*, 66(9):1107, 1995.

[32] F. M. Matinaga, A. Karlsson, S. Machida, Y. Yamamoto, T. Suzuki, Y. Kadota, and M. Ikeda. Low-threshold operation of hemispherical microcavity single-quantum-well lasers at 4K. *Applied Physics Letters*, 62(5):443, 1993.

[33] K. An and M. S. Feld. Role of standing-wave mode structure in microlaser emission. *Physical Review A*, 52(2):1691, 1995.

[34] M. Wilkins, Z. Bialynicka-Birula, and P. Meystre. Spontaneous emission in a Fabry-Perot cavity: The effects of atomic motion. *Physical Review A*, 45(1):477, 1992.

[35] W. Ren, J. D. Cresser, and H. J. Carmichael. Spontaneous emission in a standing-wave cavity: quantum mechanical center-of-mass motion. *Physical Review A*, 51(1):752, 1995.

[36] H. J. Carmichael. Photon antibunching and squeezing for a single atom in a resonant cavity. *Physical Review Letters*, 55(25):2790, 1985.

[37] E. T. Jaynes and F. W. Cummings. Comparison of quantum and semiclassical radiation theories with application to the beam maser. *Proceedings of the IEEE*, 51:89, 1963.

[38] R. P. Feynman, F. L. Vernon Jr., and R. W. Hellwarth. Geometrical representations of the Schrödinger equation for solving maser problems. *Journal of Applied Physics*, 28:49, 1957.

[39] R. H. Dicke. Coherence in spontaneous radiation processes. *Physical Review*, 93:99, 1954.

[40] M. Tavis and F. W. Cummings. Exact solutions for an N-molecule-radiation-field Hamiltonian. *Physical Review*, 170:379, 1968.

[41] P. Filipowicz, J. Javanainen, and P. Meystre. Theory of a microscopic maser. *Physical Review A*, 34:3077, 1986.

[42] H. J. Carmichael. Photon antibunching and squeezing for a single atom in a resonant cavity. *Physical Review A*, 33:3262, 1986.

[43] W. Y. Hsu and R. Glauber. Radiation by atoms in resonant cavities. In Michael S. Feld, John E. Thomas, and Aram Mooradian, editors, *Laser Spectroscopy IX*, Proceedings of the Ninth International Conference on Laser Spectroscopy, San Diego, CA, 1989. Academic Press. Held at Bretton Woods, NH, June 18-23, 1989.

[44] G. S. Agarwal. Vacuum-field Rabi splittings in microwave absorption by Rydberg atoms in a cavity. *Physical Review Letters*, 53(18):1732, 1984.

[45] G. S. Agarwal. Vacuum-field Rabi oscillations of atoms in a cavity. *Journal for the Optical Society of America, B*, 2:480, 1985.

[46] P. R. Rice and H. J. Carmichael. Nonclassical effects in optical spectra. *Journal for the Optical Society of America B*, 5:1661, 1988.

[47] H. J. Carmichael, R. J. Brecha, M. G. Raizen, H. J. Kimble, and P. R. Rice. Subnatural linewidth averaging for coupled atomic and cavity-mode oscillators. *Physical Review A*, 40(10):5516, 1989.

[48] P. L. Knight and P. W. Milonni. The Rabi frequency in optical spectra. *Physics Reports*, 66(2):59, 1980.

[49] M. Lewenstein and T. W. Mossberg. Spectral and statistical properties of strongly driven atoms coupled to frequency-dependent photon reservoirs. *Physical Review A*, 37:2048, 1988.

[50] L. Tian and H. J. Carmichael. Quantum trajectory simulations of the two-state behavior of an optical cavity containing one atom. *Physical Review A*, 46(11):R6801, 1992.

[51] B. R. Mollow. Power spectrum of light scattered by two-level systems. *Physical Review*, 188:1969, 1969.

[52] J. J. Childs, K. An, R. R. Dasari, and M. S. Feld. Single atom emission in an optical resonator. In Paul R. Berman, editor, *Cavity Quantum Electrodynamics*, Advances in Atomic Molecular and Optical Physics. Academic Press, New York, 1994. Supplement 2.

[53] L. A. Lugiato. Theory of optical bistability. In Emil Wolf, editor, *Progress in Optics*, volume 21. Elsevier, New York, 1981.

[54] C. Cohen-Tannoudji and Serge Haroche. Absorption et diffusion de photons optiques par un atome en interaction avec des photons de radiofréquence. *Journal de Physique*, 30:125,153, 1969.

[55] J. J. Sakurai. *Advanced Quantum Mechanics.* Benjamin/Cummings, Menlo Park, CA., 1967.

[56] A. L. Schawlow and C. H. Townes. *Microwave Spectroscopy.* McGraw Hill, New York, 1955.

[57] M. G. Raizen, R. J. Thompson, R. J. Brecha, H. J. Kiimble, and H. J. Carmichael. Normal-mode splitting and linewidth averaging for two-state atoms in an optical cavity. *Physical Review Letters*, 63:240, 1989.

[58] A. L. Schawlow and C. H. Townes. Infrared and optical masers. *Physical Review*, 112:1940, 1958.

[59] W. Heitler. *The Quantum Theory of Radiation.* Dover Publications, Inc., New York, third edition, 1984.

[60] R. Loudon. *The Quantum Theory of Light.* Oxford University Press, Oxford, second edition, 1983. p.295.

[61] A. Siegman. *Lasers.* University Science Books, Mill Valley, Ca., first edition, 1986.

[62] P. M. Alsing, D. A. Cardimona, and H. J. Carmichael. Suppression of fluorescence in a lossless cavity. *Physical Review A*, 45(3):1793, 1992.

[63] A. Yariv. *Quantum Electronics.* John Wiley and Sons, New York, NY, second edition, 1975.

[64] H. Kogelnik and T. Li. Laser beam and resonators. *Proceedings of the IEEE*, 54(10):1312, 1966.

[65] M. Prentiss and A. Cable. Slowing and cooling an atomic beam using an intense optical standing wave. *Physical Review Letters*, 62(12):1354, 1989.

[66] M. Hercher. The spherical mirror Fabry-Perot interferometer. *Applied Optics*, 7(5):951, 1968.

[67] D. J. Heinzen. *Radiative Decay and Level Shift of an Atom in an Optical Resonator.* PhD thesis, Massachusetts Institute of Technology, 1988.

[68] R. Lalezari, Research Electroptics Inc., Boulder, Co.

[69] The PZT cylinders were purchased from Morgan Matroc. Their dimensions were 1" long with a diameter of 1" and wall thickness .125". The material used for the cavities in the actual experiment was PZT-8. Note that drilling holes in such a material is difficult because it is extremely brittle, but a local company, Ferro-Ceramic, performed the necessary machining.

[70] H. J. Kimble, private communication.

[71] M. Born and E. Wolf. *Principles of Optics.* Pergammon, Oxford, 6 edition, 1986.

[72] To be published.